Production of Dark Matter in Cosmological Models with Low Reheating Temperature

Dissertation
zur
Erlangung des Doktorgrades (Dr. rer. nat.)
der
Mathematisch-Naturwissenschaftlichen Fakultät
der
Rheinischen Friedrich-Wilhelms-Universität Bonn

vorgelegt von

Fazlollah Hajkarim

aus
Gorgan, Iran

Bonn, 19.07.2018

Angefertigt mit Genehmigung der Mathematisch-Naturwissenschaftlichen Fakultät der Rheinischen Friedrich-Wilhelms-Universität Bonn

1. Gutachter:	Prof. Dr. Manuel Drees
2. Gutachter:	Prof. Dr. Herbert K. Dreiner
Tag der Promotion:	09.10.2018
Erscheinungsjahr:	2018

Abstract

In standard cosmology it is assumed that dark matter (DM) is thermally produced during the radiation dominated era after an inflationary period. This has led to the prediction of weakly interactive massive particles (WIMPs) as the most popular candidates for DM. However, current indirect, direct, and collider searches for the WIMPs have not found any clear evidence yet. This issue motivates us to investigate cosmological scenarios with matter domination before big bang nucleosynthesis (BBN). The theories unifying the four fundamental forces of nature at high energy scales, like superstring theory, can have proposals for the early universe cosmology after the inflationary reheating and before BBN. In such cases the universe can be dominated by heavy long–lived fields (moduli) with low reheating temperatures which can decay to DM and radiation. To explore such scenarios, we precisely compute the degrees of freedom (DoF) of standard model particles using lattice quantum chromodynamics (QCD) results for QCD equation of state around the temperature of quark–gluon confinement. Afterwards, we study the production of DM in an early matter dominated era from the annihilation of thermal bath particles and decay of moduli, using the computed DoF and assuming initially vanishing and nonvanishing radiation and DM densities. In that case new production mechanisms for DM beyond the thermal WIMP production are also possible. Finally, we focus on studying the production of neutralinos, as the most popular DM candidate in supersymmetric models, in low reheating scenarios and its status in current experimental searches.

Acknowledgements

I would like to thank Prof. Dr. Manuel Drees for his helps, support, and being my PhD supervisor and my collaborator.

I should thank Prof. Dr. Herbi Dreiner and Prof. Dr. Hans Peter Nilles for their helps and support. Also, I use this opportunity to thank Prof. Dr. Klaus Desch and Prof. Dr. Helmut Baltruschat for accepting to be the examiners of the oral presentation of my Ph.D. thesis.

Also, I am grateful to Dr. Andreas Wißkirchen for his support and helps on computer problems and other issues.

I never forget the grateful helps and kindness of PI secretaries Petra Weiß, Patricia Zündorf, Christa Börsch, and Dagmar Faßbender.

I acknowledge the help of Manimala Chakraborti, Bardia Najjari Farizhendi, and Rahul Mehra for reading the draft of this thesis. I also thank Bardia, Rahul, Meng Shi, and Raghuveer Garani as my officemates.

I am also thankful for the rest of my friends and colleagues at Bonn: Ernany Rossie Schmitz, Stefano Colucci, Swasti Belwal, Young Xu, Zhongyi Zhang, Abtin Narimani, Reza Safari, Christoph Liyanage, Cesar Fierro Cota, Manuel Krauß, Annika Reinert, Andreas Trautner, Victor Martin Lozano, Simon Zeren Wang, Alireza Babaei, and those I have forgotten their names.

Finally, I should thank my parents and grandparents, and my brother for their support and love during my life and studies.

Contents

CHAPTER 1

Introduction

"What hurts you, blesses you. Darkness is your candle. Your boundaries are your quest."

The Big Red Book
Rumi
Translated by Coleman Barks

"I am part of the part that once was everything, part of the darkness which gave birth to light."

Faust
Johann Wolfgang von Goethe
Translated by Walter Arnold Kaufmann

1.1 Dark Matter Paradigm

The standard model (SM) of particle physics and general relativity (GR) are two main triumphs of modern physics in explaining nature. The SM illustrates three out of four fundamental forces (electromagnetic, weak and strong interactions) which govern the interactions between building blocks of matter (i.e. elementary particles) in nature. Nevertheless, it does not contain any solution to the dark matter (DM) paradigm, hierarchy problem in electroweak sector, inflation, neutrino masses, baryon asymmetry, etc. Beyond the standard model (BSM) physics is an attempt to solve these problems by introducing new symmetries, particles, etc. The fourth force i.e. gravity is described by Einstein's theory of general relativity. GR works well at the scale of solar system to predict the behaviour of massive objects. However, it fails in the regimes where gravity is strong (e.g. near black holes and the Big Bang) or for cosmic acceleration scale (dark energy problem). Modified gravity theories that try to solve these issues using different approaches. The main focus of this thesis is to study the production of a particle dark matter candidate in the early universe.

The first evidence for the existence of dark matter came from rotation curves of galaxies which does not match the prediction of Einstein's theory of gravity and its Newtonian limit [1, 2]. Observation of galaxies in the Coma cluster [3] also confirm the presence of an invisible matter component which influences the gravitational potential without any known interaction beyond the gravity. Moreover, the predictions of the standard model of cosmology ΛCDM, where Λ stands for cosmological constant and CDM for cold dark matter, confirm the presence of a non–luminous matter component through its effect on the cosmic microwave background (CMB) [4–6], which appears in the CMB power spectrum, and the formation of large structures of the universe (galaxies, clusters, etc.) [7]. Observations of the Bullet [8, 9] and Abell 3827 [10, 11] clusters are other confirmations of DM and putting limits on the interaction of DM particles due to discrepancies in the motion of visible matter compared to the expectation given by gravity laws.

Some modified gravity theories have tried to explain the mentioned discrepancies by modifying the laws of gravity at galactic and cosmic scales without assuming any new invisible matter [12–14]. However, based on our explanation in the previous paragraph and also looking at observational difficulties of the modified gravity theories, we believe that dark matter is a new type of matter and indeed exists in the universe. Consequently, it can not be explained only by changing the gravity equations or laws of motion.

The nature of Dark Matter (DM) has been a mystery for many decades. Most proposals for its explanation [1] need new particle physics, since astrophysical and cosmological observations imply that DM consists of cold particles (which were non–relativistic at the begininng of structure formation) [15, 16]. The SM of particle physics does not contain any such particle, while many BSM theories do.

In the ΛCDM, cosmology the universe after Big Bang has developed through inflation, radiation domination, matter domination, dark energy domination eras [7]. In such models of the universe, DM particles were in thermal equilibrium with SM particles during radiation domination. When the universe expanded the temperature decreased. This reduced the probability of annihilation of DM particles to SM ones and vice versa. Consequently, after some time DM particles started to decouple from the thermal bath, and afterwards their number became constant (freeze–out). The DM relic density which is proportional to DM number density after freeze–out and the inverse of radiation entropy density, should match the observed value at present time. Using this fact, the cross section of thermally produced DM should be at the order of weak scale [15]. This is the well–known candidate for DM i.e. weakly interacting massive particles (WIMPs). To compute the relic density for a DM candidate, in addition to having the details of interaction via the Lagrangian that respects gauge symmetry and renormalizability, we should consider the precise thermal features of SM particles interacting with DM. These features appear in the energy and entropy densities of SM particles and become very important in a strongly interacting fluid regime; especially, around the time quarks and gluons begin to confine inside hadrons.

Supersymmetry (SUSY) is one of the BSM theories that tries to solve some of the problems of SM like the DM paradigm, hierarchy problem in the electroweak sector, gauge unification, etc. SUSY works as a symmetry corresponding every SM fermion (boson) to its bosonic (fermionic) superpartner. The quadratic divergences coming from the top–quark loop contribution to the Higgs mass is cancelled by that of its superpartner, "s–top", thereby alleviating the hierarchy problem [17]. Supersymmetric theories propose different candidates for DM. The highly motivated one which can play the role of WIMP DM is the neutralino [18].

Many attempts have been made to detect the WIMPs (especially neutralino DM) and other DM candidates (like axion) in the indirect [19–23], direct [24–29], and collider [30–35] experiments. Indirect searches can measure the annihilation or decay of DM to SM particles in the halo of our galaxy (or other astronomical sources). In direct detection, it has been tried to detect a rare scattering of DM off nuclei at Earth based experiments using the properties of local DM halo. Finally, the collision of SM

particles at high energies can produce DM in colliders like the Large Hadron Collider (LHC). However, unfortunately all efforts to observe the WIMP and other DM candidates have failed so far.

Maybe starting to doubt the naive assumption of a radiation dominated universe after inflation and thermally produced WIMPs can light our path to find DM and BSM physics. Many BSM theories like superstring theory propose heavy long–lived fields (moduli) coming from the compactification of extra dimensions [16, 36]. These fields can dominate the universe after inflationary reheating and before big bang nucleosynthesis (BBN). This imposes a period of matter domination which does not exist in standard cosmology. In such a case, DM can also be produced via the late decay of moduli (non–thermal production) changing the final abundance of DM. As a consequence, new production mechanisms and ranges of DM mass and cross sections beyond the thermal WIMP, satisfy the observed relic density will be available [16, 36].

In this thesis we will study the production of particle DM in the early universe especially in scenarios with low reheating temperatures. The subjects studied in this thesis are briefly mentioned in the next Section.

1.2 Thesis Chapters

This PhD thesis includes five chapters. The current Chapter is the Introduction of this thesis. In the next Chapter, the precise calculation of degrees of freedom (DoF) of standard model thermal bath and its effect on the properties of WIMP dark matter is described (Chapter 2). To compute the DoF of SM we used the recent result of lattice quantum chromodynamics (QCD) and hadron resonance gas model for strongly interacting QCD sector around the QCD transition temperature ($\sim$ 150 MeV). Also, we considered the evolution of neutrino temperature with respect to photon temperature assuming the rest of particles in the standard model are free. This leads to a precise result for the temperature evolution of DoF. In the framework of the minimal cosmological model, detailed measurements on the CMB by the PLANCK collaboration [5] fix the scaled CDM relic density to $\Omega_{DM}h^2 = 0.1193 \pm 0.0014$, with an error of less than 1.5%. In order to fully exploit this observational precision, theoretical calculations should have a comparable or smaller error. In Chapter 2, we use recent lattice QCD calculations to improve the description of the thermal plasma. This affects the predicted relic density of thermal WIMPs, which once were in chemical equilibrium with SM particles. We also use these results to compute the thermally averaged annihilation cross section of WIMP that reproduces the correct CDM relic density, for a large range of WIMP masses [37].

Chapter 3 is about the production of DM in an early matter dominated epoch assuming the presence of a heavy long lived (modulus) field. This heavy long–lived particle decays to radiation and DM. In addition to DM annihilation into, and thermal DM production from, radiation, we include direct DM production from the decay of the long–lived particle. In contrast to earlier treatments, the temperature dependence of the number of DoF in the SM plasma is treated carefully. Besides the well–known cases of thermal hot and cold DM, additional regions of parameter space with the approximately correct DM relic density appear. In some of these regions the temperature dependence of DoF can change the final DM density by several hundred percent. Furthermore, we analyze the effect of allowing vanishing and nonvanishing initial abundances for radiation and DM. We find an upper bound on the mass of the long–lived particle (modulus) if the DM annihilation cross section is below that corresponding to the thermal WIMP DM in standard cosmology [38].

In Chapter 4 we discuss the production of neutralino dark matter in scenarios with low reheating temperatures, are introduced in Chapter 3. In such scenarios, various production mechanisms beyond the thermally produced WIMPs can happen. This causes different regions of parameter space of neutralinos,

as the most popular supersymmetric (SUSY) DM, gain the required relic abundance. These regions with over and under production in thermal scenario which now have obtained the correct relic density can still respect the constraints from direct, indirect and collider searches. However, their production mechanism is determined by the type of neutralino. Relaxing the condition on the thermal production of neutralino shows that low scale SUSY is a phenomenologically viable candidate to explain DM and BSM physics. The bino–like neutralino DM which is over produced in the thermal scenario and is less constrained by current experiments can gain the correct relic density in the non–thermal scenario. Also, in case of a successful detection of a neutralino DM in experiments we can gain information about its production in the early universe with a low reheating scenario and estimate the reheating temperature of the modulus field and its corresponding mass [39].

Finally, the last Chapter is devoted to the conclusion of this thesis (Chapter 5).

1.3 List of Publications

This thesis is based on the following papers which are published or in the process of publishing in the journals:

- "The Effects of QCD Equation of State on the Relic Density of WIMP Dark Matter," M. Drees, F. Hajkarim and E. R. Schmitz, JCAP **1506**, no. 06, 025 (2015) [arXiv:1503.03513 [hep-ph]] [37].
- "Dark Matter Production in an Early Matter Dominated Era," M. Drees and F. Hajkarim, JCAP **1802**, no. 02, 057 (2018) [arXiv:1711.05007 [hep-ph]] [38].
- "Neutralino Dark Matter in Low Reheating Scenarios," M. Drees and F. Hajkarim, [arXiv:180X.XXXXX [hep-ph]] [39].

CHAPTER 2

Precise Calculation of Degrees of Freedom in the Thermal Bath of the Early Universe

2.1 Introduction

Einstein's theory of general relativity and its newtonian limit have been successful in explaining the gravitational force at the scale of solar system. However, to illustrate gravity in astronomical and cosmological scales it is required to consider that most of the matter in our Universe consists of invisible and some neutral matter, called the dark matter (DM). DM encompasses $\sim 85\%$ of all matter [6, 40, 41]. There are different possible candidates for DM [42]. Among which weakly interacting massive particles (WIMPs) have been the most favorable one. One of the reasons for the popularity of WIMPs is that in the hot plasma of the early universe they could had been in full chemical equilibrium with the standard model (SM) particles. This could had happened after the last period of entropy production, when the maximum temperature of the universe reaches more than about 5% of the WIMP mass. Then in a given cosmological model, independent of initial conditions, the relic abundance of WIMPs can be calculated by using only particle physics quantities i.e. masses, couplings and cross sections. The thermodynamic equation is widely used for this purpose is called Boltzmann equation [7]. Using this equation to compute the final relic density of WIMPs and compare with its observational value gives the approximate weak scale interaction for WIMP [43–47]. This shows a possibly deep connection between DM paradigm and beyond the standard model (BSM) theories like supersymmetry (SUSY) [48–52]. Moreover, it opens the experimental ways in which WIMPs can be investigated.

Experimental searches for WIMPs have not gained a confirmed signal yet. The WIMP candidates which satisfy the observational value for thermal relic abundance should also respect the constraints from direct [53–55] and indirect [19, 56–59] detection experiments. In direct searches, the nuclear recoil from the interaction of WIMP and detector nucleons can be measured. In indirect detection probes the interaction of WIMPs with the particles in astronomical objects or the annihilation of WIMPs to SM particles can be detected.

The metric of spacetime in the standard cosmology is the Friedmann–Robertson–Walker (FRW) metric [7]. The standard model of cosmology can explain the expansion of the Universe after inflationary period in the presence of radiation, (baryonic and dark) matter, cosmological constant. In such a scenario the comoving entropy density has remained constant since the WIMPs were fully in thermal equilibrium with the SM particles. DM yield (Y_χ) is the quantity that we are interested in. It depends on the ratio of the WIMP number density n_χ and the entropy density s. We need to know the precise temperature evolution of s to estimate the temperature dependence of n_χ. Additionally, we know that in FRW framework the

Hubble parameter H shows the expansion rate of the universe. It is proportional to the square root of the total energy density ρ of all matter content. To compute the precise value of Hubble rate we need $\rho(T)$ at temperature T. These issues were ignored in earlier studies [7, 48] assuming the relativistic limit for SM particles and neglecting the interaction in the thermal bath although it was a reliable approximation for almost all temperatures. Using this assumption is wrong for the temperatures close to QCD deconfinement transtion (~ 150 MeV). At that time, partons (quarks, gluons) starts to confine and form the hadrons (pions, kaons, ...). This causes a rapid reduction in the relativistic degrees of freedom corresponding to s and ρ. In recent studies [60, 61] it is also mentioned that for temperatures above the QCD transition the plasma has strongly interacting effects from quarks and gluons which should be considered in precise estimations.

This Chapter is based on our published paper titled "The effects of QCD equation of state on the relic density of WIMP dark matter" [37]. Some details not mentioned in the paper, are addressed here. In this Chapter we intend to precisely consider the effect of strong interactions on the radiation entropy and energy densities which depend on the temperature of SM particles in quark–gloun plasma. To that end, we use the recent calculations of lattice quantum chromodynamics (LQCD) studies [62] which is smoothly matched to the result of the hadron resonance gas (HRG) [63] model at the temperature $T = 100$ MeV. Our results represents the variation of WIMP relic density can reach more than 5% in comparison with earlier treatments [60, 61, 64] including the effects of QCD part of matter on the SM thermal plasma.

In order to find the required value of temperature dependent $\langle\sigma v\rangle$, the thermally averaged cross section of WIMPs multiplied by the relative velocity of annihilating DM particles, which satisfies the observed relic abundance, we use the effects of QCD mentioned in the previous paragraphs. There is an earlier calculation by Steigman et al. [65] which shows that the deviation in $\langle\sigma v\rangle$ for a corresponding WIMP mass up to ~ 1.5 from the "canonical" value of $3 \cdot 10^{-26}$ cm^{3}s^{-1}. Experiments have begun to probe this region of cross section. Current experiments like FermiLAT can observe nearby dwarf galaxies in the gamma ray region and probe the diffusion of gamma ray emission in the galaxy. They have constrained different sets of WIMP masses and final states of WIMP annihilation cross section to values lower than the canonical one [56–58].

In the rest of this Chapter (based on [37]) we review the calculations required to find the relic abundance of thermal WIMPs in Sec. 2.2. We briefly discuss the earlier treatments of $s(T)$ and $\rho(T)$ along with the details of our calculation for these quantities in Sec. 2.3. We show the values of $\langle\sigma v\rangle$ based on our result for energy and entropy densities in comparison with previous ones. The bounds from indirect detection of WIMP and cosmic microwave background (CMB) anisotropy is considered in Sec. 2.4. The last Section of this Chapter (Sec. 2.5) is devoted to a summary of our results.

2.2 Boltzmann Equation and the Relic Abundance

2.2.1 Basic Framework

We start our calculation of relic density for particle DM from Boltzmann equation which is widely studied in the literature [7]. If we consider DM to be a stable particle species χ, which annihilates to a pair of SM particles, then this equation shows the time evolution of number density of DM n_χ [7]

$$\frac{dn_\chi}{dt} + 3Hn_\chi = -\langle\sigma v\rangle\left(n_\chi^2 - n_{\chi,\mathrm{eq}}^2\right). \tag{2.1}$$

The cosmological time is denoted by t. The Hubble parameter is defined as

$$H = \frac{1}{a}\frac{da}{dt}\,, \tag{2.2}$$

where a is the time dependent scale factor in the FRW metric. The thermally averaged product of WIMP annihilation cross section and Möller[1] velocity is shown by $\langle\sigma v\rangle$. The number density of χ, at thermal equilibrium is $n_{\chi,\mathrm{eq}}$. Here the χ particles are assumed self–conjugate (Majorana) particles. If this assumption does not hold, which is the case for particles that are not self–conjugate, one should consider two sets of separate Boltzmann equations for particles and antiparticles. Assuming the radiation dominated era without any phase transitions in the FRW framework the total entropy of the universe is constant i.e.

$$S = s\,a^3 = const\,, \tag{2.3}$$

where s is the entropy density. It is convenient to define a new variable, independent of comoving volume i.e. a^3. It is called DM yield $Y_\chi \equiv n_\chi/s$. Using eq. (2.2) the term $3Hn_\chi$ on the left–hand side of the Boltzmann eq. (2.1) can be cancelled with the other term produced from changing the variable number density to DM yield.

The derivate in eq. (2.1) is with respect to time, however, the variables s and $n_{\chi,\mathrm{eq}}$ explicitly depend on temperature. So we define a new variable $x \equiv m/T$ which depends on temperature and it is in the direction of time. Then, the entropy density for relativistic particles can be written as

$$s(T) = \frac{2\pi^2}{45}h_{\mathrm{eff}}(T)T^3\,, \tag{2.4}$$

which comes from the Stephan–Boltzmann law. In the above formula, $h_{\mathrm{eff}}(T)$ is the effective number of relativistic degrees of freedom (DoF) that appears in the definition of s. For temperatures much higher than the mass of SM particles, $T \gg m_i$, the quantity $h_{\mathrm{eff}}(T)$ reduces to the sum of all DoF i.e. $h_{\mathrm{eff}}(T) \to \sum_i \mathbf{g}_i$, where $\mathbf{g}_i$'s is the number of internal DoF for each particle species i. For example, the contribution of a massless photon is $\mathbf{g}_\gamma = 2$. However, for a massless Dirac fermion like electron (considering both helicities at thermal equilibrium) we have $\mathbf{g}_e = 4 \cdot 7/8 = 3.5$. The DoF for all of the SM particles at very high temeratures are shown in Table (2.1). Using eqs. (2.3) and (2.4) we have

$$\frac{d}{dt}\left[h_{\mathrm{eff}}(T)T^3a^3\right] = 0\,, \tag{2.5}$$

then the evolution of temperature with respect to time can be deriven as

$$\frac{dT}{dt} = -\frac{TH}{1+\frac{1}{3}\frac{d\,\log h_{\mathrm{eff}}(T)}{d\,\log T}}\,. \tag{2.6}$$

Moreover, we require to know the dependence of Hubble parameter on temperature. Consequently, we use the following Friedmann equation

$$H^2 = \frac{8\pi G_N}{3}\rho_{tot}\,, G_N = \frac{1}{M_{Pl}^2}\,, \tag{2.7}$$

where ρ_{tot} is the total energy density of the universe, which at the time of radiation domination, is equal to the radiation energy density i.e. $\rho(T)$. Newton's gravitational constant and Planck mass are denoted by

[1] The Möller velocity represents the relative velocity between the annihilating WIMPs in the non–relativistic limit.

G_N and M_{Pl}, respectively. Then, the radiation energy density in the radiation dominated era where the universe behaves like a gas of particles can be obtained via

$$\rho(T) = \frac{\pi^2}{30} g_{\rm eff}(T) T^4 \,. \tag{2.8}$$

The effective number of relativistic DoF contributing to energy density is denoted by $g_{\rm eff}(T)$. At high temperatures where all particle masses can be ignored (for SM particles, higher than a few TeV) the DoF of entropy and energy densities become equal i.e. $g_{\rm eff}(T) = h_{\rm eff}(T)$. However, this is not true in general for lower temperatures, then they should be calculated separately.

By implementing eqs. (2.8), (2.7), and (2.6) in (2.1) we obtain

$$\frac{dY_\chi}{dx} = \lambda g_{\rm eff,*}^{1/2} \frac{1}{x^2} \left(Y_{\chi,\rm eq}^2 - Y_\chi^2 \right) , \tag{2.9}$$

where we have introduced

$$g_{\rm eff,*}^{1/2} = \frac{h_{\rm eff}}{g_{\rm eff}^{1/2}} \Big[1 + \frac{1}{3} \frac{d(\log h_{\rm eff})}{d(\log T)} \Big], \tag{2.10}$$

and

$$\lambda = \sqrt{\frac{\pi}{45 G_N}} m_\chi \langle \sigma v \rangle \,, \tag{2.11}$$

where m_χ is the WIMP mass. For a WIMP mass of 1 GeV and thermally averaged cross section of 10^{-26} $\rm cm^3 s^{-1}$ we have the numerical factor $\lambda \equiv 2.76 \times 10^9$. The DoF $g_{\rm eff}$ and $h_{\rm eff}$ defined by eqs. (2.8) and (2.4) appear in $g_{\rm eff,*}^{1/2}$ in eq. (2.10). Since both of these DoF exist in the definition of $g_{\rm eff,*}^{1/2}$ and also they appear in the scaled equilibrium yield density $Y_{\chi,\rm eq}$, we require the temperature evolution of both to determine the DM abundance. The decoupling of WIMPs occur when they are non–relativistic and then we have the following value for $Y_{\chi,\rm eq}$

$$Y_{\chi,\rm eq}(x) = \frac{n_{\chi,\rm eq}}{s} = \frac{45}{2\pi^4} \Big(\frac{\pi}{8} \Big)^{1/2} \frac{\mathbf{g}_\chi}{h_{\rm eff}} \, x^{3/2} \exp(-x), \tag{2.12}$$

where for a neutral Majorana fermion $\mathbf{g}_\chi = 2$. The dependence of $Y_{\chi,\rm eq}$ on $h_{\rm eff}$ is shown above.

2.2.2 Energy and Entropy Density Degrees of Freedom: $g_{\rm eff}(T)$ and $h_{\rm eff}(T)$

In the DM literature, most of the studies concentrate on the annihilation cross section of DM by introducing new terms in the Lagrangian or adding new symmetries, etc. Here, our focus is instead on the precise estimation of degrees of freedom during temperature evolution of the thermal bath of the early universe. These DoF as mentioned in the last section are denoted by $g_{\rm eff}(T)$ and $h_{\rm eff}(T)$. To achieve our purpose, we should first calculate the energy density $\rho(T)$ and the pressure $p(T)$ (it is also shown in eq. A.9). The entropy density will then be given by

$$s(T) = \frac{\rho(T) + p(T)}{T} \,. \tag{2.13}$$

We can find the contribution of a particle species i to energy density and pressure by knowing its distribution function $f_i(\vec{k}, T)$ as follows

$$\rho_i(T) = \mathbf{g}_i / (2\pi)^3 \cdot \int d^3k E_i(\vec{k}) f_i(\vec{k}, T) \,, \tag{2.14}$$

$$p_i(T) = \mathbf{g}_i/(2\pi)^3 \cdot \int d^3k(\vec{k})^2 f_i(\vec{k}, T)/(3E_i(\vec{k}))\,. \tag{2.15}$$

The number of DoF for species i is denoted by $\mathbf{g}_i$ and the three momentum is shown by $\vec{k}$.

Particle	Mass	Relativistic Degrees of Freedom
γ	0	2
e	0.511 MeV	$4 \times \frac{7}{8}$
μ	105.658 MeV	$4 \times \frac{7}{8}$
τ	1776.86 ± 0.12 MeV	$4 \times \frac{7}{8}$
ν_e	< 2 eV	$2 \times \frac{7}{8}$
ν_μ	< 2 eV	$2 \times \frac{7}{8}$
ν_τ	< 2 eV	$2 \times \frac{7}{8}$
u	$2.2^{+0.6}_{-0.4}$ MeV	$12 \times \frac{7}{8}$
d	$4.7^{+0.5}_{-0.4}$ MeV	$12 \times \frac{7}{8}$
c	1.27 ± 0.03 GeV	$12 \times \frac{7}{8}$
s	96^{+8}_{-4} MeV	$12 \times \frac{7}{8}$
t	173.21 ± 0.51 GeV	$12 \times \frac{7}{8}$
b	$4.18^{+0.04}_{-0.03}$ GeV	$12 \times \frac{7}{8}$
g	0	16
h	125.09 ± 0.24 GeV	1
W^+	80.385 ± 0.015 GeV	3
W^-	80.385 ± 0.015 GeV	3
Z	91.187 ± 0.0021 GeV	3
	Sum of DoF	106.75

Table 2.1: Relativistic degrees of freedom [7] versus masses of SM particles are shown in the above table from the data of Particle Data Group [42].

For a free (non–interacting) particle with mass m_i, the distribution function is the Bose–Einstein or Fermi–Dirac distribution function. These functions depend on the ratio of the energy of that species $E_i = \sqrt{m_i^2 + \vec{k}^2}$ and the temperature T [7]. We introduce $y_i = E_i/m_i$ and $x_i = m_i/T$ which are dimensionless quantities to compute the following DoF for each species

$$g_i(T) = \frac{15\mathbf{g_i}}{\pi^4} x_i^4 \int_1^\infty \frac{y_i^2\sqrt{y_i^2-1}}{\exp(x_i y_i) \pm 1} dy_i\,; \tag{2.16}$$

$$h_i(T) = \frac{45\mathbf{g_i}}{4\pi^4} x_i^4 \int_1^\infty \frac{\sqrt{y_i^2-1}}{\exp(x_i y_i) \pm 1} \frac{4y_i^2-1}{3} dy_i\,. \tag{2.17}$$

The $+1$ and -1 in the denominators of the above integrals denote fermionic and bosonic contributions, respectively [7].

eqs. (2.16) and (2.17) are not good approximations if the thermodynamic system is strongly interacting like QCD. Before beginning our approach to compute these functions, we review other results briefly as used in DM packages for studying DM properties like `DarkSUSY` [66], `micrOMEGAs` [67] and `SuperIso` [68]

Describing the thermodynamics of the early universe around QCD transition requires careful investiga-

tion as had been mentioned in the early works on WIMP properties. Olive et al. in [69] approximated the interactions between partons and hadrons by simple non–relativistic potentials. However, in ref. [70] free particles approximation is used. They described the transition temperature from the hadronic to the partonic phase by the temperature at which the two calculations give the same entropy density. As the number of hadrons increases with temperature a rapid rising appears in $h_{\rm eff}(T)$. We also use this "hadron resonance gas model" as it was done in all previous calculations at sufficiently low temperatures.

Assigning a simple definition to the transition temperature is problematic and leads to a discontinuity in $g_{\rm eff}(T)$ and $h_{\rm eff}(T)$ [70]. Using interpolating functions that smoothly treat the transition between the hadronic and partonic phases is a possible solution which is done in [71]. Srednicki et al. [71] also guaranteed that these DoF functions along with their derivatives are smooth without considering dynamical effects in the thermal bath. Moreover, they assumed two different estimation for QCD transition temperature, 150 MeV and 400 MeV, to estimate the uncertainty in their calculations. In ref. [64] the same functions are used which assume a transition temperature of 150 MeV. The computer packages mentioned in previous paragraphs use their data by default.

The results of lattice QCD calculations were first included in the calculation of DoF by Hindmarsh and Philipsen [60] when the effects of dynamical quarks were not comprised in the most precise lattice QCD calculations (Appendix A is about thermodynamic variables and their relation with lattice QCD studies). Some evidence has been found that the ratio of the true pressure to the corresponding value for free particles very slightly depends on the number of quark flavors [72]. Hence, Hindmarsh et al. [60] used the similar correction function to scale the contributions of all strongly interacting quarks and gluons. This was done by pure glue lattice calculations [72] and being matched to perturbative calculations [73] at $T = 1.2$ GeV.

The result of Laine and Schroeder [61] is rather similar. However, they have used two different sets of pure glue lattice QCD calculations [74–78]. In addition, they have done the matching to perturbative calculations at a very low temperature of 350 MeV. At the end, their result consists of the quark mass dependence up to next–to–leading order, $O(g_s^2)$, in the perturbative expansion. Particularly, they indicate that the contribution of charm quarks are not negligible at low temperatures around a few hundred MeV.

Here we illustrate our treatment for the calculation of DoF using lattice QCD results. We regard all SM particles without strong interactions at temperature much higher than the electron mass as free particles and therefore we use eqs. (2.16) and (2.17) for them. These particles consist of the leptons, the electroweak gauge bosons and the single physical Higgs boson of the SM. We emphasize that in the Standard Model for the physical Higgs mass, $m_H \simeq 125$ GeV, the electroweak symmetry breaking is not a phase transition. However, it is a smooth cross–over transition [79–81]. This causes the comoving entropy density to remain constant as we supposed in the derivation of eq. (2.9). Consequently, even at temperatures higher than the transition we assume free massive $W^{\pm}$ and Z bosons (with three DoF each, see Table. 2.1) and a single physical Higgs boson [2].

Our main focus in this Chapter is to include the effect of QCD interactions around the deconfinement transition. This is very important since at that temperature a large reduction in DoF happens. Free quarks and gluons confine to form hadrons. Based on lattice studies it is known that QCD transition is a smooth crossover with conserved entropy [82]. In ref. [62] QCD equation of state (EoS) derived by lattice methods for $N_f = 2 + 1$ active flavors is given which we use in our treatment. The range of temperatures which this EoS covers is between 100 and 400 MeV. This is consistent with another calculation of DoF by a different group [83]. Here we use the following parameterized formula for pressure provided by

[2] In a more precise calculation massless gauge bosons (with two DoF each) and a massive complex Higgs doublet (with four DoF) can be used. However, in such a case the relic density of WIMPs with masses above 2 TeV will only be affected. Also, the final relic density will change very little in these different approaches. So we neglect such effects in our setup.

[62] which includes the effects of u, d, s quarks and gluons in the mentioned range of temperature

$$\frac{p}{T^4} = \frac{1}{2}\left[1 + \tanh\left(c_t(\bar{t} - t_0)\right)\right] \cdot \frac{p_{\rm id} + a_n/\bar{t} + b_n/\bar{t}^2 + d_n/\bar{t}^4}{1 + a_d/\bar{t} + b_d/\bar{t}^2 + d_d/\bar{t}^4}\,, \tag{2.18}$$

where $\bar{t} = T/T_c$ and QCD transition temperature is denoted by $T_c = 154$ MeV. In the above formula, the ideal gas value of p/T^4 for gluons and three massless quarks is shown by $p_{\rm id} = 19\pi^2/36$. Table 2.2 shows the numerical parameters in eq. (2.18). Since the function $\tanh(z)$ becomes close to unity for large values of z, eq. (2.18) reaches the ideal gas limit as $T \gg T_c$, or $\bar{t} \gg 1$. Additionally, as it is demonstrated in [62] that at higher temeperatures eq. (2.18) is in agreement with the available perturbative calculations. Consequently, we use the parameterization of eq. (2.18) to represent the contribution of three light quarks, i.e. u, d, s, and gluons for temperatures higher than 100 MeV.

c_t	a_n	b_n	d_n	t_0	a_d	b_d	d_d
3.8706	-8.7704	3.9200	0.3419	0.9761	-1.2600	0.8425	-0.0475

Table 2.2: Parameters used in eq. (2.18) to describe the pressure of (2+1)–flavor QCD.

If we have the pressure p of a thermodynamic system, we can find the energy density ρ using the trace anomaly (Appendix A and eq. (A.9)), which is the relation between trace of the energy–momentum tensor and the pressure as the following equation shows [62]

$$\frac{I(T)}{T^4} = \frac{\rho - 3p}{T^4} = T\frac{d}{dT}\left(\frac{p}{T^4}\right). \tag{2.19}$$

We can compute the derivative of eq. (2.18) and then by using that we can get the trace anomaly $I(T)$. From the first equation in (2.19) and eq. (2.22) one can calculate the energy density $\rho(T)$. Then, the entropy density can be found from eq. (A.9).

From the result of [61] we know that the effect of charm quark is not negligible at temperatures near QCD transition T_c. We considered this effect in the evaluation of DoF functions $g_{\rm eff}$ and $h_{\rm eff}$ from the lattice QCD data of Table 6 of [84]. We take the physical ratio of charm and strange quark masses to be $m_c/m_s = 11.85$ which is based on [85]. The data for charm quark contribution to pressure is given by p_c/T^4. Then we use it to compute its contribution to ρ and s which are shown in eqs. (2.19) and (2.13). This set of data is valid for temperatures up to 1 GeV. For temperatures larger than that we use a fitting function like (2.18) with $p_{id} = 7\pi^2/60$ to match it with ideal gas results (2.16) and (2.17). The interpolating function is given by

$$\frac{p}{T^4} = \frac{1}{2}\left[1 + \tanh\left(c_t(\bar{t} - t_0)\right)\right] \cdot \frac{p_{\rm id} + a_n/\bar{t} + b_n/\bar{t}^2 + d_n/\bar{t}^{3.75}}{1 + a_d/\bar{t} + b_d/\bar{t}^2 + d_d/\bar{t}^{4.5}}\,, \tag{2.20}$$

where different values for coefficients are shown in Table 2.3. This function helps us to have both DoF ($g_{\rm eff}$ and $h_{\rm eff}$) and their derivatives behaving smoothly at all temperatures.

c_t	a_n	b_n	d_n
1.0	-7.98258×10^8	3.5261×10^{17}	-4.82168×10^{31}
t_0	a_d	b_d	d_d
-1.0	-7.08432×10^8	3.68056×10^{17}	2.32149×10^{38}

Table 2.3: Parameters found for eq. (2.20) to fit the result of [84] for the pressure of charm quark from lattice QCD calculation.

At high temperatures where the QCD interactions are small the contribution of bottom and top quarks to DoF is significant. As a consequence we assume them to be free quarks in our calculation using their on–shell masses provided by the Particle Data Group [42].

Hadron resonance gas model describes the thermodynamic behaviour of QCD at temperatures lower than T_c, where all hadrons and hadron resonances are assumed as non–interacting particles which contribute to the thermal bath. This model has been used in the early calculations [69, 70], as mentioned above. For temperatures between 100 MeV and T_c this model matches well to the parametrization of QCD equation of state in (2.18) as shown by the authors in ref. [62]. A paramaterized formula for trace anomaly in this model is computed in ref. [63]

$$\frac{I(T)}{T^4} = \frac{\rho - 3p}{T^4} = a_1 T + a_2 T^3 + a_3 T^4 + a_4 T^{10}\,, \tag{2.21}$$

where the parameters are shown in Table 2.4. The validity range of this equation is 70 MeV $\leq T \leq T_c$. It will be used to show the contribution of strongly interacting particles for temperatures below 100 MeV. Using cubic spline interpolation we smoothly match it to the QCD equation of state at $T > 100$ MeV. We ignore the effect of charm quark at this temperature since its contribution is negligible below the QCD transition [3].

a_1	a_3	a_4	a_{10}
4.654 GeV^{-1}	-879 GeV^{-3}	8081 GeV^{-4}	-7039000 GeV^{-10}

Table 2.4: Parameters used in eq. (2.21) to describe the trace anomaly of hadron resonance gas model.

We integrate the two sides of eq. (2.19) to find the following relation for pressure

$$\frac{p(T)}{T^4} = \frac{p_0}{T_0^4} + \int_{T_0}^{T} dT' \frac{I(T')}{T'^5}\,, \tag{2.22}$$

where $p(T_0)/T_0^4 = 0.1661$ at $T_0 = 70$ MeV is taken from the result of [63]. We can solve the integral in eq. (2.22) analytically from $I(T)$ as given by eq. (2.21). Then we have a parameterzied formula for pressure from which the energy and entropy density can be calculated by using eqs. (2.19) and (2.13).

We intend to include the effect of neutrino decoupling at temperatures below 1 MeV. When the temperatures of the universe is around several MeV, the decoupling begins. At this point the Hubble parameter becomes larger than the rate of interactions changing the ν_μ and ν_τ number densities. However,

[3] We should mention that the contribution of hadrons to $g_{\rm eff}$ and $h_{\rm eff}$ is exponentially small at $T \ll m_\pi = 140$ MeV. Then eq. (2.21) is not very precise at very low temperatures. However, it is not important for our goal. Since for $T \ll 100$ MeV the effect of hadrons is very small, it is not required to be treated very carefully.

at first the expansion of the universe affects the photons and neutrinos in the same way even after neutrino decoupling, i.e. the photon and neutrino temperatures remain the same. This changes only once e^+e^- pairs begin to annihilate, at $T \simeq m_e$. Since neutrinos are already (almost) decoupled by this time, the entropy that was stored in electrons and positrons gets transferred (almost) entirely to photons, not to neutrinos. In the limit where neutrino decoupling was complete when electron decoupling began, this argument shows that for $T \ll m_e$ the ratio of relic photon and neutrino temperatures is $T_\gamma/T_\nu = (11/4)^{1/3}$. Actually (electron) neutrinos were not completely decoupled at $T \sim m_e$, when e^+ and e^- start to annihilate. Therefore, some energy and entropy from e^+e^- annihilation goes to the neutrinos. This effect can be described by writing

$$h = 2\left[1 + \frac{7}{8} N_{\rm eff}\left(\frac{4}{11}\right)\right], \tag{2.23}$$

$$g = 2\left[1 + \frac{7}{8} N_{\rm eff}\left(\frac{4}{11}\right)^{4/3}\right], \tag{2.24}$$

where the number effective neutrinos in the SM is $N_{\rm eff} \simeq 3.046$ [86] [4]. We should note that in the above equations the effect of photons with $\mathbf{g}_\gamma = 2$ is considered. eqs. (2.23) and (2.24) are applicable for $T \ll m_e$, in practice for $T \leq 50$ keV. As mentioned above, for $T > 1$ MeV we have $T_\nu = T_\gamma$. For 50 keV $< T <$ 1 MeV we use numerical results from Fig. 1 of [87] to determine the evolution of T_ν with respect to T_γ. This can then be plugged into eqs. (2.23) and (2.24) instead of $T_\nu/T_\gamma = (4/11)^{1/3}$ to compute the photon and neutrino contribution to $g_{\rm eff}(T)$ and $h_{\rm eff}(T)$. Note that the temperature T is defined to be that of the photons, $T = T_\gamma$.

2.3 Results and Comparison with Previous Studies

Here we present our numerical results for DoF and its consequence on WIMP DM production. Figures 2.1 and 2.2 show the functions $h_{\rm eff}(T)$ (entropy density DoF) , $g_{\rm eff}(T)$ (energy density DoF), and $g^{1/2}_{\rm eff,*}(T)$ (shows the thermodynamic effects in Boltzmann equation (2.9)) we defined in eqs. (2.4), (2.8), and (2.10). Our results are shown by black solid curves, while other results from refs. [64], [60], and [61] are drawn by green dashed, red dot–dashed, and blue dotted curves, respectively [5].

We regard the effect of e^+e^- decoupling on the neutrino background by $N_{\rm eff} \simeq 3.046$ in eq. (2.23). As a result, we find $h\left(T_{\gamma,0}\right) = 3.9387$ in our calculation where the present photon temperature is $T_{\gamma,0} = 2.7255 \pm 0.0006$ K [42]. Hence, the value we obtained for $h_{\rm eff}$ is slightly higher than $h\left(T_{\gamma,0}\right) = 3.9138$ in ref. [60] and $h\left(T_{\gamma,0}\right) = 3.9139$ in ref. [66]. We should mention that the final relic density $\Omega_\chi h^2$ is proportional to $h(T_{\gamma,0})T^3_{\gamma,0}$ for a given value of $Y_\chi(T_{\gamma,0})$, as eq. (2.25) shows.

[4] Since the distribution of neutrinos is non–thermal after electron decoupling, any temperature can not be assigned to them, though the behavior of the functions $g_{\rm eff}$ and $h_{\rm eff}$ at $T \ll m_e$ is delineated by eqs. (2.23) and (2.24) precisely. Most of energy that goes to neutrinos from e^+e^- annihilation goes to the ones with $E \simeq m_e$. Their annihilation also distorts the thermal spectrum of individual neutrinos.

[5] To extract the data from diagrams of [61], which did not exist in `micrOMEGAs`, and also [65] we used `Inkscape` and `WebPlotDigitizer` (a web based program).

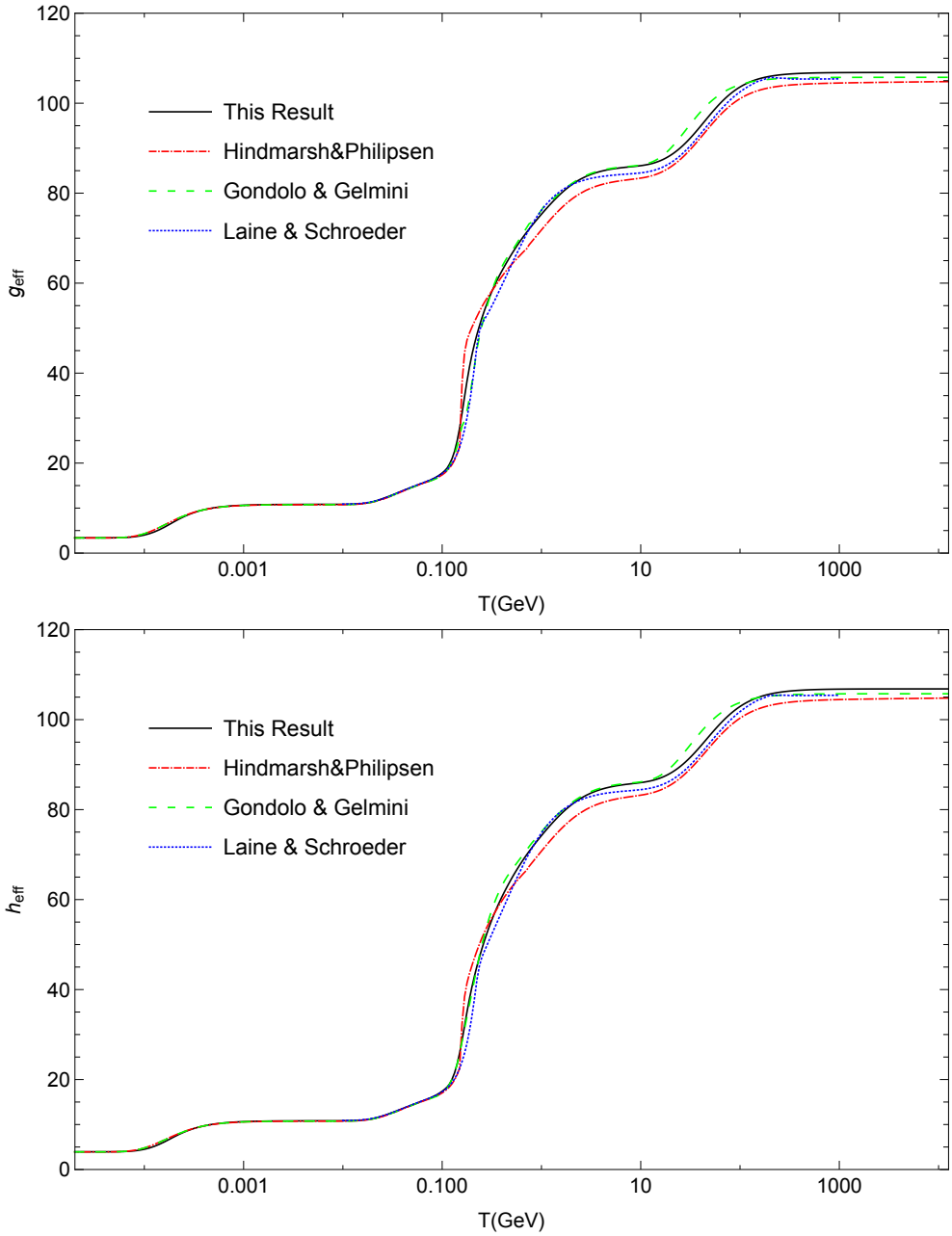

Figure 2.1: Energy density DoF $g_{\rm eff}(T)$ (up) and entropy density DoF $h_{\rm eff}(T)$ (bottom) defined in eqs. (2.8) and (2.4). The black solid line represents our result based on lattice calculations with $N_f = 2 + 1$ dynamical quark flavors [62] plus the result for charm quark effects on the equation of state [84]. The green dashed curve is the calculation by Gondolo and Gelmini [64], based on results from ref. [71]. The results of refs. [60] and [61] which are based on pure glue lattice QCD calculations are shown by red dot–dashed and blue dotted curves, respectively.

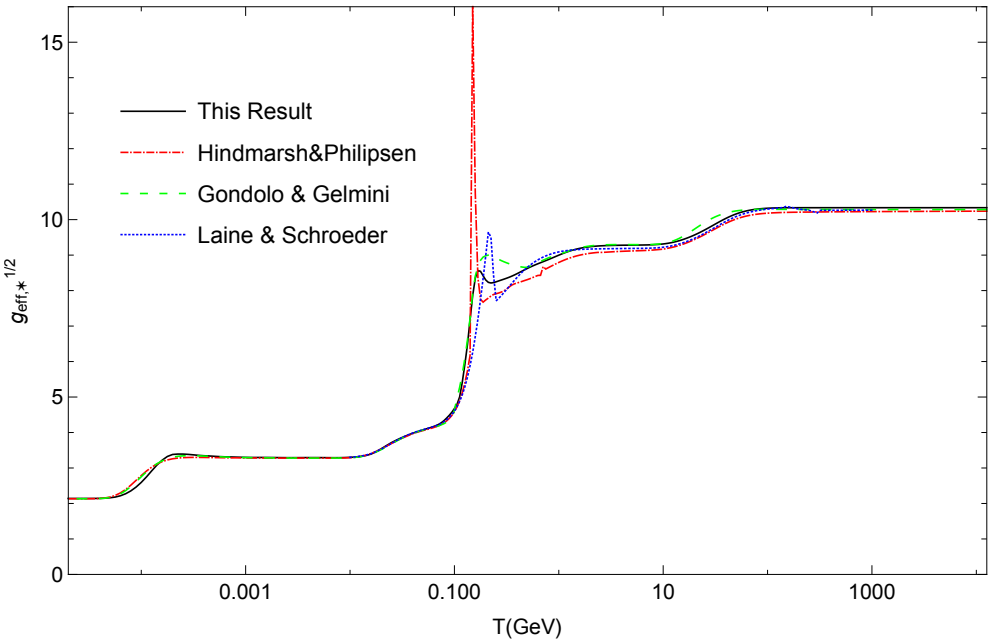

Figure 2.2: The function $g_{\rm eff,*}^{1/2}(T)$ defined in eqs. (2.4) and (2.10). The original calculation by Gondolo and Gelmini [64], based on results from ref. [71], are shown by the green dashed curves. The red dot–dashed and blue dotted curves show results from refs. [60] and [61], which are based on pure glue lattice QCD calculations. The black solid curves depict our results, which are based on lattice calculations with $N_f = 2 + 1$ dynamical quark flavors.

As we described in the previous section, both deconfinement of partons and the restoration of the electroweak gauge symmetry in the SM are smooth cross–over transitions. As a consequence, the DoF functions $g_{\rm eff}(T)$ and $h_{\rm eff}(T)$ are smooth at every temperature. This could not happen if we had real phase transitions for QCD and electroweak sectors. The smoothness of these functions are ensured by cubic spline interpolation between two relevant regions.

Obviously, there are several differences between our calculation and the three others. These differences are crucial mostly around the deconfinement transition. Furthermore, they appear in the diagram of $g_{\rm eff,*}^{1/2}$, largely due to the derivative of $h_{\rm eff}$ in eq. (2.10), which makes the discrepancies between various treatments more noticeable. In Fig. 2.2 we can see the calculation of [71] used in [64]. It overestimates $g_{\rm eff,*}^{1/2}$ for temperatures around $T \simeq 0.1$ GeV, in comparison to all other calculations using lattice QCD equation of state. A discontinuity at $T = T_c$ appears in the data of ref. [60] which causes a divergence in the derivative. This is visible as an infinite spike in $g_{\rm eff,*}^{1/2}$. We took the numerical results of [60] for $h_{\rm eff}$ and $g_{\rm eff}$ from `micrOMEGAs` [67] package. This discontinuity and its consequent spike is smoothed out there in the thermal relic density calculation. We can still see this noted spike of $g_{\rm eff,*}^{1/2}$ in the Fig. 2.2. Ref. [60] predicts a smaller value of $g_{\rm eff,*}^{1/2}$ in the range of temperature around QCD transition than we do, except for the mentioned spike. Eventually as it is shown by blue dotted line in Fig. 2.5 the result of ref. [61] for $g_{\rm eff,*}^{1/2}$ is the closest one to ours, apart from the oscillatory shape visible just above the QCD transition temperature.

To understand how the changes in $h_{\rm eff}$ and $g_{\rm eff,*}^{1/2}$ affect the WIMP relic density, we must numerically solve the Boltzmann equation (2.9). When we numerically calculate this equation the final result is independent of the input value of yield $Y_\chi(x_i)$ for $x_i \lesssim 10$, where the initial value of x is denoted by x_i.

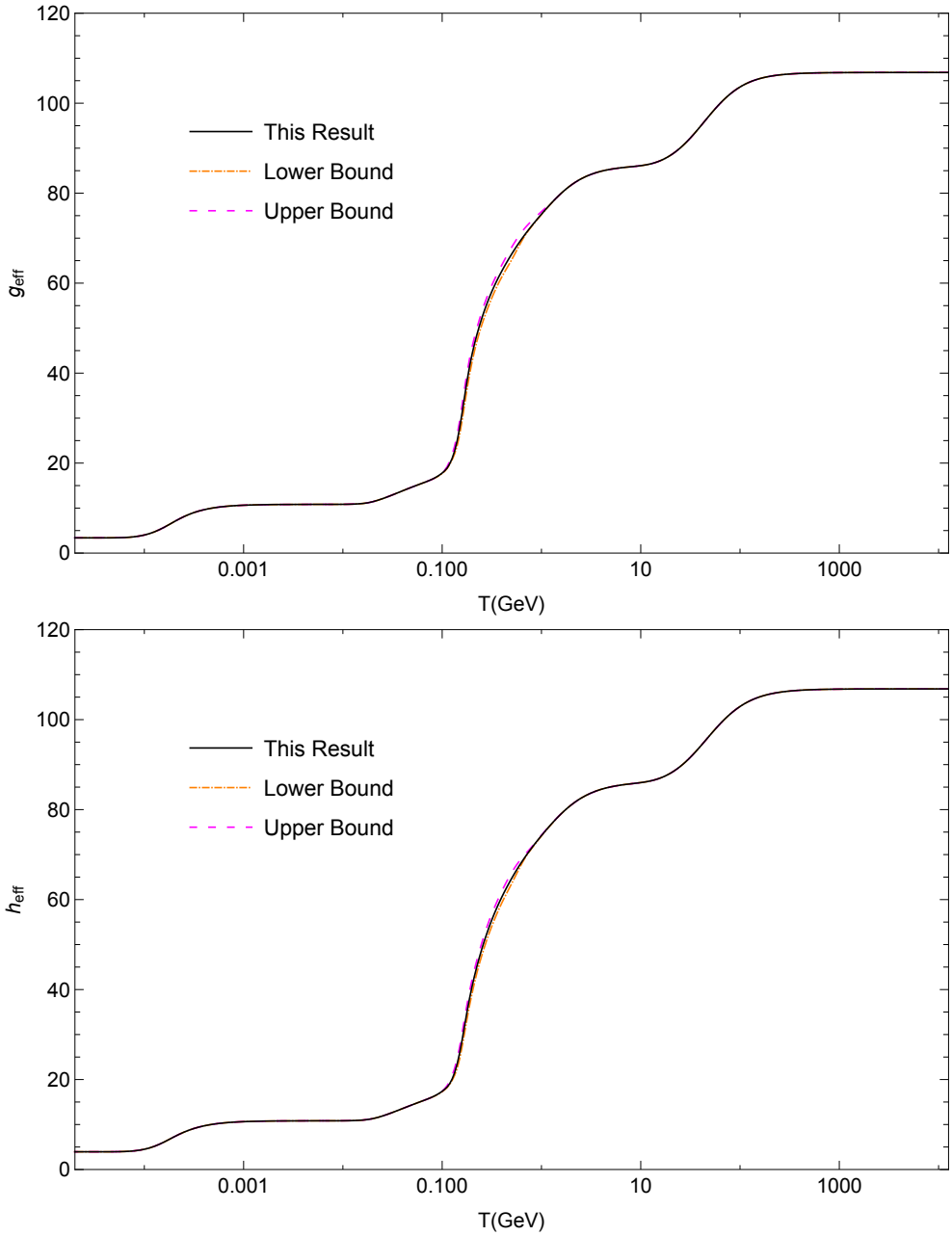

Figure 2.3: Energy density DoF $g_{\rm eff}(T)$ (up) and entropy density DoF $h_{\rm eff}(T)$ (bottom) defined in eqs. (2.8) and (2.4). The black solid line represents our result based on lattice calculations with $N_f = 2 + 1$ dynamical quark flavors [62] plus the result for charm quark effects on the equation of state [84]. The two different estimations of DoF based on upper (dashed magenta) and lower (orange dotted dashed line) bounds on lattice QCD studies are also shown.

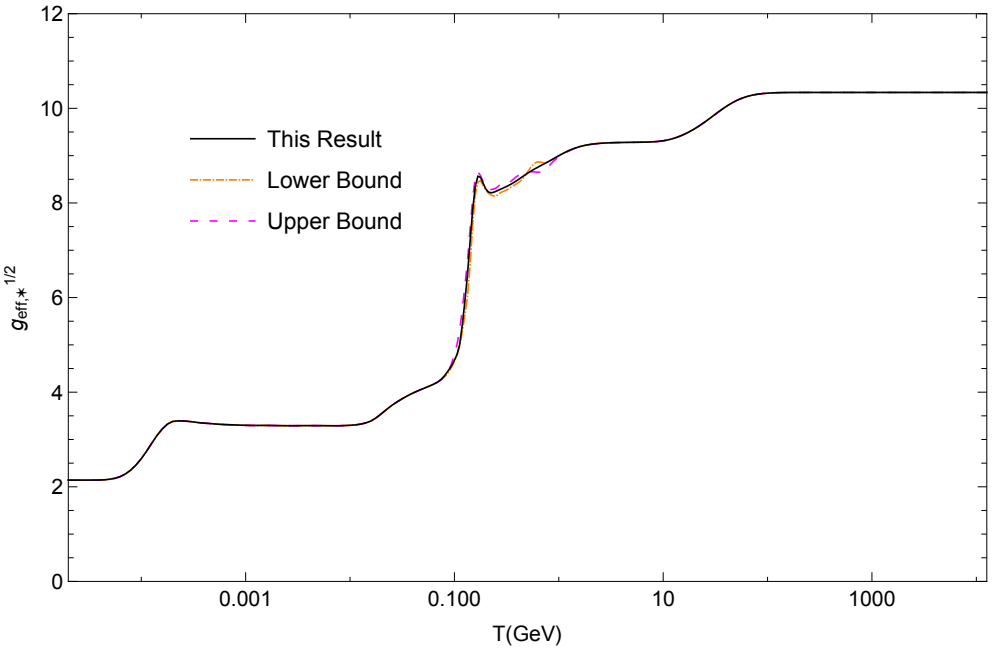

Figure 2.4: The function $g_{\rm eff,*}^{1/2}(T)$ defined in eqs. (2.10). The black solid curve depict our results, which are based on lattice calculations with $N_f = 2 + 1$ dynamical quark flavors. This plot also depicts the two different estimations of $g_{\rm eff,*}^{1/2}(T)$ based on upper (magenta dashed line) and lower (orange dotted dashed line) bounds on lattice QCD studies of [62] and [84].

We compute the numerical value of $Y_\chi(x)$ up to $x = 1000$, at which the final yield Y_χ is going to be approximately constant.

$$\Omega_\chi h^2 = \frac{\rho_\chi}{\rho_{crit}} h^2 = \frac{m_\chi Y_{\chi,0} s_0}{3H_0^2/8\pi G_N} \left(\frac{H_0}{100 \text{ km s}^{-1} \text{ Mpc}^{-1}} \right)^2 . \tag{2.25}$$

Here, the present yield, denoted by lower index 0, is assumed to be equal to yield at $x = 1000$ i.e. $Y_{\chi,0} = Y_\chi(x = 1000)$. Also, the entropy of photons in the present time is experimentally obtained as $s_0 = 2891.2 \text{ cm}^{-3}$ [42]. Moreover, we should emphasize that H_0 on the right–hand side of eq. (2.25) cancels so the relic density is usually evaluated as $\Omega_\chi h^2$. Finally, what we numerically calculate is $\Omega_\chi h^2 = 2.7889 \cdot 10^8 Y_{\chi,0} m_\chi/(1 \text{ GeV})$.

The effect of our precise treatment for DoF of SM $h_{\rm eff}$, $g_{\rm eff}$, and $g_{\rm eff,*}^{1/2}$ on the relic density is illustrated in Fig. 2.5. The results for a temperature independent thermally averaged cross section is shown in the upper frame, whereas, the result for $\langle \sigma v \rangle \propto 1/x$ which is temperature and also velocity dependent is displayed in the lower frame. These two approaches show $\langle \sigma v \rangle$ away from the poles (where the WIMPs can annihilate into any particle ψ with $m_\psi \simeq 2m_\chi$) and thresholds (at which the WIMPs are much heavier than all final–state particles from annihilation) at small velocity, when the initial states are pure S–wave and pure P–wave, respectively. The examples for P–wave annihilation cross section are the annihilation of a pair of Majorana WIMPs into light SM fermions or two complex scalars via $s-$channel exchange of a gauge boson. As we expect for freeze–out temperatures around the QCD transition which corresponds to WIMP masses of a few GeV, we see the largest discrepancies between our result and previous studies. These differences are up to 9% for the pure S–wave cross section, and up to 12% for the pure P–wave one.

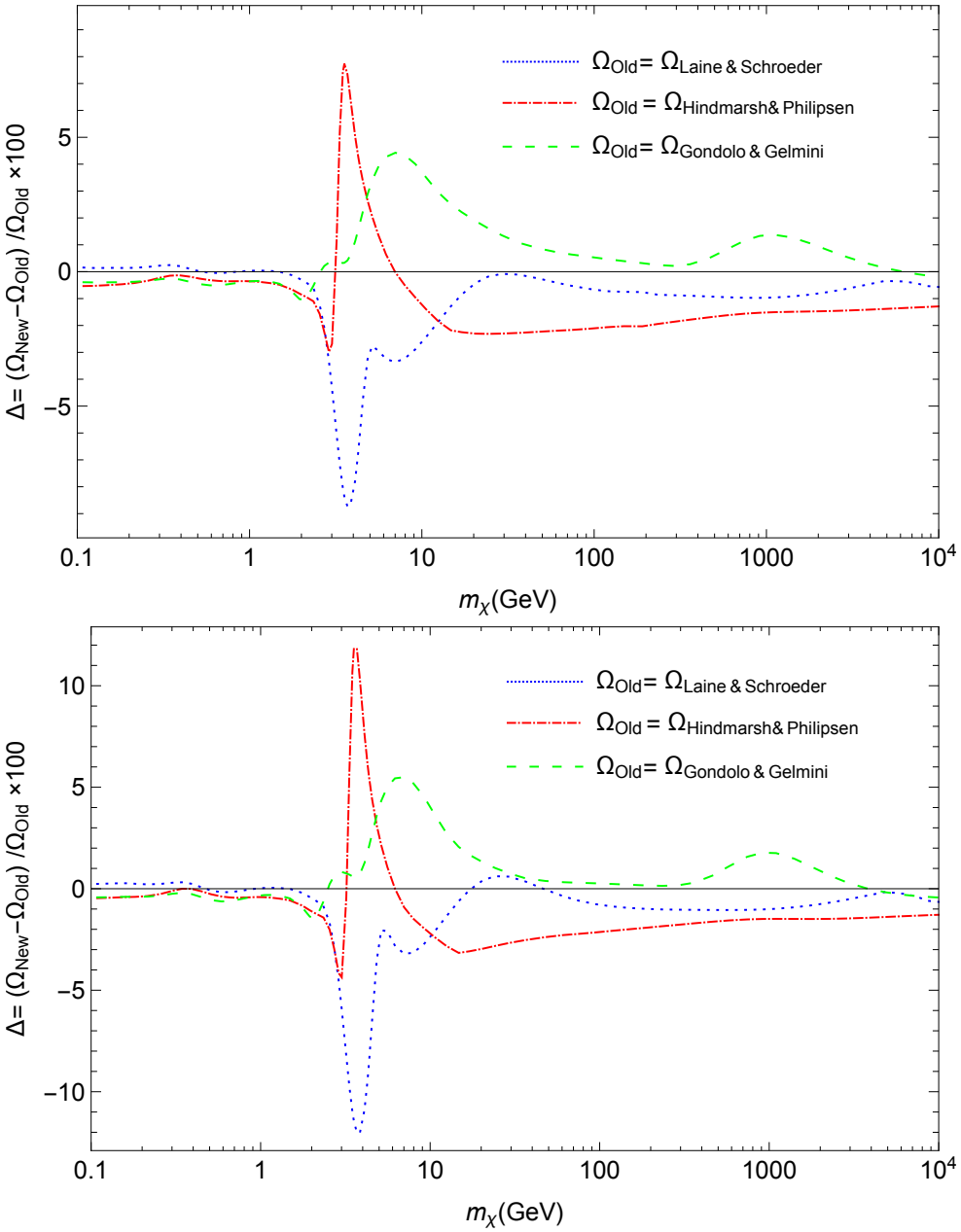

Figure 2.5: The relative difference between the predicted relic density of a Majorana WIMP between our calculation and a calculation using the same older results for the functions $h_{\rm eff}$, $g_{\rm eff}$, and $g_{\rm eff,*}^{1/2}$ shown in Figs. 2.1 and 2.2, as functions of the WIMP mass. The upper frame is for a constant $\langle\sigma v\rangle$, chosen such that our prediction for $\Omega_\chi h^2 = 0.1193$, while the lower frame is for a pure $P-$wave annihilation, with $\langle\sigma v\rangle = 1.2 \cdot 10^{-24}\ {\rm cm}^3{\rm s}^{-1} \cdot T/m_\chi$. These results are almost independent of the numerical size of the annihilation cross section.

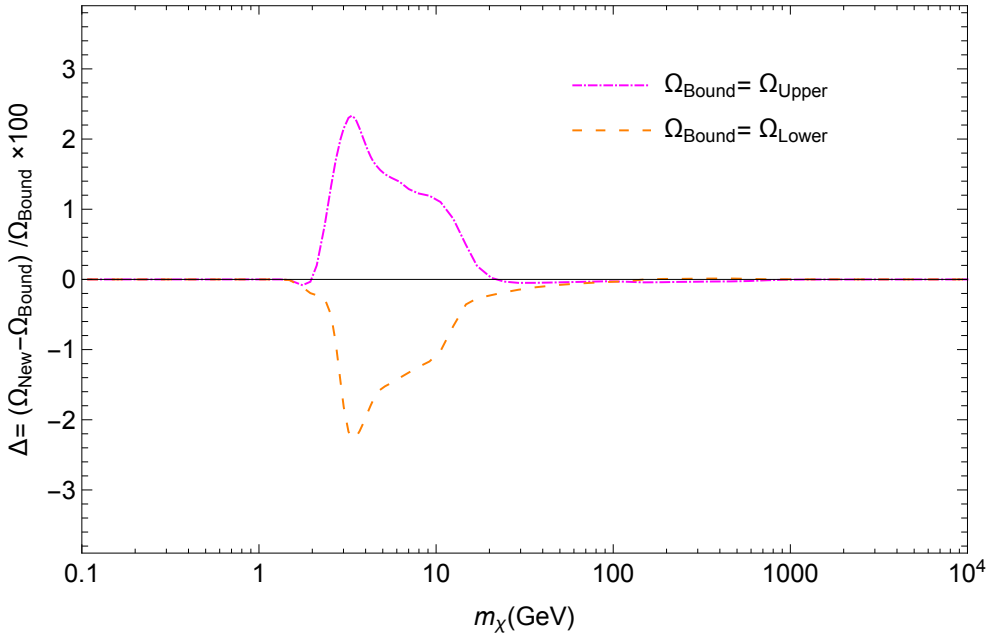

Figure 2.6: This plot shows the relative difference between the predicted relic density for two different estimations of DoF based on upper (magenta dashed line) and lower (orange dotted dashed line) bounds on lattice QCD studies [62] and [84]. The data for upper and lower bounds of $h_{\rm eff}$, $g_{\rm eff}$, and $g_{\rm eff,*}^{1/2}$ are shown in Figs. 2.3 and 2.4. In this frame the constant $\langle\sigma v\rangle$ is chosen such that it satisfies the prediction for $\Omega_\chi h^2 = 0.1193$ as shown in Fig. 2.7.

Here, we use the approximate analytical solution of Boltzmann eq. (2.9) based on freeze–out approximation which roughly shows the moment that the annihilation rate of WIMP became equal to Hubble rate ($n_{\chi,\rm eq}\langle\sigma v\rangle = H$). This is computed in ref. [7] as follows

$$Y_{\chi,0} \propto \frac{x_{\rm FO}}{g_{\rm eff,*}^{1/2}(T_{\rm FO})\langle\sigma v\rangle(T_{\rm FO})}\,, \quad x_{\rm FO} \propto \log\left(m_\chi g_{\rm eff,*}^{1/2}(T_{\rm FO})\langle\sigma v\rangle(T_{\rm FO})/h_{\rm eff}(T_{\rm FO})\right)\,, \tag{2.26}$$

where for the relevant range of masses and cross sections for WIMPs the value that approximately quantifies the freeze–out is $x_{\rm FO} \sim 20$. The above equation shows that $g_{\rm eff,*}^{1/2}$ influences the final relic much more than $h_{\rm eff}$, since the latter one only appears logarithmically in $x_{\rm FO}$. In eq. 2.26, the DoF are assumed to be roughly constant around the freeze–out temperature of WIMP $T_{\rm FO} = m_\chi/x_{\rm FO}$. However, wherever this functions change drastically, it is not satisfactory to follow this approximation anymore. This is the case around QCD transition temperature as Fig. 2.2 shows. Though, this is not important at higher temperatures, since the yield Y_χ does not depend on $g_{\rm eff,*}^{1/2}$. As the temperature of the universe decreases below the decoupling temperature $T_{\rm FO}$, the right hand side of Boltzmann equation (2.9) is suppressed by a factor $1/x^2$. In case the cross section is P–wave with $\langle\sigma v\rangle \propto 1/x$ the suppression is stronger when $T_{\rm FO} < T$. Consequently, whenever the derivative of $h_{\rm eff}$ sharply changes, so also $g_{\rm eff,*}^{1/2}$ does, leading to a variation in the final relic density larger for the P–wave case than the S–wave case.

We previously pointed out that the result of ref. [64] overestimates $g_{\rm eff,*}^{1/2}$ for temperatures above the QCD transition T_c. Eq. (2.26) shows that this causes a smaller predicted relic density, as Fig. 2.5 confirms it. The effect of overestimation in the value of $g_{\rm eff,*}^{1/2}$ extends over a large range of temperatures and thus is up to around 5% near the peak of the dashed green line shown in Fig. 2.5. There is another peak much lower than the first one near $m_\chi = 1$ TeV which could probably be thanks to lack of knowledge of the top

quark mass at the time when ref. [64] was written.

The spike in $g_{\rm eff,*}^{1/2}$ predicted by the `micrOMEGAs` treatment of the results of ref. [60] gives prominent spikes in the ratios shown in Fig. 2.5. These spikes are numerical artefacts that result from the smoothing procedure used in `micrOMEGAs`. As argued in ref. [60], a true δ function spike in $g_{\rm eff,*}^{1/2}$ should not affect the numerical solution of the Boltzmann equation, which necessarily entails some discretization. The probability that the program then has to evaluate the right–hand side of the Boltzmann equation at the precise value of x where the δ function diverges is zero. We nevertheless show results including this spike since it results from the "standard treatment" encoded in `micrOMEGAs`. Outside the mass range affected by this spike, the results of ref. [60] predict a slightly too large relic density, consistent with our observation that it predicts smaller values of $g_{\rm eff,*}^{1/2}$ and $h_{\rm eff}$ than our treatment does. Note that for fixed $g_{\rm eff,*}^{1/2}$, reducing $h_{\rm eff}$ will (slightly) increase $x_{\rm FO}$, leading to an increase of the predicted relic density. A decrease of $h_{\rm eff}$ therefore goes into the same direction as a decrease of $g_{\rm eff,*}^{1/2}$. However, the fact that the relative difference between our calculation and the prediction based on ref. [60] is almost the same in both frames of Fig. 2.5 at large WIMP masses shows that the main effect still comes from the change of $g_{\rm eff,*}^{1/2}$.

As seen in Fig. 2.2 the prediction of $g_{\rm eff,*}^{1/2}$ from ref. [61] is below ours except for a small range of temperature around the QCD transition. Therefore, based on eq. 2.5 the predicted relic density from the treatment of ref. [61] for pure S–wave cross section lies above our result for WIMP masses heavier than 2 GeV. As we noted, this also occurs for pure P–Wave annihilation in a smaller range of temperatures. This is the reason why in the lower frame of Fig. 2.5 the blue curve for masses around 25 GeV goes slightly above 1%. We should also note that except for the range of masses between 2 and 20 GeV the prediction for relic density based on our set of DoF is in agreement with the one from ref. [61] to better than 1%. For the mentioned range of mass the difference in the relic density reaches 9 (12)% for pure $S-$ ($P-$)wave cross section.

Note that the energy and entropy densities from lattice QCD calculation that we included in our work based on the Table 1 of [62], have large uncertainties which are around 14% at $T = 130$ MeV to about 3% at $T = 400$ MeV. This roughly leads to an uncertainty in the relic density up to 2.5% for 2 GeV $\leq m_\chi \leq 20$ GeV as shown in Fig. 2.6. Eventually, we should mention that neglecting the effect of charm quark from lattice studies, and assuming it as a free particle increases the relic density up to 2.2% for dark matter masses around 30 GeV.

As Fig. 2.5 shows, the final results are roughly independent of the WIMP annihilation cross section, as long as the calculated relic abundance is approximately correct, even though, as in the lower panel of figure is shown, they are sensitive to the dependency of $\langle\sigma v\rangle$ on temperature in P–wave case. Thermodynamic effects affect the relic density through $g_{\rm eff,*}^{1/2}(x_{\rm FO})$, and $x_{\rm FO}$ only logarithmically depends on the WIMP annihilation cross section.

Using the observational value of DM abundance in standard ΛCDM cosmology $\Omega_\chi h^2 = 0.1193\pm0.0014$ [5]; we can precisely determine the value of the annihilation cross section of WIMP, that does depend on the functions $h_{\rm eff}(T \sim T_{\rm FO})$ and $g_{\rm eff}(T \sim T_{\rm FO})$ at $T_{\rm FO}$, and mostly on $g_{\rm eff,*}^{1/2}(T \sim T_{\rm FO})$ due to the appearance of derivative of DoF in it. To determine the free parameters of thermal WIMPs models we require to precisely compute this cross section. Besides, indirect detection experiments (see Appendix B) have started to measure the annihilation cross sections close to values of $\langle\sigma v\rangle$ which satisfy the observed relic density, if it does not depend on the temperature approximately (S–wave).

We display the required value of $\langle\sigma v\rangle$ for S–wave annihilation cross section of a Majorana fermion in Fig. 2.7. This result is obtained by using our interpolated calculation of $h_{\rm eff}$, $g_{\rm eff}$, and $g_{\rm eff,*}^{1/2}$. It is also an update on the result of ref. [65] which uses the DoF from the data of ref. [61] to obtain the DM relic $\Omega_\chi h^2 = 0.11$. In that figure the result of ref. [65] scaled by $0.11/0.1193$ is also shown, which is based on

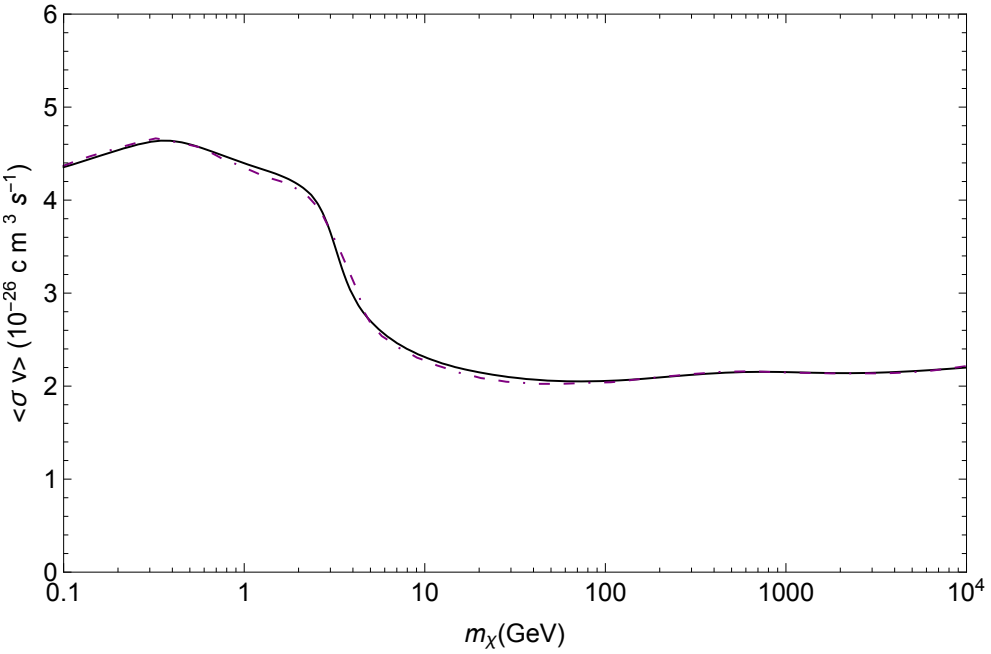

Figure 2.7: The value of $\langle\sigma v\rangle$, assumed to be completely independent of temperature, required to obtain a thermal relic density $\Omega_\chi h^2 = 0.1193$ within standard cosmology, as a function of WIMP mass (black solid line). Also, the result of ref. [65] scaled to $\Omega_\chi h^2 = 0.1193$ is shown (purple dash-dash-dotted line).

the different assumptions for DoF to compute $\Omega_\chi h^2$.

The "canonical" value of thermally averaged cross section of WIMP is known to be $3 \cdot 10^{-26}$ cm^{3}s^{-1}. However, we see that it is closer to $2 \cdot 10^{-26}$ cm^{3}s^{-1} for masses in the range 10 GeV $< m_\chi <$ 10 TeV, as shown by Fig. 2.5. The required cross section is approximately constant over this region of mass due to an "accidental" cancellation of two effects. We can understand this issue using the approximate solution of Boltzmann eq. 2.26. For larger DM masses $x_{\rm FO}$ increases, also $T_{\rm FO} = m_\chi / x_{\rm FO}$ gets bigger, since the dependence of $x_{\rm FO}$ on m_χ is only logarithmic. This increases $g^{1/2}_{\rm eff,*}(T_{\rm FO})$ which makes the relic density smaller as Fig. 2.2 shows. At high temperatures (roughly higher than 200 GeV) the function $g^{1/2}_{\rm eff,*}$ gains its asymptotic value of 106.75, which is independent of T. For WIMP masses larger 10 TeV, in order to cancel the growth of $x_{\rm FO}$, the required value of $\langle\sigma v\rangle$ should increase logarithmically with m_χ. However, WIMPs with such large masses are problematic, since from dimensional analysis and unitarity arguments [88] $\langle\sigma v\rangle \propto 1/m_\chi^2$, thus finding DM with mass larger than 10 TeV is very difficult.

Alternatively, for WIMP masses below 10 GeV, as $T_{\rm FO}$ decreases, $g^{1/2}_{\rm eff,*}(T_{\rm FO})$ reduces quickly, as shown in Fig. 2.2. This needs a rather rapid growth of $\langle\sigma v\rangle$, to a maximum value of around $4.5 \cdot 10^{-26}$ cm^{3}s^{-1}. The $g^{1/2}_{\rm eff,*}(T_{\rm FO})$ roughly becomes a constant again for masses below 0.35 GeV. This contains the contribution of electrons, positrons, neutrinos, and photons to the DoF so that we have $g^{1/2}_{\rm eff,*} \simeq 3.29$. When m_χ decreases, $x_{\rm FO}$ also keeps decreasing; then as WIMP mass for very light WIMPs reduces, $\langle\sigma v\rangle$ should become smaller to keep the relic density constant.

By rescaling the result of ref. [65] we obtain a slightly smaller value of $\langle\sigma v\rangle$ with respect to our calculation for most of the range of WIMP masses. This effect is consistent with the result of $g_{\rm eff}(T)$ and

$h_{\rm eff}(T)$ done in ref. [61] so that a larger relic density is produced than our treatment [6].

2.4 Experimental Constraints on $\langle\sigma v\rangle$

In the next to last section of this Chapter, we have compared our predicted result for $\langle\sigma v\rangle$ according to the observed relic density (shown in Fig. 2.7) against the constraints from indirect searches of WIMP (see Appendix B) and cosmic microwave background (CMB) studies. The decoupling of CMB happens at temperatures lower than WIMP decoupling (~ 0.3 eV rather than $\sim m_\chi/20$). Whereas, the average kinetic energy of WIMPs in galaxies is $\sim 10^{-6} m_\chi$, only when $\langle\sigma v\rangle$ is highly independent of the temperature this comparison is meaningful. In case of P–wave cross section for which $\langle\sigma v\rangle \propto T$ (also for even stronger $T-$dependence) the constraints on $\langle\sigma v\rangle$ from indirect WIMP searches and from the CMB are still some orders of magnitude above the observed value for the correct relic density.

Currently the strongest and most robust upper bounds on $\langle\sigma v\rangle$ from indirect WIMP searches come from searches for hard γ rays by the FermiLAT collaboration [19, 56–58]. Photons travel in straight lines through our galaxy, whereas charged particles get deflected by the galactic magnetic field. This not only introduces a sizable uncertainty, since our knowledge of this magnetic field is far from perfect, it also isotropizes the arrival directions of the charged annihilation products of WIMPs, making it impossible to focus on regions of space where the WIMP signal should be particularly strong. Another advantage of γ rays is that they are present in nearly all possible final states: hard photons can be emitted directly off final or intermediate state particles, can originate from the decay of neutral pions and other hadrons that result from the hadronization of $q\bar{q}$ final states or the decay of τ leptons, and can be produced from energetic electrons or positrons through "inverse Compton" upscattering of ambient photons.

We anticipate to observe the strongest WIMP signal from the center of the Milky Way galaxy, since it is the closest dense region to us where DM particles have high chance to meet each other. However, lots of backgrounds in this region in the form of point sources and also extended emission make the detection difficult. There are some claims about the evidence of an additional component in the GeV γ flux near the center of our galaxy which could be explained through the annihilation of WIMPs [89–92]. However, refs. [93–95] interpret this observation differently . Moreover, we should mention that there is not any published analysis of the data on the galactic center by the FermiLAT collaboration itself.

Hence, in this Chapter we focus on the observations of nearby dwarf galaxies by FermiLAT [19, 56–58]. The mass density of dwarf galaxies contrary to large galaxies like the Milky Way should be dominated by dark matter even in the central region, thus it gives a significantly better signal–to–background ratio for indirect searches of WIMPs. We illustrate our result based on the recent 6–year "Pass 8" analysis [19]. We should mention no signal from WIMP has been found yet.

We show the experimental results in Fig. 2.8. The strongest upper bound on $\langle\sigma v\rangle$ comes from predominant annihilation of WIMPs into $u\bar{u}$ final states while the bound for the $b\bar{b}$ final state is only a little weaker. The upper bound on the $\langle\sigma v\rangle$ is similar for WIMP masses lighter than 40 GeV if WIMPs annihilate to $\tau^+\tau^-$ final state; however, it is slightly weaker for heavier WIMPs. For larger DM masses the γ flux per WIMP annihilation is higher for hadronic final states because of higher multiplicity. But the photon multiplicity is independent of the WIMP mass for the $\tau^+\tau^-$ final state. The S–wave annihilation of WIMPs ($\langle\sigma v\rangle$ independent of T) into hadrons or τ leptons is excluded for masses in the range $m_\chi \leq 70$ to 100 GeV.

As already stated, the annihilation of WIMPs into e^+e^- results hard photons (through upscattering of ambient, e.g. visible sector particles, photons). This gives an upper bound on $\langle\sigma v\rangle$. However, this bound

[6] Since we required to read the data from ref. [65] and we used scaling based on $\Omega_\chi h^2 \propto 1/\langle\sigma v\rangle$, comparing the results in Fig. 2.7 is not as precise as Fig. 2.5.

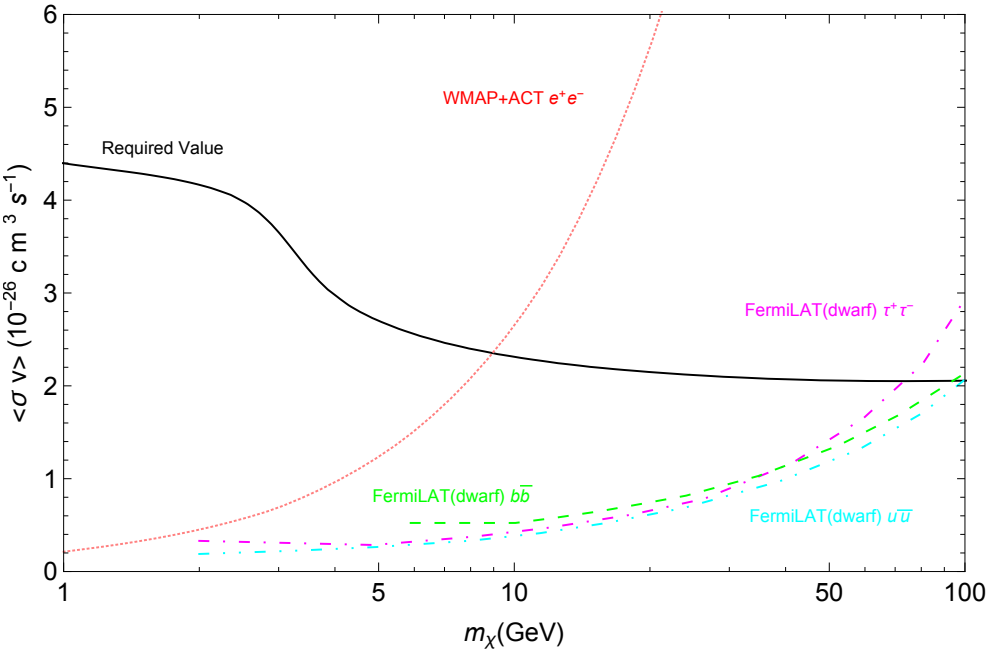

Figure 2.8: The result of Fig. 2.7 is compared with several observational upper bounds on $\langle\sigma v\rangle$, which is assumed to be independent of temperature. The cyan, green and magenta curves follow from the FermiLAT upper bound [19] on the γ flux from dwarf galaxies, for different dominant WIMP annihilation channel ($u\bar{u}$, $b\bar{b}$ or $\tau^+\tau^-$), whereas the red curve results from an upper bound on spectral distortions of the CMB, assuming WIMP annihilation into e^+e^- pairs.

is worse than the one from the annihilation of WIMPs into $\tau^+\tau^-$ by a factor of about two to three [19].

It is known that the annihilation of WIMPs has an important impact on CMB. Actually, their annihilations increase the temperature of CMB plasma during the "recombination" epoch (when neutral atoms are first formed) [96, 97] which postpones the decoupling of the CMB photons and causes the distortion of the pattern of CMB anisotropies. This puts the strongest limit on $\langle\sigma v\rangle$. Such limit for the WIMP annihilation cross section into e^+e^- pairs is shown in Fig. 2.8. These limits are from the analysis of data from the WMAP and ACT collaborations [59]. This constrains a thermal WIMP masses lighter than 8 GeV.

The data of PLANCK can give much better constraints [5, 98]. However, the mentioned papers only consider the multiplication of the efficiency factor $f_{\rm eff}$ and the WIMP annihilation cross section. This factor measures the amount of absorbed energy by thermal bath particles from the WIMP annihilation. The results of ref. [99] along with PLANCK put some constraints on dark matter annihilating into e^+e^- pairs with an S–wave cross section (temperature independent). For our calculation of $\langle\sigma v\rangle$, the bound is effective for masses below 50 GeV, see also the paper by Steigman et al. [100]. In fact the difference between our result and [100] is due to different values of efficiency factor we take $f \simeq 0.8$, following ref. [99], while in [100] $f = 1$ is assumed.

Since the efficiency factor should be similar for the other final states considered in Fig. 2.8, the CMB constraint should also be similar for all channels. The current CMB constraint is thus weaker than the bounds derived from the most recent FermiLAT data if WIMPs mostly annihilate into $q\bar{q}$ or $\tau^+\tau^-$ final states, but is stronger for WIMPs annihilating predominantly into e^+e^-. However, one should keep in mind that the CMB constraint is less direct. It is conceivable that additional non–standard ingredients

to the CMB fit – e.g., the presence of sterile neutrinos, a significant running of the spectral index of inflation, and/or a large contribution from tensor modes – can (partly) compensate the distortions caused by early WIMP annihilation, thereby weakening the constraint on $\langle\sigma v\rangle$. On the other hand, the constraint derived from the observation of dwarf galaxies depends on the assumed dark matter distribution [56]. In any case, it is encouraging that recent astrophysical and cosmological observations begin to probe relatively light thermal WIMPs with temperature independent annihilation cross section.

2.5 Summary and Conclusions

In this Chapter we used the QCD equation of state from results of lattice QCD with dynamical quarks to obtain the DoF of SM for energy and entropy densities. Our emphasis is on temperatures around the QCD deconfinement transition at $T_c = 154$ MeV. The functions $g_{\rm eff}(T)$ and $h_{\rm eff}(T)$ explain the evolution of DoF of SM with temperature. The quantity $g_{\rm eff,*}^{1/2}$ defined in eq. 2.10 is particularly important for the calculation of relic density, since the derivative of $h_{\rm eff}(T)$ appears in it, which the effect of QCD transition highly affects it and also the relic density of WIMPs. At the time of writing our paper [37] we suggested that these DoF functions can be embedded in computer packages for dark matter [66–68] [7].

The WIMP relic density we calculated for various masses based on our treatment of $h_{\rm eff}$ and $g_{\rm eff}$ differs from earlier DoF results using phenomenological models or pure glue lattice QCD calculations. The difference between previous results and ours is noticeable for WIMP masses between 3 and 15 GeV where the error reaches up to 9% for a constant $\langle\sigma v\rangle$ (S–wave), and up to 12% if $\langle\sigma v\rangle \propto T$ as in pure P–wave annihilation cross sections away from poles and thresholds. The source of difference is somewhat due to a sharp change in the data of $h_{\rm eff}(T)$ leading to a sharp spike or divergent behaviour in its derivative which also appear as spike in the previous treatments of $g_{\rm eff,*}^{1/2}$. This makes important to consider the continuity of $h_{\rm eff}(T)$ at all temperatures, especially around the times that cosmological transitions occur like QCD transition, which we considered here, and electroweak transition around 100 GeV, which we essentially ignored it in our calculation.

We should note that there are some uncertainties in the lattice QCD result that we used. We should emphasize that these uncertainties cause up to 2.5% difference in the predicted relic density for the WIMP masses between 3 and 10 GeV which is significantly larger than the observational value (in the framework of the standard ΛCDM cosmology) as Fig. 2.6 shows. Nonetheless, our result for $m_\chi > 20$ GeV is in agreement with the best former of result ref. [65] to better than 1%.

We used our improved treatment of the thermodynamics of the very early universe to update the calculation of the WIMP annihilation cross section required to reproduce the observed dark matter relic density, assuming the thermal average $\langle\sigma v\rangle$ to be independent of temperature [37]. We found that this cross section is indeed nearly constant for 10 GeV $< m_\chi <$ 10 TeV, thanks to a fortuitous cancellation between two competing effects; however, as also pointed out in ref. [65], the required value is closer to $2 \cdot 10^{-26}$ cm^{3}s^{-1} than to the often–cited "canonical" value of $3 \cdot 10^{-26}$ cm^{3}s^{-1}. On the other hand, for $m_\chi \lesssim 3$ GeV the required value of $\langle\sigma v\rangle$ exceeds $4 \cdot 10^{-26}$ cm^{3}s^{-1}. Producing a sufficiently large annihilation cross section for such light WIMPs typically requires the introduction of new light "mediators" between the WIMPs and SM particles. If the mediator mass is $\lesssim m_\chi/10$, the contribution of the mediator particles to the entropy and energy densities should be included, slightly modifying our results for the required annihilation cross section shown in Fig. 2.7.

Moreover, we used the upper bounds on $\langle\sigma v\rangle$ from probes of energetic γ rays produced in WIMP annihilation and from CMB constraints to compare with the required value that satisfies the observed relic density. The strongest upper bound comes from the PLANCK data for WIMPs annihilating into

[7] Currently, two of these codes i.e. `DarkSUSY` [66] and `SuperIso` [68] have added these set of DoF to their routine.

e^+e^- [8]. In addition, the bounds from γ ray searches, give stronger limits for WIMPs annihilating into hadronic or $\tau^+\tau^-$ final states. These are more important than the CMB bound based on standard ΛCDM cosmology which can easily be avoided. If most of the WIMPs annihilate into neutrinos, all of these constraints can be avoided [101–103].

It should be noted that both our calculation of the required WIMP annihilation cross section and our analysis of observational upper bounds on this quantity assumed that the thermal average $\langle\sigma v\rangle$ is independent of temperature, or, equivalently, that the annihilation cross section is independent of the invariant center–of–mass energy. Theoretically this assumption is not well motivated. For non–relativistic WIMPs the annihilation cross section can usually (but not always [104]) be expanded in terms of the relative velocity v, $\sigma v = a + bv^2 + \cdots$. Even if the constant term a is not suppressed, i.e. if annihilation from an $S-$wave is allowed, one would generically expect b to be of the same order as a. This would reduce the required value of $\langle\sigma v\rangle$ in today's universe by about 10%. If the constant term in σv is suppressed, the upper bounds on $\langle\sigma v\rangle$ that follow from observations in today's universe do not constrain thermal WIMP models significantly [37].

However, even in this case it is important to calculate the relic density as accurately as possible. This leads to a constraint on the free parameters of the underlying WIMP model, which can hopefully one day be compared to direct measurements at colliders. Only then we will be able to say with some confidence that this WIMP model is indeed correct. This Chapter of my thesis based on this paper [37], makes a small contribution to this ambitious long–term program.

In the next Chapter (chapter 3) the production of dark matter in an early matter dominated epoch will be discussed. We intend to use the result of this Chapter along with other assumptions to verify the effect of evolution of degrees of freedom in a non–thermal period of cosmology dominated by a heavy long–lived scalar field. Also, the effects of assuming different initial conditions for the dark matter and radiation densities will be studied there.

[8] Although a dedicated analysis for specific final states still had not been performed at the time of publication of our paper [37].

CHAPTER 3

Dark Matter Production in an Early Matter Dominated Era

3.1 Introduction

Weakly Interacting Massive Particles (WIMPs) are the most extensively studied class of DM candidate particles [15]. These particles are theoretically assumed to be thermally produced in the early universe. They had been produced when they were in thermal equilibrium with the plasma (thermal bath) of SM particles at an adequately high temperature. However, WIMP abundance reduced when the universe expanded and temperature decreased, until their annihilation rate became equal to the Hubble expansion rate. At the moment of this equality WIMPs roughly decoupled ("froze out") which means that their co–moving density basically became a constant. This mechanism in the standard cosmology approximately needs a value for the thermally averaged WIMP annihilation cross section (the so called "canonical" value) in order to yield the observed value of DM relic density. This canonical cross section is roughly of the order of typical weak interaction cross section; the term "weakly" in WIMP's name corresponds to this fact. Supersymmetric (SUSY) extensions of the SM include WIMP candidates such as neutralino DM [105].

Since the thermal WIMPs can be probed in different types of experiments, they are the most interesting DM candidates. However, none of the current direct detection [24–26, 106] and indirect [19–21] WIMP experiments have observed any signal so far. Moreover, collider searches for particles beyond the standard model have not provided any positive evidence as yet except some new constraints on the parameter space of attractive models. Overall, having no evidence in WIMP experiments have caused renewed interest in DM scenarios beyond the thermal WIMP.

There are some possibilities to consider DM production beyond the naive assumption of thermal WIMP in standard cosmology. One of them is to modify the expansion history of the universe using theoretical motivations. In the standard cosmology it is assumed that the universe is radiation dominated after the inflationary era until the temperature reaches about 1 eV (radiation–matter equality time), and afterwards matter (mostly dark one) starts to dominate the universe. However, UV–complete theories like string theory suggest that there may have been an epoch of early matter domination after inflationary reheating and before Big Bang Nucleosynthesis (BBN), which must have occurred in a radiation–dominated era. The mentioned period of early matter domination is formed by heavy long–lived scalar particles (moduli) with the longevity due to very weak couplings to SM particles. In string theory the vacuum expectation values (VEVs) of such (heavy) "moduli" fields control the couplings of the low energy theory [107, 108]. In fact, supergravity theories contain scalar ("Polonyi" [109]) fields with similar properties so that these

fields gained mass by the mechanism that caused supersymmetry breaking in a hidden sector. Moduli fields obtained large values during inflation, if their mass was smaller than the Hubble scale during inflation [110–114]. They began to oscillate coherently later, which mimicks an ensemble of scalar particles at rest in the cosmic rest frame. Since supersymmetry, supergravity, and superstring theories are vastly studied in the literature [17, 115–120], we do not discuss their details in here.

The decay of moduli fields after dominating the energy density of the universe can produce a large amount of entropy which affects the thermal history afterwards via the dilution of all particles produced before. Additionally, their decay can influence the (to high extent) successful predictions of standard BBN if it happened very late; this is the so called cosmological moduli (or Polonyi) problem [121–125]. The detailed analysis [126, 127] showed that the reheat temperature, i.e. the highest temperature of the radiation dominated epoch, must have been at least ~ 4 MeV in order not to threaten the success of standard BBN; this bound has more recently been confirmed in [128]. In this Chapter we have shown that the scalar mass should be heavier than 100 TeV to have a reheat temperature above 4 MeV. The existence of such a heavy particle is a problem if visible sector superparticle masses are also at this mass scale, since we expect that SUSY effects, as a solution to hierarchy problem should appear at TeV scale. However, large superparticle masses are still acceptable for "split" Supersymmetry [129, 130]. Consequently, any DM model that assumes its production during an early epoch of matter domination by a heavy scalar [131, 132] should respect the BBN bound on the reheat temperature.

Some possible scenarios for non–thermal production of DM particles with emphasis on the reheating era after inflationary period are studied in the literature by several authors [133–136]; more recently in [137].

If the gravitino (the super partner of graviton) in supersymmetric or superstring theories decays at early moments of the universe, this can also affect the production of baryons during BBN (gravitino problem). This problem can be solved in some models that predict an early matter dominated era due to the presence of a heavy long–lived modulus [138]. In other scenarios gravitino decays do not overproduce DM [139], or the gravitino is itself a stable DM candidate [140, 141]. There are some supersymmetric scenarios where gravitinos can be produced via the decay of modulus so that the gravitino should be heavy enough not to decay at BBN time (moduli-induced gravitino problem) [125, 139, 142]. On the other side as noted in [138, 143, 144], if the gravitino is heavier than the moduli fields, finding a solution of moduli problem can automatically solve the gravitino problem as well. In this Chapter we will not consider the gravitino and its possible effects on BBN, so in practice we assume that one of the above solutions for gravitino problem implicitly works in our scenario.

In general, there are two mechanisms for DM to be produced thermally. We described the WIMP DM production scenario via freeze–out (FO) mechanism briefly above and in more details in previous Chapter (Chapter 2). This mechanism happens when the expansion of the universe reduces the temperature to around 5% of the WIMP mass; this is the so called freeze–out temperature. However, dark matter production occurs at temperatures above the mass of the DM particle in the freeze–in (FI) mechanism. As an example, this scenario can happen due to the decay of a heavier particle. In such a case DM thermally averaged cross section is very small that DM annihilation to SM thermal bath is negligible [134, 145]. In this Chapter we intend to consider DM production in an early matter dominated epoch where both of these two general scenarios can happen. FI and FO can occur in matter domination and radiation domination produced after the decay of the heavy scalar (modulus), respectively. Nevertheless, other DM production mechanisms are possible during modulus domination. These other scenarios are investigated in [146] along with considering the decay of a visible sector particle (which is WIMP–like) into a lighter DM particle that exists in a dark (hidden) sector and DM annihilates only to dark sector particles (radiation). However, in this paper [38] which is the main source of this Chapter we assume that DM particles interact with SM particles and finally annihilate to them and not to other particles in a

possible hidden sector.

Our analysis in this Chapter is based on our paper [38] titled "Dark Matter Production in an Early Matter Dominated Era" motivated by the work of Kane et al. [146] on non–thermal cosmological history and DM production. Here, unlike ref. [146] we do not consider the presence of dark radiation since it is strongly constrained by current experimental data. However, in our analysis we only assume DM interacts with the visible sector particles. Moreover, we concentrate on the details of thermal history of the universe. Our study includes the effects coming from the temperature dependence of the effective number of relativistic degrees of freedom for energy and entropy density of radiation which are shown by $g_{\rm eff}$ and $h_{\rm eff}$. We will use the results of [37] (Chapter 2 of this thesis is about this paper and its details), which assumes free electroweak gauge and Higgs bosons, as appropriate for a smooth crossover electroweak transition [79–81]. Moreover, it uses results from lattice QCD around the QCD transition temperature, matched to a hadron resonance gas at lower temperatures [62, 63]. Additionally, the effect of neutrino decoupling at MeV temperatures is included using the study of Lesgourgues et al. [87]. Eventually, we investigate scenarios with non-vanishing radiation and DM densities at the beginning of a period of early matter domination.

The remainder of this Chapter is organized as follows. In the next Section we describe the general formalism for computing the DM relic density in a cosmology with an early matter dominated epoch. Here we largely follow ref. [146], but with improved treatment of the radiation component using the data of [37]. In Sec. 3.3 we map out regions of parameter space giving the correct DM relic density assuming initially vanishing DM and radiation content, with special emphasis on the effect of the temperature dependence of $g_{\rm eff}$ and $h_{\rm eff}$. In Sec. 3.4 we then consider non–vanishing initial radiation and DM density. Finally, we summarize the outcome of our work and conclude in Sec. 5.

3.2 The General Framework for Non-Thermal Dark Matter Production

In this Section we describe the calculational framework for computing the DM relic density in a scenario with an early epoch of matter domination. In the first Subsection we define the variables we use, and the equations that determine their evolution during the early universe. Our analysis is model–independent in the sense that all relevant particle physics quantities – particle masses, the DM annihilation cross section and the decay width of the heavy scalar particle – are assumed as free parameters. This approach is based on ref. [146], but we extend it by correctly considering the temperature dependence of the number of relativistic degrees of freedom in the thermal plasma of the early universe. In the second Subsection we briefly describe the numerical solution of the evolution equations, and the relation of the dimensionless quantities introduced in the first Subsection to the scaled DM relic density [38].

3.2.1 Evolution Equations

In the standard thermal DM production scenarios (both freeze–in and freeze–out) one only needs to solve a single evolution equation, namely the Boltzmann equation for the number density of the DM particles. In these scenarios all the relevant dynamics happens during the radiation dominated epoch, so the state of the universe is essentially determined uniquely by the temperature T. In particular, both the Hubble parameter and the entropy density are functions of T only; moreover, the co–moving entropy density is constant in this case, since the universe evolves adiabatically.

This is no longer true in the case we are interested in, where the energy density of the universe was dominated for a while by slowly decaying scalar ϕ particles [1]. We therefore need to track three coupled

[1] The spin of the decaying particles is not relevant for us. However, the by far best motivated particle physics examples of this

evolution equations: for the DM particles, for the ϕ particles, and for the radiation content.

Following [108, 134, 146] we introduce dimensionless quantities in order to describe the evolution of the universe. To this end all dimensionful quantities are divided by appropriate powers of the "reheat temperature", defined as

$$T_{\rm RH} = \sqrt{\Gamma_\phi M_{\rm Pl}} \left(\frac{45}{4\pi^3 g_{\rm eff}(T_{\rm RH})} \right)^{1/4} . \tag{3.1}$$

Here $M_{\rm Pl} \simeq 1.22 \times 10^{19}$ GeV is the Planck mass, Γ_ϕ is the total decay width of the ϕ particles, and $g_{\rm eff}$ is the number of relativistic degrees of freedom in the thermal plasma (numerically computed in Chapter 2), defined via the energy density of radiation [7]:

$$\rho_R(T) = \frac{\pi^2}{30} g_{\rm eff}(T) T^4 . \tag{3.2}$$

We should note that the $T_{\rm RH}$ is defined to some extent ideally. It is the temperature the universe would have if all the energy stored in ϕ was instantaneously transformed into radiation at the time

$$H_{\rm RH} = \Gamma_\phi, \quad H_{\rm RH}^2 = \frac{8\pi}{3M_{\rm Pl}^2} \rho_R(T_{\rm RH}) , \tag{3.3}$$

where the Hubble rate at reheating is denoted by $H_{\rm RH}$. This equation is computed under the assumption that ϕ particles completely dominated the energy density of the universe before their decay [36, 108, 128, 133, 136]. Nevertheless $T_{\rm RH}$ is a good estimate of the highest temperature of the radiation–dominated epoch that begins after most ϕ particles have decayed. Note, however, that the thermal bath during moduli domination can be considerably hotter than $T_{\rm RH}$; we will illustrate this point below.

The decay width of moduli (or Polonyi) fields ϕ are Planck suppressed, but the precise coupling strength is model dependent. Therefore, we write

$$\Gamma_\phi = \alpha \frac{M_\phi^3}{M_{\rm Pl}^2} , \quad \alpha = \frac{C}{8\pi} = \text{ constant} , \tag{3.4}$$

where M_ϕ is the mass of ϕ, and C is a constant whose value depends on the UV–complete theory. The value of $T_{\rm RH}$ is obtained by computing Γ_ϕ (which requires fixing M_ϕ and C or α), and inserting this into eq. (3.1). Note that this is an implicit equation, since the right–hand side (rhs) depends on $T_{\rm RH}$ via $g_{\rm eff}$. We use results from ref. [37] to compute the temperature dependence of $g_{\rm eff}$.

As noted above, the success of standard BBN requires $T_{\rm RH} \gtrsim 4$ MeV. This implies $M_\phi \gtrsim 100$ TeV for $\alpha \sim 1$ [126–128]. In Fig. 3.1 the dependence of the reheating temperature on the modulus mass according to eq. (3.1) is shown for different couplings α between 10^{-4} and 1. Here we have assumed that only SM particles contribute to $g_{\rm eff}$. If some new particles are found, as predicted e.g. by supersymmetric extensions of the SM, this figure will definitely change at higher reheating temperatures, i.e for larger M_ϕ. For comparison, Fig. 3.1 also shows results for fixed $g_{\rm eff}(T_{\rm RH}) = 10.75$, as appropriate for the SM at temperatures before BBN but after the decoupling of muons. In this plot, with its logarithmic axes, the differences between the two sets of curves become apparent only for $T_{\rm RH}$ of order the QCD transition temperature $T_c \sim 150$ MeV [62] or higher[2]. However, this is by far not the only way in which the temperature dependence of $g_{\rm eff}$ affects the final result.

mechanism use scalar moduli or Polonyi fields, as discussed in the Introduction.

[2] The curves also differ slightly for $T_{\rm RH}$ below the electron mass, where the actual $g_{\rm eff}(T_{\rm RH})$ is less than 10.75. However, scenarios with such a low reheat temperature will not reproduce standard BBN.

The set of Friedmann–Boltzmann equations we use in this Chapter to study the production of dark matter in an early matter dominated era are

$$\begin{aligned} \dot{\rho}_\phi + 3H\rho_\phi &= -\Gamma_\phi \rho_\phi \,, \\ \dot{\rho}_R + 4H\rho_R &= (1-\bar{B})\Gamma_\phi \rho_\phi + 2E_{X'}\langle\sigma v\rangle' \left(n_{X'}^2 - {n_{X',\mathrm{EQ}}}^2\right) \,, \\ \dot{n}_{X'} + 3Hn_{X'} &= \frac{B_{X'}}{M_\phi}\Gamma_\phi \rho_\phi - \langle\sigma v\rangle' \left(n_{X'}^2 - {n_{X',\mathrm{EQ}}}^2\right) \,, \end{aligned} \tag{3.5}$$

$$H^2 = \frac{8\pi}{3M_{\mathrm{Pl}}^2}\left(\rho_\phi + \rho_R + \rho_{X'}\right) \,. \tag{3.6}$$

Here $\rho_\phi = M_\phi n_\phi$ is the energy density stored in ϕ particles, $n_{X'}$ is the number density of the DM particles and $\rho_{X'} = M_{X'} n_{X'}$ is their energy density, which we call X' following ref. [146]. Moreover, the Hubble rate for all contents of the universe is shown by H and defined in eq. (3.6). Moreover, $E_{X'} \approx (M_{X'}^2 + 3\,T^2)^{1/2}$ is the average energy per X' particle; this approximation is sufficient for our purposes since the contribution of DM particles to the total energy density is always subdominant in the epoch we are interested in[3].

As in ref. [146] we assume that ϕ particles can decay into X' particles with effective branching ratio $B_{X'}$; the average energy per ϕ decay that goes into DM particles is then given by $\bar{B}M_\phi$, with

$$\bar{B} = \frac{E_{X'} B_{X'}}{M_\phi} \,. \tag{3.7}$$

A fraction $1-\bar{B}$ of the ϕ energy will then go into SM particles, i.e. into radiation. In many cases a discrete symmetry ensures that X' particles can only be produced pairwise. If $\phi \to X'X'$ is the dominant X' production mode from ϕ decays, then $B_{X'} = 2\Gamma(\phi \to X'X')/\Gamma_\phi$.[4] Note that we will mostly be interested in scenarios where $B_{X'} \ll 1$, i.e. $\bar{B} \ll 1$; the exact expression for $E_{X'}$ is then again not important.

In the following analysis we assume that the decay products of ϕ thermalize immediately, i.e. radiation always refers to a relativistic plasma in full thermal equilibrium, again following ref. [146]. This is an idealization. If ϕ particles decay into two body final states, these final state particles will initially have energy $M_\phi/2$, which can be much higher than T. These energetic SM particles could produce DM particles before they thermalize. This has been analyzed in [148], where it was shown that this source of X' particles can be significant if $M_{X'}$ is relatively close to M_ϕ. We are mostly interested in $M_{X'} \ll M_\phi$, in which case the approximation of instantaneous thermalization of the ϕ decay products should be applicable. Recently, it has been claimed that considering the details of thermalization process can change the maximum temperature of the universe and affect the process of DM production during and after early matter domination [149–151]. We postpone to consider these details for future studies.

Finally, the equilibrium number density of DM particles $n_{X',\mathrm{EQ}}$ is given by

$$n_{X',\mathrm{EQ}} \equiv \frac{g_{X'} T {M_{X'}}^2}{2\pi^2} K_2\left(\frac{M_{X'}}{T}\right) \to \begin{cases} \frac{\tilde{g}_{X'}\,\zeta(3) T^3}{\pi^2} & \text{if } T \gg M_{X'} \\ g_{X'}\left(\frac{M_{X'}T}{2\pi}\right)^{\frac{3}{2}} \exp(-M_{X'}/T) & \text{if } T \ll M_{X'} \,. \end{cases} \tag{3.8}$$

[3] This ansatz implicitly assumes that X' particles are at least in kinetic equilibrium with the SM radiation. Note that kinetic equilibrium is much easier to attain than full chemical equilibrium.

[4] ϕ particles might decay predominantly into heavy SM particles, e.g. top quarks or Higgs bosons, with masses larger than the temperature. However, these heavier SM particles will then decay almost immediately into light SM particles, i.e. into radiation. ϕ particles could also decay into some partners of X', e.g. a pair of gluinos in supersymmetric models, which then decay almost immediately into X' (e.g. neutralino) plus radiation [147]. All these cases are covered by this formalism.

Here $g_{X'}$ counts the internal degrees of freedom of X', $\tilde{g}_{X'} = g_{X'}\,(3g_{X'}/4)$ for bosonic (fermionic) X', and K_2 is the modified Bessel function of second kind. In our numerical calculations we assume $g_{X'} = 2$, as appropriate for a spin$-1/2$ Majorana (self–conjugate) fermion.

The reason why we use the above equation even at relativistic limit is that the number density of a particle species at temperature T in the context of quantum mechanics should be computed from Fermi–Dirac or Bose–Einstein distributions for fermions and bosons, respectively. However, the integral for such number density does not have any analytical solution for all range of temperatures except in the relativistic and non–relativistic limits. As a consequence, to avoid more numerical calculations for finding $n_{X',\mathrm{EQ}}(T)$, which is time consuming, we use the above definition for the equilibrium number density of DM which is based on Maxwell–Boltzmann distribution. This function behaves smoothly at all temperatures and is a very good approximation.

Our main interest is the calculation of the Dark Matter relic density, by deriving and solving the above set of Boltzmann equations. To that end, we use T_{RH} to define the dimensionless scale parameter

$$A \equiv a T_{\mathrm{RH}}\,; \tag{3.9}$$

multiplying the scale factor in the Friedmann–Robertson–Walker metric a with T_{RH} improves the stability of the numerical solution [108]. This in turn allows us to define co–moving densities for ϕ particles, radiation and DM particles in the following

$$\Phi \equiv \frac{\rho_\phi A^3}{T_{\mathrm{RH}}^4}\,,\; R \equiv \rho_R \frac{A^4}{T_{\mathrm{RH}}^4}\,,\; X' \equiv n_{X'} \frac{A^3}{T_{\mathrm{RH}}^3}\,. \tag{3.10}$$

Note that R and X' approach constants when ϕ decays (Φ vanishes) as well as the pair production and annihilation of X' particles can be neglected. Finally, we use the co–moving densities to define a co–moving Hubble parameter

$$\widetilde{H} \equiv \left(\Phi + \frac{R}{A} + \frac{E_{X'} X'}{T_{\mathrm{RH}}}\right)^{1/2}\,. \tag{3.11}$$

$\widetilde{H}$ is related to the usual (dimensionful) Hubble parameter in eq. (3.6) via

$$H = \widetilde{H} T_{\mathrm{RH}}^2 A^{-3/2} c_1^{-1/2} M_{\mathrm{Pl}}^{-1}\,, \tag{3.12}$$

where we have introduced the constant $c_1 = 3/(8\pi)$. Using eqs. (3.2) and (3.10) we find

$$T = \left(\frac{30}{\pi^2 g_{\mathrm{eff}}(T)}\right)^{1/4} \frac{R^{1/4}}{A} T_{RH}\,, \tag{3.13}$$

The effective number of degrees of freedom g_{eff}, defined via the radiation energy density as in eq. (3.2), depends on the temperature, since only particles with mass of order of or less than the temperature contribute significantly [7]. In the SM the temperature dependence is not severe for $T \gtrsim 1$ GeV. As a first approximation one can therefore ignore terms proportional to the derivative dg_{eff}/dT. This allows to derive an evolution equation for R from energy conservation. Therefore, the set of equations one needs to solve is then as follows

$$\begin{aligned}
\widetilde{H}\frac{d\Phi}{dA} &= -c_\rho^{1/2} A^{1/2} \Phi, \\
\widetilde{H}\frac{dR}{dA} &= c_\rho^{1/2} A^{3/2}(1-\bar{B})\Phi + c_1^{1/2} M_{\mathrm{pl}} \left[\frac{2E_{X'}\langle\sigma v\rangle'}{A^{3/2}}\left(X'^2 - {X'_{\mathrm{EQ}}}^2\right)\right],
\end{aligned} \tag{3.14}$$

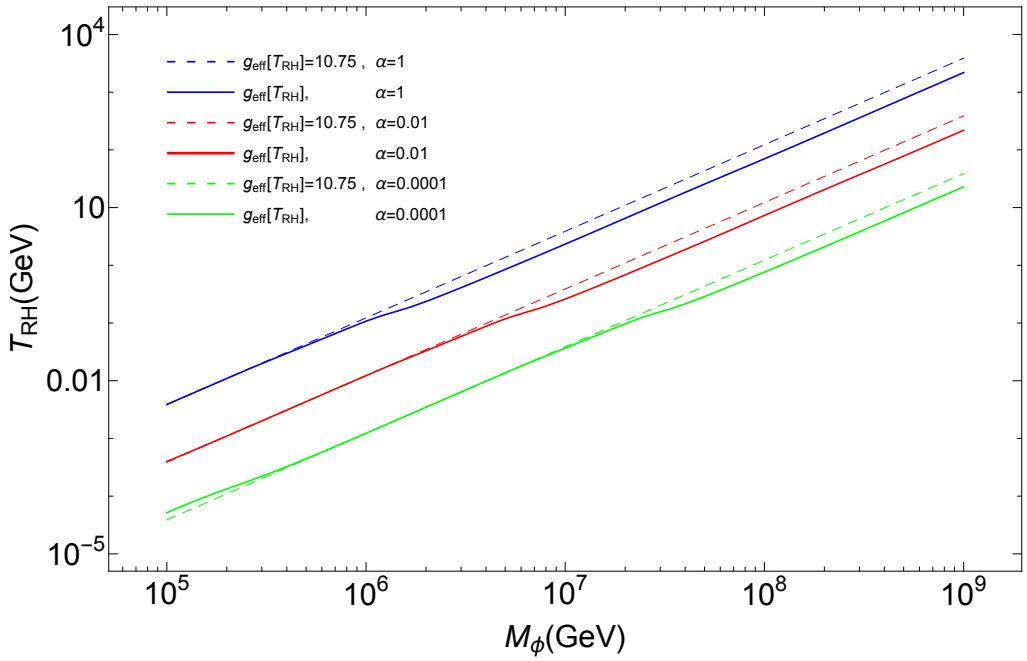

Figure 3.1: Reheating temperature $T_{\rm RH}$ as function of the mass M_ϕ of the particle whose energy density dominates in the early matter dominated epoch, for different coefficients α defined in eq. (3.4). The solid curves have been obtained including the temperature dependence of $g_{\rm eff}$ as predicted by the SM, whereas the dashed curves are for fixed $g_{\rm eff}(T_{RH}) = 10.75$.

$$\widetilde{H}\frac{dX'}{dA} = \frac{c_\rho^{1/2} T_{\rm RH} B_{X'}}{M_\phi} A^{1/2}\Phi + c_1^{1/2}\, M_{\rm pl} T_{\rm RH} A^{-5/2} \langle\sigma v\rangle' \left(X'^2_{\rm EQ} - X'^2\right).$$

Here c_1 is as in eq. (3.12), and we have defined a second constant $c_\rho = \frac{\pi^2 g_{\rm eff}(T_{\rm RH})}{30}$.

The first eq. (3.14) describes ϕ decays. Unfortunately it is not entirely straightforward to see in this formalism that Φ becomes constant when ϕ decays can be neglected. Eq. (3.1) shows that $T_{\rm RH} \to 0$ as $\Gamma_\phi \to 0$, so eqs. (3.10) become ill–defined in this case. Note, however, that initially Φ, and hence $\widetilde{H}$, are much bigger than unity if moduli are to dominate the universe for an extended epoch. Initially $d\Phi/dA$ is thus much less than Φ. One can show that $Ad\Phi/dA$ becomes of order Φ_I only when $H \simeq \Gamma_\phi$.

In the second eq. (3.14) we recognise a positive contribution to the rhs proportional to Φ stemming from ϕ decays, and a contribution describing the pair production from and annihilation of X' particles into radiation. A similar term appears on the rhs of the third equation with opposite sign; this third equation also features a positive contribution from direct $\phi \to X'$ decays.

In order to follow the evolution of the universe more accurately we must consider the precise evolution of $g_{\rm eff}$ (and related quantities) in the thermal bath. As shown in ref. [7] the evolution of the radiation component is then more easily described via the entropy density, which is given by

$$s_R(T) = \frac{\rho_R(T) + p_R(T)}{T} = \frac{2\pi^2}{45} h_{\rm eff}(T) T^3 \,. \tag{3.15}$$

The second equation defines $h_{\rm eff}(T)$, which is another measure of the effective number of relativistic degrees of freedom; in the SM, $g_{\rm eff}(T) \simeq h_{\rm eff}(T)$ before neutrinos decouple at MeV temperatures. In standard cosmology, the co–moving entropy density is constant after the end of inflation. However, in

the scenario considered here ϕ decays lead to entropy production. This is described by the evolution equation in the following

$$\frac{d\,s_R}{dt} + 3Hs_R = \frac{1}{T}[(1-\bar{B})\Gamma_\phi \rho_\phi + 2E_{X'}\langle\sigma v\rangle' \left(n_{X'}^2 - {n_{X',\mathrm{EQ}}}^2\right)]. \tag{3.16}$$

The factor $(1-\bar{B})$ in the first term of the rhs of eq. (3.16) should not be there if $T > M_{X'}$; recall, however, that $\bar{B} \ll 1$ in cases of interest, so that we make only a small mistake by including this factor. The second term describes entropy production from out–of–equilibrium annihilation of X' particles; we find that this term is always numerically insignificant. Also, this is true for the last term on the rhs of the second eq. (3.14).

This leads to the following equation describing the evolution of the temperature

$$\begin{aligned}\frac{dT}{dA} = \left(1 + \frac{T}{3h_{\mathrm{eff}}}\frac{dh_{\mathrm{eff}}}{dT}\right)^{-1}\Bigg[\quad & -\frac{T}{A} + \frac{15T_{\mathrm{RH}}^6}{2\pi^2 c_1^{1/2} M_{\mathrm{Pl}} H T^3 h_{\mathrm{eff}} A^{\frac{11}{2}}}\Bigg(c_\rho^{1/2} A^{3/2}(1-\bar{B})\Phi \\ & + c_1^{1/2} M_{\mathrm{pl}} \frac{2E_{X'}\langle\sigma v\rangle'}{A^{3/2}}\left(X'^2 - {X'_{\mathrm{EQ}}}^2\right)\Bigg)\Bigg].\end{aligned} \tag{3.17}$$

Note that the rhs of eq. (3.17) depends both on $h_{\mathrm{eff}}(T)$ and (via c_ρ) on $g_{\mathrm{eff}}(T)$. We will use the results of [37] for them which were also represented in Figs. (2.1) and (2.2) of Chapter 2. This equation replaces the second eq. (3.14); the first and third of these equations remain unchanged. We also need eq. (3.2) to compute the radiation density from T, and eqs. (3.11) and (3.10) to compute the scaled Hubble parameter $\widetilde{H}$. This is a closed system of equations.

As mentioned above, in the early epoch of matter domination the radiation component can be much hotter than T_{RH}. If terms proportional to the derivative of h_{eff} or g_{eff} with respect to temperature are ignored, the evolution of the temperature for $H \gg \Gamma_\phi$ can be computed analytically. If initially $\rho_R = 0$, using the third equation of (3.14) and assuming $\widetilde{H} \approx \Phi_I^{1/2}$ in early matter domination one can find [134]

$$R \simeq \frac{2}{5}\left(\frac{\pi^2 g_{\mathrm{eff}}(T)}{30}\right)^{1/2}\left(A^{5/2} - 1\right)\Phi_I^{1/2}, \tag{3.18}$$

where we neglected the contribution of annihilation of DM to radiation, since it is negligible at that time and also afterwards. By applying eq. (3.13) the following equation for temperature evolution can be obtained

$$T \simeq \left(\frac{8^8}{3^3 5^5}\right)^{1/20}\left(\frac{g_{\mathrm{eff}}(T_{\mathrm{max}})}{g_{\mathrm{eff}}(T)}\right)^{1/4} T_{\mathrm{max}}\left(A^{-3/2} - A^{-4}\right)^{1/4}. \tag{3.19}$$

The temperature reaches its maximum at $A_{max} \equiv (8/3)^{2/5}$ which can be deriven by computing the derivative of above equation [134]. The maximum temperature during modulus domination T_{max} is given by [134]

$$T_{\mathrm{max}} = \left(\frac{3}{8}\right)^{2/5}\left(\frac{5}{\pi^3}\right)^{1/8}\left(\frac{g_{\mathrm{eff}}(T_{\mathrm{RH}})^{1/2}}{g_{\mathrm{eff}}(T_{\mathrm{max}})}\right)^{1/4}(M_{\mathrm{pl}} H_I T_{\mathrm{RH}}^2)^{1/4}. \tag{3.20}$$

Using $H_I = \Phi_I^{1/2} T_{\mathrm{RH}}^2/(c_1^{1/2} M_{\mathrm{Pl}})$ we find $T_{\mathrm{max}} \sim T_{\mathrm{RH}}\Phi_I^{1/8}$, up to $O(1)$ factors, where Φ_I is the initial co–moving density of ϕ. The assumption of vanishing initial ρ_R is reasonable only if the matter dominated epoch lasts sufficiently long to basically erase all clues of possible earlier radiation dominated epochs. This requires $H_I \gg \Gamma_\phi$, and hence $\sqrt{\Phi_I} \gg 1$. In consequence, even if T_{RH} is well below the temperature T_c of the QCD transition, frequently $T_{\mathrm{max}} > T_c$, in which case an accurate treatment of the temperature

dependence of $g_{\rm eff}$ and $h_{\rm eff}$ becomes important.

3.2.2 Dark Matter Abundance in an Early Matter Dominated Epoch

As in case of standard cosmology, the dark matter annihilation cross section plays an important role. Here we will not consider specific particle physics candidates for X'. Instead we use the standard parametrization,

$$(\sigma v)' = a + bv^2\,, \tag{3.21}$$

which is applicable for particles whose final relic density is set at temperature $T < M_{X'}$. Here a is nonzero only if X' particles can annihilate from an $S-$wave initial state, whereas a non-vanishing b can be generated also by annihilation from the $P-$wave. Thermal averaging then gives [64, 118]

$$\langle\sigma v\rangle' = a + 6b\frac{T}{M_{X'}}\,. \tag{3.22}$$

In the following sections we will present exact numerical solutions of the evolution equations discussed in the previous subsections. These have been obtained with the help of `Mathematica`. We found it convenient to rewrite the equations in terms of the logarithmic derivative $d/d(\log A) = Ad/dA$, i.e. we multiplied eqs. (3.14) and (3.17) with A [5]. We always use initial conditions

$$A = 1,\ \Phi = \Phi_I = \frac{3H_I^2\, M_{\rm pl}^2}{8\pi\, T_{\rm RH}^4}\,; \tag{3.23}$$

in the next Section we will follow ref. [146] in initially setting [6]

$$R_I = X_I' = 0\,. \tag{3.24}$$

The assumption of initial density for radiation and dark matter particles can be reasonable if ϕ particles completely dominate the universe for some time after inflationary reheating, so that all dependence on conditions before the ϕ dominated epoch is erased. Recall that in the absence of ϕ decays the ratio of radiation and matter densities scales like $1/A$. A possible initial radiation component can then become irrelevant if $A_{\rm decay} \gg 1$, where $A_{\rm decay}$ is the value of the dimensionless scale factor where most ϕ particles decay. Until this time to good approximation H_I = constant. The first eq. (3.14) can then be solved analytically [146]

$$\Phi(A) = \Phi_I\, \exp\left[-\frac{2}{3}\left(\frac{c_\rho}{\Phi_I}\right)^{1/2}\left(A^{3/2}-1\right)\right], \tag{3.25}$$

where we have used the initial value $A = 1$. Most moduli particles decay when $\Phi \simeq \Phi_I\, \exp(-1)$, which occurs at $A \simeq A_{\rm decay}$ with

$$A_{\rm decay} = \left[\frac{3}{2}\left(\frac{\Phi_I}{c_\rho}\right)^{1/2} + 1\right]^{2/3}\,. \tag{3.26}$$

[5] Actually, for very stiff Riccati type differential equations which is the case for Boltzmann equation it would be better to consider higher powers of variable under integration (here A) instead of only considering exponential. Here a large factor which depends on Planck mass, DM cross section, and mass appears in the equation which makes the integration process time consuming over the large interval of integration for A. Changing the variable A reduces the length of integration interval by some orders of magnitude.

[6] Practically, in the initially vanishing radiation density case we consider the numerical value for the initial temperature to be $T_I = 10^{-13}$ GeV.

Writing

$$H_I = \gamma \Gamma_\phi \,, \tag{3.27}$$

and using the fact that $H_I \propto \sqrt{\Phi_I}$, it is easy to see that $A_{\rm decay} \gg 1$ requires $\gamma \gg 1$.

In this case, and with eqs. (3.24) imposed, the final computed relic dark matter abundance will be essentially independent of the initial Φ_I, or, equivalently, of γ. Note that the final scaled densities introduced in eqs. (3.10) do depend on Φ_I. For example, again setting $\widetilde{H} = \sqrt{\Phi_I}$ = constant, a good analytical approximation for the final value of R can be derived [146]

$$R_F \equiv R(A_F) \simeq L \left(\frac{\Phi_I}{c_\rho}\right)^{1/3} \Phi_I \,, \tag{3.28}$$

where we have defined

$$L \equiv (1 - B_{\rm eff})\, \Gamma\left(\frac{5}{3}\right) \left(\frac{3}{2}\right)^{2/3} \quad \text{with } B_{\rm eff} \equiv \frac{B_{X'} \left(M_{X'}{}^2 + 3 T_{\rm RH}{}^2\right)^{1/2}}{M_\phi} \,. \tag{3.29}$$

Here A_F should be so large that the co–moving abundances of radiation and matter have become constant and ϕ decays have been completed, i.e. $A_F \gg A_{\rm decay}$ with $A_{\rm decay}$ given by eq. (3.26). On the other hand, A_F should still be within the radiation dominated epoch.

Evidently $R_F \propto \Phi_I^{4/3}$. This dependence cancels once we normalize the final dark matter density to today's energy density carried by photons, which is known very well from measurements of the Cosmic Microwave Background (CMB). We thus compute the final X' relic abundance from the following relation [38][7]

$$\begin{aligned} \Omega_{DM} h^2 &= \frac{\rho_{X'}(T_{\rm now})}{\rho_\gamma(T_{\rm now})} \Omega_\gamma h^2 = \frac{\rho_{X'}(T_F)}{2\rho_R(T_F)} \frac{g_{\rm eff}(T_F) h_{\rm eff}(T_{\rm now})}{h_{\rm eff}(T_F)} \frac{T_F}{T_{\rm now}} \Omega_\gamma h^2 \\ &= M_{X'} \frac{X'(T_F)}{R(T_F)} \frac{A_F T_F g_{\rm eff}(T_F) h_{\rm eff}(T_{\rm now})}{2 T_{\rm now} T_{\rm RH} h_{\rm eff}(T_F)} \Omega_\gamma h^2 \,. \end{aligned} \tag{3.30}$$

Here Ω_{DM} is the dark matter mass density in units of the critical density, h is today's Hubble constant in units of 100 km/(s $\cdot$ MPc), and $T_F = T(A_F)$ is in the radiation dominated era, as mentioned above. In the second step we have written $\rho_\gamma = 2\rho_R / g_{\rm eff}$, and used the fact that the matter density $\rho_{X'}$ scales exactly like the entropy density s_R for $A \geq A_F$, i.e. after all ϕ decays and X' annihilations ceased. Note also that $h_{\rm eff}$ becomes constant after electrons decoupled, i.e. for $T \ll m_e$. The present observational values of the current temperature and density of (CMB) photons, as collected by the Particle Data Group [42], are:

$$\begin{aligned} \Omega_\gamma h^2 &= 2.473 \times 10^{-5} \,; \\ T_{\rm now} &= 2.7255 \text{ K} = 2.35 \times 10^{-13} \text{ GeV} \,. \end{aligned} \tag{3.31}$$

We use these values in our numerical calculations. Cosmological observations also determine the total present density of non-baryonic dark matter quite accurately [42]

$$\Omega_{DM} h^2 = 0.1186 \pm 0.002 \,. \tag{3.32}$$

[7] In ref. [146] the final DM relic density is expressed via today's radiation density. The latter is, strictly speaking, not known very well, since we do not know whether the lightest neutrino is still relativistic, and hence contributes to radiation, or not. Alternatively we could normalize to the entropy density, which was co–moving constant for $A \geq A_F$; this closely mirrors the usual treatment of thermal WIMPs. Note also that we do know today's entropy density of neutrinos, which also remained co–moving constant for $T \ll 1$ MeV.

This can be used to effectively reduce the dimension of the allowed parameter space by one. However, in this paper we are more interested in mapping out the predicted relic density as function of the relevant free parameters. These include the reheat temperature, the branching ratio for $\phi \to X'$ decays, the X' annihilation cross section as parameterized in eq. (3.22), and the masses of the ϕ and X' particles. In Sec. 3.4 we will in addition allow non–vanishing initial values for the radiation and X' densities.

In the next Section we will compute the dark matter abundance numerically. To that end, first we require to have an analytical understanding of different parameter regions that satisfy the relic density. To achieve that we use eqs. (3.28), (3.30) and (3.31) to obtain the approximate relic density in an early matter dominated epoch as follows [38, 146]

$$\Omega_{DM}h^2 \approx \frac{M_{X'}X'(T_F)}{L^{3/4}\,\Phi_I}\,\frac{g_{\rm eff}(T_F)h_{\rm eff}(T_{\rm now})}{2T_{\rm now}h_{\rm eff}(T_F)}\Omega_\gamma h^2\,. \tag{3.33}$$

The details of different DM production mechanisms are given in the following Section.

3.3 Dark Matter Relic Density for Initially Vanishing Radiation

In this Section we show numerical results for the predicted X' relic density for vanishing initial radiation and X' densities, i.e. for initial conditions given by eqs. (3.23) and (3.24). All X' particles – and all other particles in today's universe – then originate from ϕ decay, either directly or via the radiation that originates from ϕ decay.

Before presenting numerical results, it is useful to briefly discuss the different DM production mechanisms in non–thermal cosmology. Here we again closely follow ref. [146], where analytical approximations based on eqs. (3.14) were developed. As discussed in the previous Section, these equations ignore terms that depend on the derivative of $g_{\rm eff}$ or $h_{\rm eff}$ with respect to temperature. While our numerical treatment fully includes these effects, the analytical approximations remain useful as a guide to the (quite large) parameter space. We also remind the reader that, unlike ref. [146], we do not include a dark radiation component.

It should be clear that the usual thermal WIMP scenario can also be reproduced in our framework, if $T_{\rm RH}$ is above the conventional decoupling temperature $T_{\rm FO}$ defined in the radiation dominated epoch. This requires rather large reheat temperatures, and hence very large ϕ masses as shown in Fig. 1, or else quite small masses for the dark matter particle X'. In the latter case one would typically need additional light mediators in order to achieve a sufficiently large X' annihilation cross section. Of course, here we are mostly interested in scenarios that differ from this standard thermal WIMP scenario.

A first important observation is that for not too small X' annihilation cross section, the rhs of the third eq. (3.14) essentially vanishes over an extended range of A. In the absence of $\phi \to X'$ decays this corresponds to X' particles being in full thermal equilibrium, but in the present context this "quasi–static equilibrium" (QSE) can also be obtained through a balance between X' production from ϕ decay and X' annihilation, with negligible X' production from the thermal plasma. Using eq. (3.14) the general QSE solution can be found as

$$X'_{\rm QSE}(A) = \left[\frac{A^3}{\langle\sigma v\rangle'}\left(\frac{c_\rho^{1/2}B_{X'}}{c_1^{1/2}M_\phi M_{\rm Pl}}\Phi\right) + {X'_{\rm EQ}}^2\right]^{1/2}\,. \tag{3.34}$$

QSE will be maintained only if the reaction rate $n_{X'}\langle\sigma v\rangle'$ is larger than the Hubble expansion rate. Clearly

QSE can only be achieved if $X'_{\rm QSE} > X'_{\rm crit}$ so that we have

$$X'_{\rm crit} \equiv (n_{X'})_{\rm crit}\frac{A^3}{T_{\rm RH}^3} = \frac{HA^3}{\langle\sigma v\rangle' T_{\rm RH}^3} = \frac{\widetilde{H}A^{3/2}}{c_1^{1/2} M_{\rm Pl} T_{\rm RH}\langle\sigma v\rangle'}\,. \tag{3.35}$$

This leads to a lower bound $\langle\sigma v\rangle'_{crit}$ on the thermally averaged X' annihilation cross section. This lower bound depends on the temperature. If T_{RH} is much smaller than $M_{X'}$, the term $\propto \left(X'_{\rm EQ}\right)^2$ in eq. (3.34) can be ignored. On the other hand, for sufficiently high temperature $\langle\sigma v\rangle'_{crit}$ can be calculated from $X'_{\rm QSE} = X'_{\rm EQ}$. The critical thermally averaged cross section can be computed as below using the mentioned assumptions [146]

$$\langle\sigma v\rangle'_{crit} \equiv \frac{8\pi M_\phi}{3T_{RH}^2 M_{\rm Pl} B_{X'}}\left(\frac{45}{4\pi^3 g_{\rm eff}(T_{RH})}\right)^{1/2}; \qquad M_{X'} \gg T_{RH} \tag{3.36}$$

$$\langle\sigma v\rangle'_{crit} \equiv \left(\frac{2}{3}\right)^{1/4}\left(\frac{4\pi^3 g_{\rm eff}(T_{RH})}{45}\right)^{1/2}\frac{\pi^2}{\zeta(3)\tilde{g}_{X'}\Gamma(5/3)^{3/8} T_{RH} M_{\rm Pl}}; \qquad M_{X'} \ll T_{RH}\,. \tag{3.37}$$

One can classify different regions of parameter space according to whether the thermally averaged X' annihilation cross section is above or below the critical one for $T \simeq T_{\rm RH}$; this is called efficient and inefficient annihilation.

Let $\hat{T}_{\rm FO}$ be the X' freeze–out temperature, computed in a radiation dominated universe. If $\hat{T}_{\rm FO} > T_{\rm RH}$ then $X'_{\rm EQ} \sim 0$ for $T \gtrsim T_{\rm RH}$. In the efficient annihilation case ($\langle\sigma v\rangle' > \langle\sigma v\rangle'_{crit}$), before the reheating DM co–moving density follows $X'_{QSE} \propto \Phi^{1/2}$ but around the reheating time and afterwards the ratio of X'_{QSE}/X'_{crit} decreases exponentially. At scale factor A_{crit} they become roughly of the same order which can be written as [146]

$$X'_{QSE}(A_{crit}) = \frac{1}{\lambda}X'_{crit}(A_{crit})\,, \tag{3.38}$$

here λ is an $O(1)$ constant. Using eqs. (3.34) and (3.35) leads to

$$\left(\frac{\Phi}{\widetilde{H}^2}\right)_{A_{crit}} = \frac{\langle\sigma v\rangle'_{crit}}{\lambda^2\langle\sigma v\rangle'}\,. \tag{3.39}$$

Since this happens in the transition between modulus and radiation dominated eras, we use $\widetilde{H} \approx \Phi^{1/2}(A_{crit})$ and eq. (3.25) and also $R(A_{crit}) \approx R_F$ to calculate A_{crit} in the following

$$\log\left(\widetilde{A}_{crit}\right) = \frac{2}{3}c_\rho^{1/2}\widetilde{A}_{crit}^{3/2} + \log\left(c_\rho^{-1/3}\left(\frac{3}{2}\right)^{2/3}\Gamma\left(\frac{5}{3}\right)\right) - \log\left(\frac{\lambda^2\langle\sigma v\rangle'}{\langle\sigma v\rangle'_{crit}} - 1\right), \widetilde{A}_{crit} = \frac{A_{crit}}{\Phi_I^{1/3}}\,. \tag{3.40}$$

We used these approximations $e^{-\frac{2}{3}\left(\frac{c_\rho}{\Phi_I}\right)^{1/2}} \approx 1$. In the last *log* we can remove the -1 since it is negligible with respect to the first term in it. Then we try to find $\widetilde{A}_{crit}$ from the following equation

$$\log\left(b_1\widetilde{A}_{crit}\right) \approx b_2\widetilde{A}_{crit}^{3/2}\,, \quad b_1 = c_\rho^{1/3}\left(\frac{3}{2}\right)^{-2/3}\Gamma\left(\frac{5}{3}\right)^{-1}\frac{\lambda^2\langle\sigma v\rangle'}{\langle\sigma v\rangle'_{crit}}\,, \quad b_2 = \frac{2}{3}c_\rho^{1/2}\,. \tag{3.41}$$

Then in the limit $\langle\sigma v\rangle' \gg \langle\sigma v\rangle'_{crit}$ we get $\widetilde{A}_{crit} \approx \left(\frac{-2}{3b_2}\right)^{2/3}\left[Productlog\left(-\frac{3}{2}\frac{b_2}{b_1^{3/2}}\right)\right]^{2/3} \approx b_1^{-1}$ [8], which can be

[8] This type of function is called "Lambert W function" or "product logarithm" which is defined as $f(z) = w$ so that the relation

written as

$$\widetilde{A}_{crit} \approx \frac{\Gamma(\frac{5}{3})\left(\frac{3}{2}\right)^{2/3} c_\rho^{-1/3}}{\lambda^2} \frac{\langle\sigma v\rangle'_{crit}}{\langle\sigma v\rangle'} \,. \tag{3.42}$$

Based on our numerical calculation [38] and the result of [146] we can approximately choose $\lambda \approx 2$.

Consequently, using eqs. (3.33), (3.38), (3.42) for "non–relativistic quasi static equilibrium" case the relic abundance can be approximated by

$$\begin{aligned}
\Omega h^2[\mathrm{QSE_{nr}}] &\approx \frac{2^{1/2}\pi^{3/4}}{3^{1/2}5^{1/4}} \frac{g_{\rm eff}(T_{\rm RH})^{1/4} B_{X'}^{1/2} M_{X'} \widetilde{A}_{crit}^{3/2} e^{-\frac{1}{3}c_\rho^{-1/2}\widetilde{A}_{crit}^{3/2}}}{L^{3/4}\left(M_{\rm Pl} M_\phi \langle\sigma v\rangle'\right)^{1/2}} \frac{g_{\rm eff}(T_F) h_{\rm eff}(T_{\rm now})}{2T_{\rm now} h_{\rm eff}(T_F)} \Omega_\gamma h^2 \\
&\approx 2^{4/3}5^{1/6}\pi^{1/6}\Gamma\left(\frac{5}{3}\right)^{1/2} \frac{\widetilde{A}_{crit} M_{X'}}{\lambda L^{3/4} g_{\rm eff}(T_{\rm RH})^{1/6} M_{\rm Pl} \langle\sigma v\rangle' T_{\rm RH}} \frac{g_{\rm eff}(T_F) h_{\rm eff}(T_{\rm now})}{2T_{\rm now} h_{\rm eff}(T_F)} \Omega_\gamma h^2 \\
&\approx \frac{120\,\Gamma\left(\frac{5}{3}\right)^{3/2}}{\pi} \frac{M_{X'} M_\phi}{\lambda^3 L^{3/4} g_{\rm eff}(T_{\rm RH}) B_{X'} M_{\rm Pl}^2 \langle\sigma v\rangle'^2 T_{\rm RH}^3} \frac{g_{\rm eff}(T_F) h_{\rm eff}(T_{\rm now})}{2T_{\rm now} h_{\rm eff}(T_F)} \Omega_\gamma h^2 .
\end{aligned} \tag{3.43}$$

In this case the final dark matter density depends on ϕ properties only via $T_{\rm RH}$. Here, the relic density is proportional to the X' mass and also proportional to the reversed squared of its thermally averaged annihilation cross section.

If X' annihilation is efficient at $T_{\rm RH}$ and $\hat{T}_{\rm FO} < T_{\rm RH}$ we are back in the standard scenario. In such case the freeze–out happens when Hubble rate becomes equal to the annihilation rate of DM particles at relativistic and non–relativistic regimes. After freeze–out the abundance of DM will be roughly constant. Using $H \equiv n_{X',\rm EQ}\langle\sigma v\rangle'$ ($H_{rad} \propto A^{-2}$ in radiation dominated epoch and $\widetilde{H}_{rad} \simeq R^{1/2}$) and eq. (3.8) for non–relativistic number density, we can derive the approximate relic density of DM in the standard freeze–out scenario. The relic density for non–relativistic and relativistic dark matter particles in the radiation domination period can then be estimated as [7, 146]

$$\Omega h^2[\mathrm{FO}^{\rm rad}_{\rm nr}] \approx \frac{4\sqrt{5}}{\sqrt{\pi}} \frac{\hat{x}'_{\rm FO}}{g_{\rm eff}(\hat{T}_{\rm FO})^{1/2} M_{\rm Pl}\langle\sigma v\rangle'} \frac{g_{\rm eff}(T_F) h_{\rm eff}(T_{\rm now})}{2T_{\rm now} h_{\rm eff}(T_F)} \Omega_\gamma h^2 \,, \tag{3.44}$$

$$\hat{x}'_{FO} \equiv \frac{M_{X'}}{\hat{T}_{FO}} = \log\left(\frac{3}{8\pi^3}\sqrt{\frac{10}{g_{\rm eff}(\hat{T}_{\rm FO})}}\langle\sigma v\rangle' g_{X'} M_{X'} M_{\rm Pl} (\hat{x}'_{FO})^{1/2}\right) ; \tag{3.45}$$

$$\Omega h^2[\mathrm{FO}^{\rm rad}_{\rm r}] \approx \frac{30\zeta(3)}{\pi^4} \frac{\tilde{g}_{X'} M_{X'}}{g_{\rm eff}(\hat{T}_{\rm FO})} \frac{g_{\rm eff}(T_F) h_{\rm eff}(T_{\rm now})}{2T_{\rm now} h_{\rm eff}(T_F)} \Omega_\gamma h^2 \,. \tag{3.46}$$

If the annihilation of DM particles is inefficient at $T_{\rm RH}$, the DM relic will be affected by X' production during the early matter dominated era and the branching ratio for $\phi \to X'$ decay. Since most ϕ decays occur at $T \sim T_{\rm RH}$ when X' annihilation is assumed to be inefficient one can write [146]

$$\Omega_{X'} h^2 = \Omega_{\rm ann} h^2 + \Omega_{\rm decay} h^2 \,. \tag{3.47}$$

Using the third equation in (3.14) and eq. (3.25) along with ignoring the annihilation term of DM particles and assuming the approximation $e^{-\frac{2}{3}\left(\frac{c_\rho}{\Phi_I}\right)^{1/2}} \approx 1$ after integration we can compute the contribution $\Omega_{\rm decay} h^2$

between w and z is $z = w\, e^w$. In the limit $z \ll 1$ we have $f(z) \approx z$.

from ϕ decays which is given by

$$\Omega_{\rm decay}h^2 \approx \frac{B_{X'}T_{\rm RH}M_{X'}}{L^{3/4}M_\phi}\frac{g_{\rm eff}(T_F)h_{\rm eff}(T_{\rm now})}{2T_{\rm now}h_{\rm eff}(T_F)}\Omega_\gamma h^2\,. \tag{3.48}$$

The first contribution to the rhs of eq. (3.47) stems from the interactions of X' particles with the thermal plasma during the matter dominated epoch. Recall that we are assuming these interactions to be negligible at $T \sim T_{\rm RH}$. However, this does not exclude the possibility that X' might have been in equilibrium at higher temperatures, still in the matter dominated epoch, and decoupled at temperature $T_{\rm FO}$ with $T_{\rm max} > T_{\rm FO} > T_{\rm RH}$. This can happen only for dark matter particles that were non–relativistic at decoupling [146, 152], i.e. $M_{X'} > T_{\rm FO}$. Using $H_{mod} \equiv n_{X',\rm EQ}\langle\sigma v\rangle'$ ($H \propto A^{-3/2}$ in the early matter dominated epoch and $\widetilde{H}_{mod} \simeq \Phi_I^{1/2}$) and eq. (3.8) for non–relativistic equilibrium number density, we can derive the approximate relic density of DM produced via freeze–out during ϕ domination. This "modified non–relativistic freeze–out" scenario [38, 146] leads to

$$\Omega_{\rm ann}h^2[{\rm FO}^{\rm mod}_{\rm nr}] \approx \frac{8}{\sqrt{5\pi}}\frac{g_{\rm eff}(T_{\rm RH})^{1/2}}{L^{3/4}g_{\rm eff}(T_{\rm FO})}\frac{T_{\rm RH}^3 {x'_{FO}}^4}{{M_{X'}}^3 M_{\rm Pl}\langle\sigma v\rangle'}\frac{g_{\rm eff}(T_F)h_{\rm eff}(T_{\rm now})}{2T_{\rm now}h_{\rm eff}(T_F)}\Omega_\gamma h^2\,, \tag{3.49}$$

$$x'_{FO} \equiv \frac{M_{X'}}{T_{FO}} = \log\left[\frac{3}{2\sqrt{10}\pi^3}\frac{g_{X'}g_{\rm eff}(T_{RH})^{1/2}}{g_{\rm eff}(T_{FO})}\frac{M_{\rm Pl}}{M_{X'}}\langle\sigma v\rangle' T_{RH}^2 {x'_{FO}}^{5/2}\right]. \tag{3.50}$$

Note that here the contribution to the relic density is again inversely proportional to the annihilation cross section, as in the case of standard thermal WIMPs. However, the dependence on $T_{\rm RH}$ and $M_{X'}$ is quite different (and stronger) than in scenarios where X' annihilation is still efficient at $T \sim T_{\rm RH}$, c.f. eq. (3.43).

On the other hand, for sufficiently small annihilation cross section the X' density never reached equilibrium. As long as this cross section is not zero, there will nevertheless be a contribution to the dark matter relic density from X' pair production from the thermal plasma [38, 146]. This can be computed from

$$X'(A_F) \approx \frac{c_1^{1/2}M_{\rm Pl}\langle\sigma v\rangle'}{T_{RH}^5}\int_{A_{max}}^{A_F} dA\,\frac{A^{7/2}n^2_{X',\rm EQ}}{\widetilde{H}}\,, \tag{3.51}$$

where $A_{max} \equiv (8/3)^{2/5}$. Using eq. (3.8) and assuming $x = M_{X'}/T$ we obtain [146]

$$X'(A_F) \approx \frac{192}{(125\pi^7)^{1/2}}\frac{T_{RH}^7 M_{\rm Pl}\langle\sigma v\rangle'\Phi_I}{M_{X'}^{12}}\frac{g_{\rm eff}^{3/2}(T_{RH})}{g_{\rm eff}^3(T_*)}\int_{\frac{M_{X'}}{T_{max}}}^{\frac{M_{X'}}{T_F}} dx'\,{x'}^{11}n^2_{X',\rm EQ}\,, \tag{3.52}$$

where T_* is the temperature at which the integrand reaches its maximum. For non–relativistic X' the equilibrium number density can be treated as Maxwell–Boltzmann distribution so in this case the integral is [146]

$$\int_{\frac{M_{X'}}{T_{max}}}^{\frac{M_{X'}}{T_F}} dx'\,{x'}^{11}n^2_{X',\rm EQ} = \frac{g_{X'}^2 M_{X'}^6}{4\pi^4}\int_{\frac{M_{X'}}{T_{max}}}^{\frac{M_{X'}}{T_F}} dx'\,{x'}^9 K_2(x')^2\,. \tag{3.53}$$

This integrand peaks at $x \simeq 3.6$ and $T_* \simeq 0.28M_{X'}$. In the limits $T_{max} \gg T_{RH}$ ($T_{max} \to \infty$) and $T_F \ll T_{RH}$ ($T_F \to 0$), we have the following estimation for the integral of eq. (3.53)

$$\chi \equiv \int_{\frac{M_{X'}}{T_{max}}}^{\frac{M_{X'}}{T_F}} dx'\; x'^9 K_2(x')^2 \approx \int_0^\infty dx'\; x'^9 K_2(x')^2 \simeq 292.571\,. \tag{3.54}$$

When the DM is relativistic and produced via inverse annihilation of SM particles we can compute the following integral using the assumption $T_* \approx T_{RH}/2$ [38, 146]

$$\int_{\frac{M_{X'}}{T_{max}}}^{\frac{M_{X'}}{T_F}} dx'\; x'^{11} n^2_{X',\mathrm{EQ}} = \frac{\zeta(3)^2 \tilde{g}^2_{X'} M^6_{X'}}{\pi^4} \int_{\frac{M_{X'}}{T_{max}}}^{\frac{M_{X'}}{T_F}} dx'\; x'^5 \approx \frac{2^6 \zeta(3)^2 \tilde{g}^2_{X'} M^6_{X'}}{6\pi^4 T^6_{RH}}\,, \tag{3.55}$$

where the degrees of freedom for the number density of relativistic bosons (fermions) is denoted by $\tilde{g}_{X'} = g_{X'}(3g_{X'}/4)$ as before. Using eqs. (3.30), (3.52), (3.53), and (3.55) the relic abundance of DM in case produced inversely from SM bath can be computed. As a consequence, the "inverse annihilation" contribution both for relativistic ($M_{X'} \ll T_{\rm RH}$) and for non–relativistic ($M_{X'} \gg T_{\rm RH}$) X' particles [38, 146]

$$\Omega_{\rm ann}h^2[\mathrm{IA_{nr}}] \approx \frac{48\,\chi\, g^2_{X'}}{5^{3/2}\pi^{15/2}L^{3/4}} \frac{g_{\rm eff}(T_{RH})^{3/2} T^7_{\rm RH} M_{\rm Pl}\langle\sigma v\rangle'}{g_{\rm eff}(T_*)^3 {M_{X'}}^5} \frac{g_{\rm eff}(T_F) h_{\rm eff}(T_{\rm now})}{2T_{\rm now} h_{\rm eff}(T_F)} \Omega_\gamma h^2\,; \tag{3.56}$$

$$\Omega_{\rm ann}h^2[\mathrm{IA_r}] \approx \frac{32\zeta(3)^2 \tilde{g}^2_{X'} 2^6}{5^{3/2}\pi^{15/2}L^{3/4}} \frac{T_{RH} M_{X'} M_{\rm Pl}\langle\sigma v\rangle'}{g_{\rm eff}(T_{\rm RH})^{3/2}} \frac{g_{\rm eff}(T_F) h_{\rm eff}(T_{\rm now})}{2T_{\rm now} h_{\rm eff}(T_F)} \Omega_\gamma h^2\,. \tag{3.57}$$

Note that this contribution is directly proportional to the annihilation cross section (which equals the X' pair production cross section); this is true also in standard cosmology if the dark matter particles never attained equilibrium, e.g. because the temperature was too low [153]. In the non–relativistic case the dependence on $T_{\rm RH}$ and $M_{X'}$ is very strong. The production of X' particles that were non–relativistic at $T_{\rm RH}$ peaks at $T_* \simeq 0.28 M_{X'}$, when the dark matter particles were in fact semi–relativistic. Note that eq. (3.56) is valid only if $T_{\rm max}$ is larger than T_*; otherwise this contribution is exponentially suppressed. In contrast, the production of relativistic X' particles peaks at $T_* \simeq T_{\rm RH}/2$.

Altogether one can thus distinguish seven different X' production mechanisms: $\mathrm{QSE_{nr}}$, $\mathrm{FO^{rad}_{nr}}$, $\mathrm{FO^{rad}_{r}}$, $\phi-$decay, $\mathrm{FO^{mod}_{nr}}$, $\mathrm{IA_r}$, and $\mathrm{IA_{nr}}$. They dominate in different regions of parameter space. Of course, these regions are smoothly connected, i.e. one can interpolate between these different regions.

Parameter regions where these different X' production mechanisms are dominant are indicated in Fig. 3.2 (and also 3.3, 3.4, and 3.5). Here and in the subsequent figures we use eq. (3.4) with $\alpha = 1$ to compute the total ϕ decay width, which in turn determines the reheat temperature via eq. (3.1). In this figure we have assumed a rather heavy ϕ particle, and hence a value of $T_{\rm RH}$ well above the temperature of the QCD deconfinement transition. Moreover, we have assumed a constant ($S-$wave) X' annihilation cross section, and fixed $B(\phi \to X') = 10^{-5}$. We do not consider values of $M_{X'}$ below 10 MeV, since for $M_{X'} \ll T_{\rm RH}$ the early $\phi-$matter dominated epoch becomes essentially irrelevant. On the other hand, we restrict ourselves to $M_{X'}$ values below a few percent of M_ϕ, since otherwise the approximation of instantaneous thermalization of ϕ decay products might loose its validity as remarked above.

We see that for $M_{X'} \leq T_{\rm RH}$ one recovers the results of standard cosmology. In particular, in the top–left part of Fig. 3.2 one recognizes the usual WIMP strip, where $\Omega_{\rm DM}h^2$ comes out near the desired value if $\langle\sigma v\rangle' \sim 10^{-8}$ GeV^{-2}. Recall that the freeze–out temperature in the radiation dominated epoch $\hat{T}_{\rm FO}$ is about $M_{X'}/20$; for $\langle\sigma v\rangle' \gtrsim 10^{-15}$ GeV^{-2} large deviations from standard cosmology therefore become evident only for $M_{X'} \geq 10$ GeV, which corresponds to $\hat{T}_{\rm FO} \gtrsim T_{\rm RH}$.

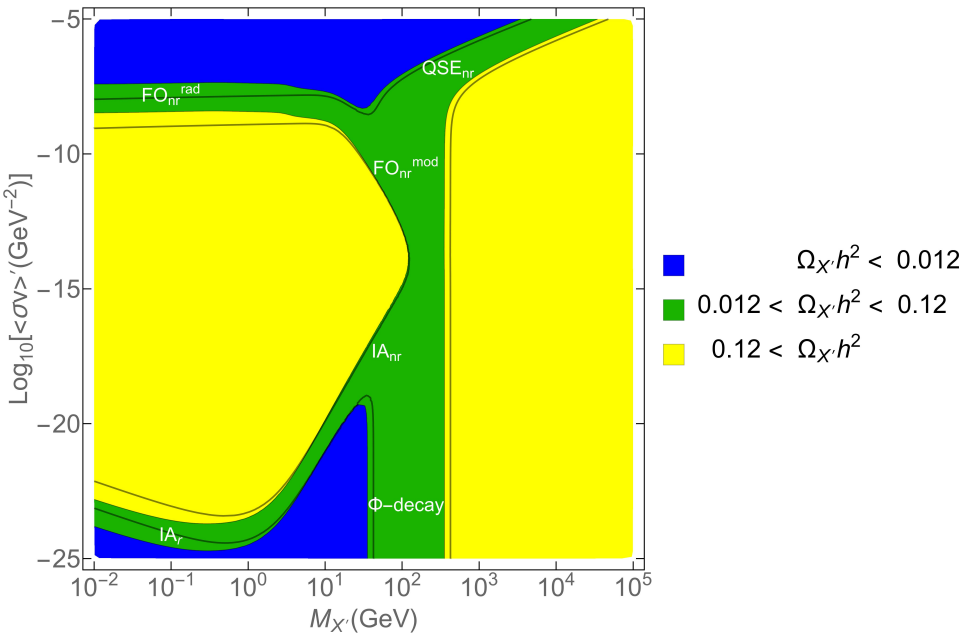

Figure 3.2: The dark matter relic density for $M_\phi = 5\times10^6$ GeV, corresponding to reheating temperature $T_{\rm RH} = 848.5$ MeV, $g_{\rm eff}(T_{RH}) = 73.46$, and branching ratio $B(\phi \to X') = 10^{-5}$. The dark matter mass $M_{X'}$ and the $S-$wave annihilation cross section $\langle\sigma v\rangle' = a$ are given on the $x-$ and $y-$axis, respectively. The colored regions represent different bins of the final dark matter relic density, computed including the full temperature dependence of $g_{\rm eff}$ and $h_{\rm eff}$, whereas the solid lines are contours of constant $\Omega_{X'}h^2 = 0.12$ (deeper inside the yellow region) and 0.012, respectively, under the approximation $g_{\rm eff} = h_{\rm eff} = g_{\rm eff}(T_{\rm RH})$.

Still in the region of small $M_{X'}$ another region with roughly correct DM relic density can be seen for much smaller cross sections. In this "inverse annihilation" region there is sufficient X' pair production from the thermal plasma, but the X' density never reaches thermal equilibrium. The results of standard cosmology are now only recovered for $M_{X'} \lesssim T_{\rm RH}$; in this part of parameter space the "inverse annihilation" mechanism can be considered to be an example of the freeze–in mechanism [145]. A review of models and constraints on DM produced via freeze–in mechanism is done in [154].

For larger $M_{X'}$ the standard WIMP region merges into a region where the correct relic density is acquired via thermal freeze–out in the ϕ matter dominated epoch. Note that this requires significantly smaller X' annihilation cross section than in the WIMP region. The reason is that here the X' density keeps getting diluted by the entropy produced by ϕ decays; recall that the relic density is inversely proportional to the annihilation cross section in both freeze–out regions, see eqs. (3.44) and (3.49).

The latter of these equations also shows that in this region the cross section required to obtain the desired relic density scales like $M_{X'}^{-3}$. As $M_{X'}$ is increased the cross section therefore rather quickly becomes too small for X' to achieve full thermal equilibrium. We should remember that the Hubble parameter in the ϕ dominated epoch is (much) larger than in the radiation dominated epoch at the same temperature, requiring a correspondingly larger cross section to obtain equilibrium. Nevertheless in Fig. 3.2 the region where the DM density for X' masses in the typical WIMP region (between 100 and 1000 GeV) comes out roughly correctly extends to very small cross sections, the dominant production mechanism being "inverse annihilation" or, for even smaller $\langle\sigma v\rangle'$, direct $\phi \to X'$ decays.

Finally, there is another region with roughly correct relic density in Fig. 3.2, where the X' annihilation cross section is significantly larger than that required for thermal WIMPs in standard cosmology. Here

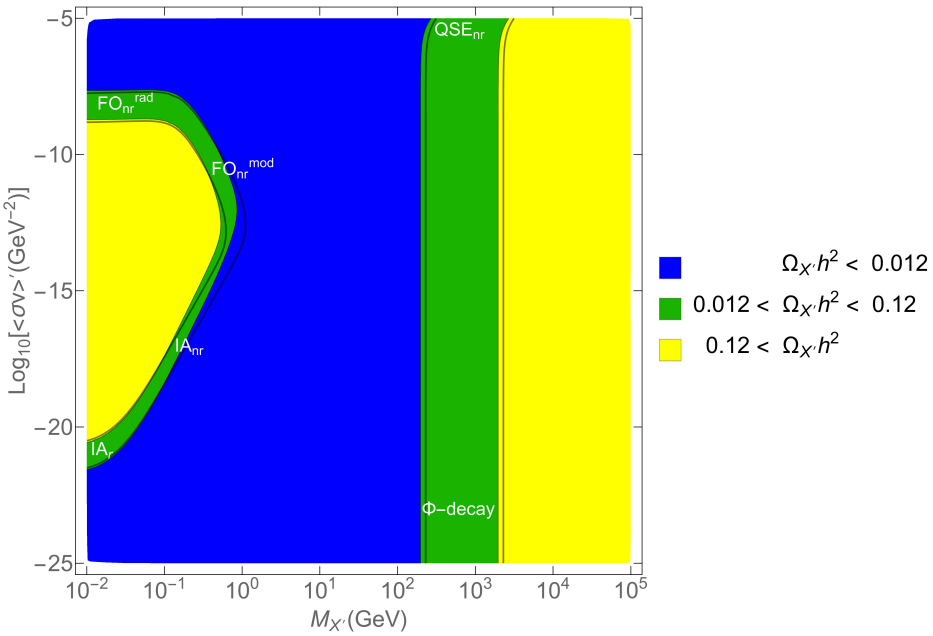

Figure 3.3: The dark matter relic density for reheating temperature $T_{\rm RH} = 10$ MeV, corresponding to $M_\phi = 1.88{\times}10^5$ GeV, $g_{\rm eff}(T_{RH}) = 10.84$, and branching ratio $B(\phi \to X') = 10^{-5}$. The $x-$ and $y-$axis represent the dark matter mass $M_{X'}$ and the $S-$wave annihilation cross section $\langle\sigma v\rangle' = a$, respectively. The details of colored regions are shown in the legend in the right hand side of figure. The solid lines are contours of constant $\Omega_{X'}h^2 = 0.12$ (deeper inside the yellow region) and 0.012, respectively, under the approximation $g_{\rm eff} = h_{\rm eff} = g_{\rm eff}(T_{\rm RH})$ (like Fig. 3.2).

quasi–static equilibrium between X' production from ϕ decays and X' annihilation is attained. Eq. (3.43) shows that here the required cross section scales like $M_{X'}$. This region therefore merges with the "modified freeze–out" region for $M_{X'} \simeq 100$ GeV, but allows to reproduce the correct relic density for very large X' annihilation cross sections if the X' mass is sufficiently large[9].

Note that in Fig. 3.2 the DM relic density comes out roughly correctly for $M_{X'}$ of a few hundred GeV almost independently of the X' annihilation cross section, as long as the latter does not exceed a few times 10^{-7} GeV^{-2}. This remains true [146] also for lower $T_{\rm RH}$, corresponding to lower α and/or lower M_ϕ; however, the ϕ decay region then directly merges into the QSE$_{\rm nr}$ region. Moreover, in Fig. 3.2 all regions with approximately correct relic density are continuous. This is no longer the case for lower $T_{\rm RH}$, where thermal effects are important only for smaller X' masses; if the effective branching ratio $B_{\rm eff}$ is kept fixed, there is then an extended region of X' masses where the X' relic density is always too low, independent of the X' annihilation cross section [146].

Similar regions for different production mechanisms like the ones in Fig. 3.2 are shown in Figs. 3.3, 3.4, and 3.5 for reheating temperatures 10 MeV, 40 MeV, and 150 MeV (corresponding to moduli masses $M_\phi = 1.88 \times 10^5$ GeV, $M_\phi = 4.94 \times 10^5$ GeV, and $M_\phi = 1.34 \times 10^6$ GeV), respectively. Other features of these last three figures are the same as Fig. 3.2.

These gross features are not affected by an accurate treatment of the number of degrees of freedom in the thermal plasma. However, the solid contours in Fig. 3.2 show that simply taking $g_{\rm eff} = h_{\rm eff} = g_{\rm eff}(T_{\rm RH})$, which seems to have been the approach used in ref. [146], can lead to sizable errors of the final DM relic density. This is further illustrated in Fig. 3.6, where we show the predicted DM relic density as

[9] The possibility to obtain the correct relic density in moduli–dominated scenarios where the annihilation cross section is too large for the normal thermal WIMP scenario was to our knowledge first discussed in ref. [155].

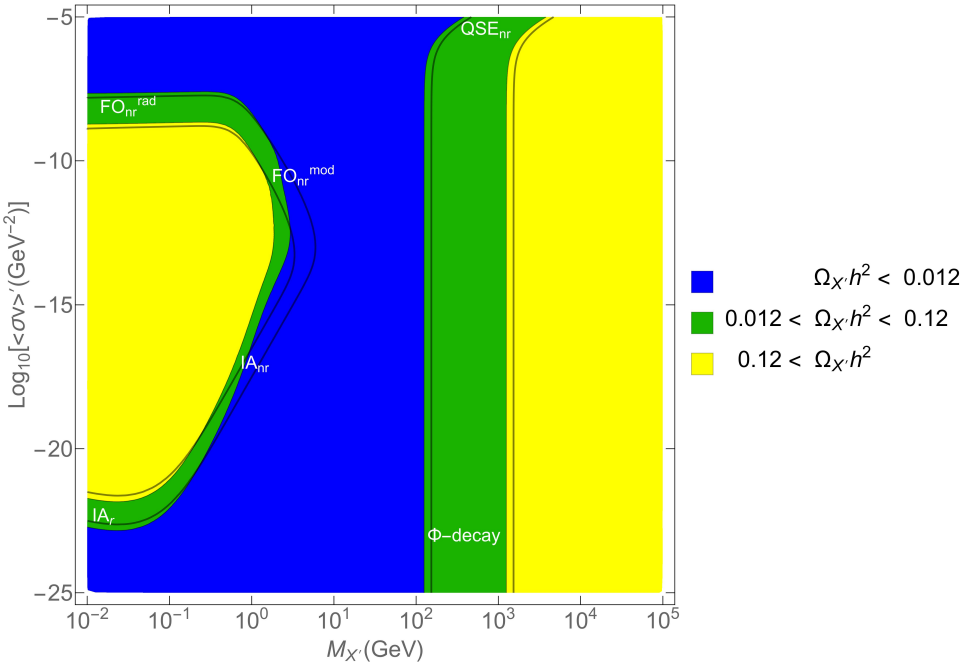

Figure 3.4: The dark matter relic density for reheating temperature $T_{\rm RH} = 40$ MeV, corresponding to modulus mass $M_\phi = 4.94 \times 10^5$ GeV, $g_{\rm eff}(T_{RH}) = 13.84$, and branching ratio $B(\phi \to X') = 10^{-5}$. The $x-$ and $y-$axis represent the dark matter mass $M_{X'}$ and the $S-$wave annihilation cross section $\langle\sigma v\rangle' = a$, respectively. The details of colored regions are shown in the legend in the right hand side of figure. The solid lines are contours of constant $\Omega_{X'}h^2 = 0.12$ (deeper inside the yellow region) and 0.012, respectively, under the approximation $g_{\rm eff} = h_{\rm eff} = g_{\rm eff}(T_{\rm RH})$ (like Fig. 3.2).

function of $M_{X'}$. The solid, dashed and dash–dotted curves have been obtained by correctly treating the full temperature dependence of $g_{\rm eff}$ and $h_{\rm eff}$, by keeping $g_{\rm eff}$ and $h_{\rm eff}$ dependent on temperature but setting $d\,h_{\rm eff}/d\,T = 0$ in eq. (3.17), and by setting $g_{\rm eff} = h_{\rm eff} = g_{\rm eff}(T_{\rm RH})$ everywhere, respectively.

We see that this last choice can over–predict the relic density by as much as two orders of magnitude; see the blue (top) curves for $M_{X'} \simeq 3$ GeV. Here the relic density is determined by freeze–out during the ϕ matter dominated epoch, with $T_{\rm FO}$ not far from the QCD transition temperature where $g_{\rm eff}$ and $h_{\rm eff}$ vary quickly. In this example, $T_{\rm RH} = 40$ MeV is well below the QCD transition, with $g_{\rm eff}(T_{\rm RH}) = 13.84$. Above the QCD deconfinement transition the actual $g_{\rm eff}$ is much higher, which means that the actual temperature is lower than that predicted in the approximation $g_{\rm eff} = h_{\rm eff} = g_{\rm eff}(T_{\rm RH})$.

Moreover, setting the $dh_{\rm eff}/dT = 0$ over–predicts the relic density by about a factor of three even for large X' masses, where the relic density is set by direct $\phi \to X'$ decays, which are independent of the thermal plasma. The reason is that the final physical DM density is obtained by normalizing the dimensionless co–moving density X' to the radiation energy density (or, equivalently, to the entropy density). Unlike in standard cosmology, the co–moving entropy density is not constant during the epoch of ϕ matter domination; the actual temperature, or entropy density, depends on the number of degrees of freedom in the thermal plasma. Moreover, if one uses eq. (3.15) to compute the entropy density, including the T dependence of $h_{\rm eff}$ but setting $dh_{\rm eff}/dT = 0$ or, equivalently, if one uses the second eq. (3.14) to describe the evolution of the radiation component, the entropy density s_R will not be conserved in the radiation–dominated epoch after ϕ decay.

This is further illustrated by Fig. 3.7, where we plot the rescaled dimensionless temperature $\bar{T} =$

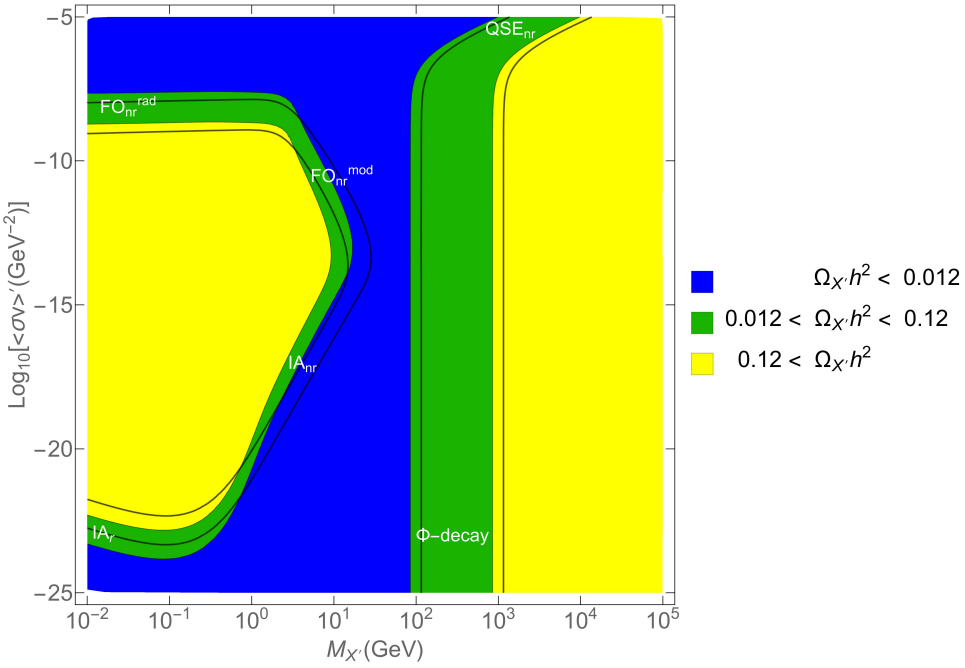

Figure 3.5: The dark matter relic density for reheating temperature $T_{\rm RH} = 150$ MeV, corresponding to $M_\phi = 1.34 \times 10^6$ GeV, $g_{\rm eff}(T_{RH}) = 27.82$, and branching ratio $B(\phi \to X') = 10^{-5}$. The $x-$ and $y-$axis represent the dark matter mass $M_{X'}$ and the $S-$wave annihilation cross section $\langle\sigma v\rangle' = a$, respectively. The details of colored regions are shown in the legend in the right hand side of figure. The solid lines are contours of constant $\Omega_{X'}h^2 = 0.12$ (deeper inside the yellow region) and 0.012, respectively, under the approximation $g_{\rm eff} = h_{\rm eff} = g_{\rm eff}(T_{\rm RH})$ (like Fig. 3.2).

$TA/T_{\rm RH}$ as a function of A for $T_{\rm RH} = 40$ MeV and $H_I = 10^{15}\Gamma_\phi$, which determines Φ_I via $\Phi_I = 3H_I^2 M_{\rm Pl}^2/(8\pi T_{\rm RH}^4)$. Note that $\bar{T}$ approaches a constant in the radiation dominated epoch if $g_{\rm eff}$ and $h_{\rm eff}$ are constant. Since we assume initial temperature $T_I = 0$, [10] see eq. (3.24), the universe goes through the QCD transition twice in this example: once early on, during the rapid heating phase which peaks at the maximal temperature estimated in eq. (3.20), and then again for much larger A, but (in this example) still in the ϕ matter dominated epoch. The case of $A < A_{max}$ for different evaluation of degrees of freedom is shown in Fig. 3.8, all parameters are chosen like Fig. 3.7. This effect for very small scale factors is not visible in Fig. 3.7. Since $dh_{\rm eff}(T)/dT \geq 0$ everywhere, the prefactor on the rhs of eq. (3.17) always tends to slow down the evolution of T, or $\bar{T}$, with A. This implies a slower increase of T, and hence a reduced $T_{\rm max}$, during reheating, but also a slower decline of T when the universe undergoes the QCD transition for a second time. In particular, the simplified treatment with $g_{\rm eff}(T) = g_{\rm eff}(T_{\rm RH})$ will considerably overestimate the temperature, and hence thermal X' production, as long as $T > T_{\rm QCD}$, as remarked above.

Note that in the ϕ matter dominated epoch the radiation content of the universe is basically determined by ϕ decays occurring in the previous $O(1)$ Hubble times; the radiation produced even earlier is quickly redshifted and becomes irrelevant after a few Hubble times. Hence $\rho_R(T)$, or T itself, basically depends on $g_{\rm eff}$ and $h_{\rm eff}$ only at temperatures $T \simeq T_{RH}$. Therefore the curves in Fig. 3.7 essentially coincide in the range of temperatures where $g_{\rm eff}(T) \simeq g_{\rm eff}(T_{\rm RH})$.

Finally, the curves diverge again at very large A, well after all ϕ particles have decayed. This is due to the decoupling of e^+e^- pairs, which increases the photon temperature by a factor 1.4 relative to

[10] Effectively, the numerical value of initial temperature is $T_I = 10^{-13}$ GeV.

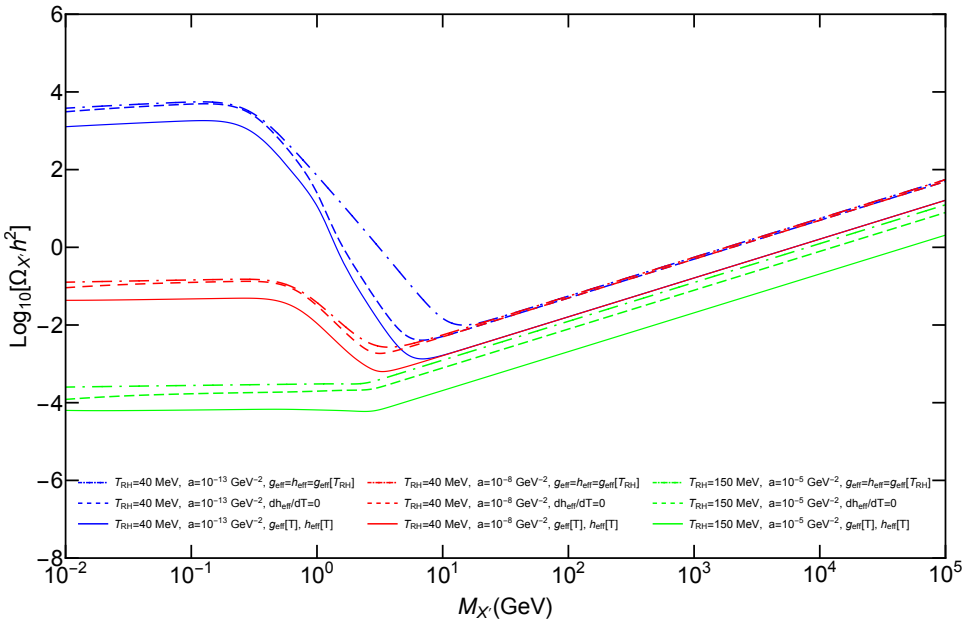

Figure 3.6: The predicted DM relic density as function of the DM mass $M_{X'}$. Different colors refer to different choices of input parameters, as indicated in the frame. The dot–dashed curves have been obtained by setting $g_{\rm eff} = h_{\rm eff} = g_{\rm eff}(T_{\rm RH})$ everywhere. The other curves use a temperature dependent $g_{\rm eff}$ when calculating ρ_R, but the dashed curves have been obtained by setting $dh_{\rm eff}/dT = 0$.

a calculation where this effect is ignored. Of course, in the case at hand one could have chosen to terminate the numerical solution of the evolution equations at a value of A_F such that $T_F > m_e$ while still satisfying $T_F \ll T_{\rm RH}$. Still, this feature shows that an accurate description of the evolution of the universe in scenarios with a ϕ matter dominated epoch requires a careful treatment of the temperature dependence of $g_{\rm eff}$ and $h_{\rm eff}$ over the entire range of temperatures.

The outcome of this discussion is that a simplified treatment that ignores the temperature dependence of $g_{\rm eff}$ and $h_{\rm eff}$ will produce reliable results only if the final temperature T_F is chosen that $g_{\rm eff}(T_F) \simeq g_{\rm eff}(T_{\rm RH})$, and if thermal X' production mechanisms are irrelevant at all temperatures T where $g_{\rm eff}(T) \neq g_{\rm eff}(T_{\rm RH})$. The former condition can only be satisfied if $g_{\rm eff}$ remains essentially constant for an extended range of temperatures around $T_{\rm RH}$, which in particular is not the case if $T_{\rm RH}$ is near the QCD transition temperature. Since the "(modified) freeze–out" and the "inverse annihilation" contributions to the X' relic density depend on some range of temperatures $T > T_{\rm RH}$ the question whether the second condition is satisfied depends on several parameters $(T_{\rm RH}, M_{X'}, \langle\sigma v\rangle', B_{X'})$ in a rather complicated manner.

So far we have assumed the thermally averaged X' cross section to be a constant. This is a good approximation for non–relativistic X' particles annihilating dominantly from $S-$wave initial states. In Fig. 3.9 we compare this to results assuming $\langle\sigma v\rangle' = 6bT/M_{X'}$ with constant b. This reproduces the correct temperature dependence for non–relativistic particles annihilating from a $P-$wave initial state. Since $T/M_{X'} \simeq 0.05$ for freeze–out in the radiation–dominated epoch, $6b$ needs to be more than one order of magnitude larger than a in order to obtain the correct relic density in the usual WIMP scenario. The difference between the allowed regions is much less in the green strip to the right, where thermal effects are either irrelevant ($\phi-$decay region) or peak at temperatures not far from $M_{X'}$ (inverse annihilation region); the one exception occurs in the QSE region, where the relevant temperature again satisfies

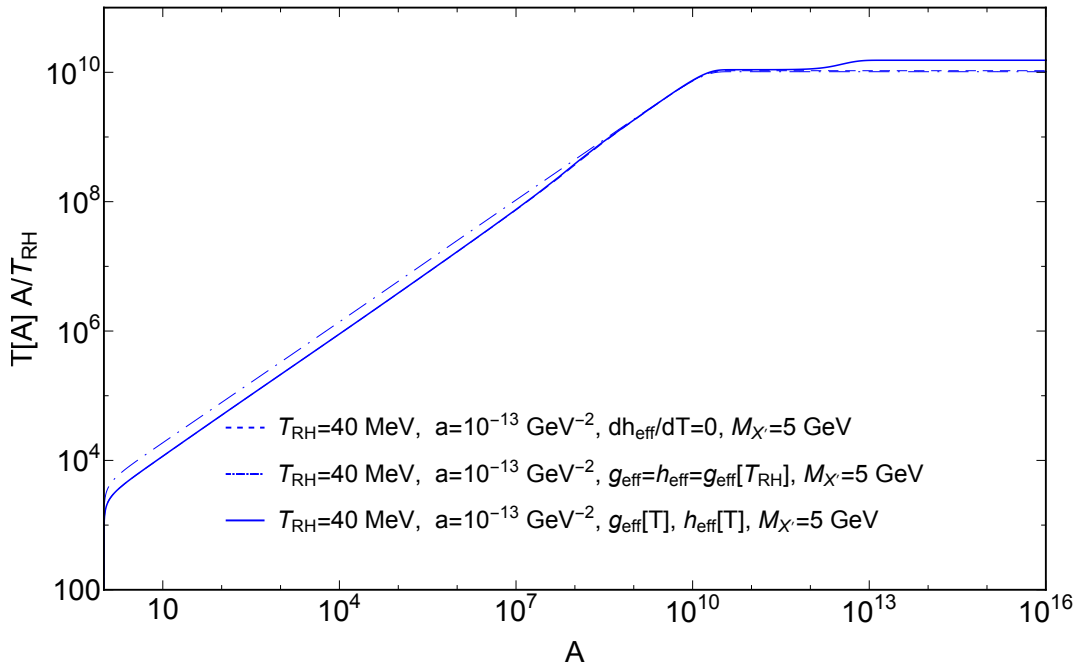

Figure 3.7: Evolution of the scaled temperature with A.

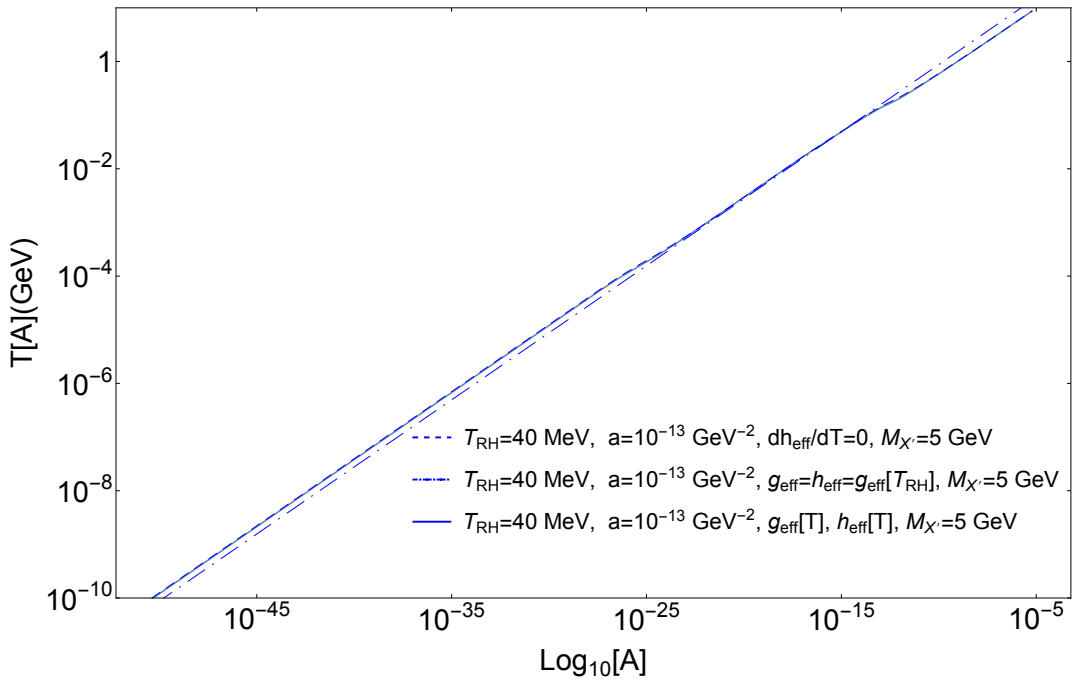

Figure 3.8: Evolution of temperature with A for very small scale factors which follows the evolution of degrees of freedom even before the temperature reaches T_{max}.

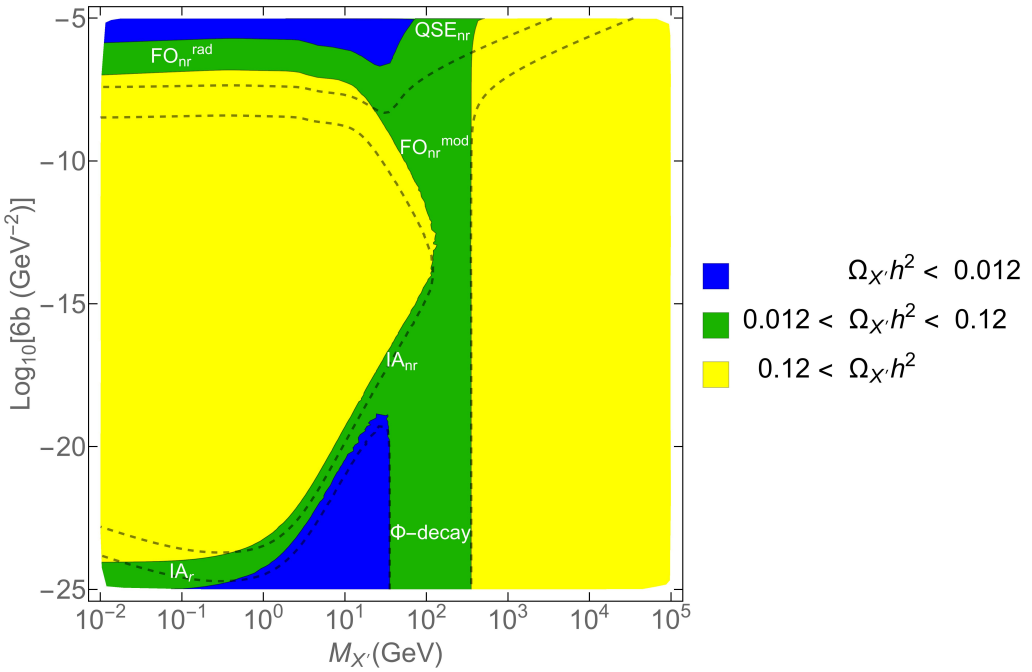

Figure 3.9: Contours of different values of the DM relic density with mass $M_\phi = 5 \times 10^6$ GeV, corresponding to $T_{\rm RH} = 848.5$ MeV. The dashed lines correspond to $\Omega_{X'}h^2 = 0.12$ (for the lines deeper inside the yellow region) and 0.012 assuming a constant cross section $\langle\sigma v\rangle' = a$, whereas the colored regions have been obtained assuming a constant parameter $6b$ in $\langle\sigma v\rangle' = 6bT/M_{X'}$.

$T \ll M_{X'}$. The biggest change occurs in the relativistic inverse annihilation region. In fact, using a constant ($T-$independent) annihilation cross section for $M_{X'} \ll T$ is unphysical; if X' particles annihilate via the exchange of mediators whose mass exceeds T, one instead expects $\langle\sigma v\rangle' \propto T^2$, i.e. an even stronger $T-$dependence. The difference in slope between the green strip and the region between the dashed curves at small X' masses and small cross sections therefore indicates that the treatment used in ref. [146] is not reliable in our discussion. However, since this concerns the region of parameter space that is not affected by the early $\phi-$dominated epoch, we will not pursue this issue any further.

In Figs. 3.10 we explore the dependence of the DM relic density on the ϕ mass and the effective branching ratio for $\phi \to X'$ decays. In these figures the temperature dependence of $g_{\rm eff}$ and $h_{\rm eff}$ has been treated carefully, but for simplicity we have assumed $\langle\sigma v\rangle' = a$ to be independent of temperature; the six frames correspond to different values of a, with fixed $M_{X'} = 100$ GeV (a typical value for a WIMP). Note that we have used eq. (3.4) with $\alpha = 1$ to compute the total ϕ decay width, which in turn determines the reheat temperature via eq. (3.1); hence $T_{\rm RH}$ scales like $M_\phi^{3/2}$ in these figures.

In frame (a) we have chosen a rather large X' annihilation cross section. Consequently the relic density is very low, unless M_ϕ is rather small (so that $T_{\rm RH}$ is well below $\hat{T}_{\rm FO}$) and $B_{X'}$ is sizable. One is then in the QSE$_{\rm nr}$ region of parameter space, where the relic density scales like $T_{\rm RH}^{-3} M_\phi$ or $M_\phi^{-7/2}$, see eq. (3.43). Note that the cross section required to achieve quasi–static equilibrium scales like $1/B_{X'}^{1/2}$.

Recall that in this region of parameter space the relic density is proportional to the inverse squared of the X' annihilation cross section. Hence the region with too high relic density is considerably larger in frame (b), which has one hundred times smaller $\langle\sigma v\rangle'$. In fact, now the relic density is in the cosmologically interesting range even in standard cosmology, which explains the large green region at large M_ϕ, where $T_{\rm RH} \geq \hat{T}_{\rm FO}$.

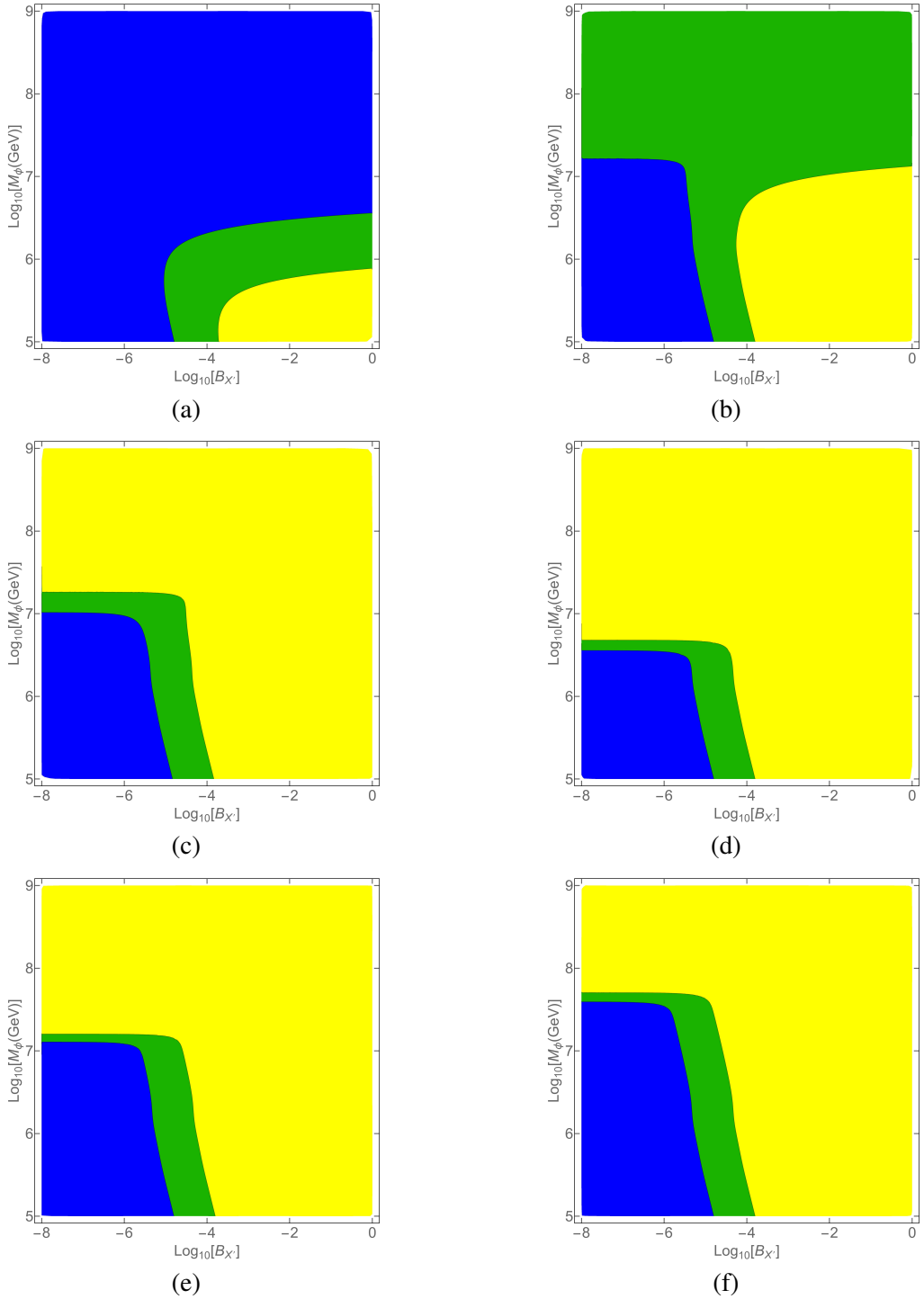

Figure 3.10: Contours of different values of DM relic density in the plane spanned by the modulus mass M_ϕ and the $\phi \to X'$ decay branching ratio $B_{X'}$. We have fixed the dark matter mass to $M_{X'} = 100$ GeV and different thermally averaged cross sections, taken to be independent of temperature. The thermally averaged cross section $\langle \sigma v \rangle'$ in the figures is a) 10^{-6} GeV^{-2}, b) 10^{-8} GeV^{-2}, c) 10^{-9} GeV^{-2}, d) 10^{-14} GeV^{-2}, e) 10^{-20} GeV^{-2}, f) 10^{-25} GeV^{-2}, respectively. These results have been obtained using a careful treatment of the temperature dependence of $h_{\rm eff}$ and $g_{\rm eff}$. The colors are as in Fig. 3.2.

In the four remaining frames the X' annihilation cross section is below that required for a thermal WIMP in standard cosmology. The final DM density will then always be too large if $B_{X'} > 10^{-4}$; for these small cross sections, there is no mechanism to sufficiently reduce a large X' density produced directly from ϕ decays. Note that even if ϕ particles do not directly couple to X' particles, ϕ decays into two SM particles plus two X' particles (or an $X'\bar{X}'$ pair, if X' is not self–conjugate) will in general still occur [148]. However, the resulting branching ratio is expected to correlate with $\langle\sigma v\rangle'$, so that a small cross section also implies a small branching ratio for these four–body modes, since both processes depend on the coupling of X' to SM particles.

Even if $B_{X'} < 10^{-4}$, the relic density will be too large for X' particles with annihilation cross section below that of standard thermal WIMPs if M_ϕ is too large. Recall that large M_ϕ implies large $T_{\rm RH}$ and hence (too) large contribution to the X' density either from inverse annihilation or, for yet larger M_ϕ, from the standard thermal freeze–out scenario.

The former dominates in the green regions at small $B_{X'}$ in the last three frames of Fig. 3.10. For the chosen DM mass $M_{X'} = 100$ GeV, we see that $M_\phi \lesssim 10^7$ GeV is required, unless the X' annihilation cross section is many orders of magnitude below that of thermal WIMPs. For non–relativistic X' particles the annihilation cross section often scales like $M_{X'}^{-2}$. In this case we find numerically that the upper bound on M_ϕ scales roughly like $M_{X'}^{2/3}$. This agrees with the estimate of eq. (3.56) for the contribution to the DM relic density from inverse annihilation during the ϕ matter dominated epoch. The same equation also shows that the upper bound on M_ϕ will scale like $M_{X'}^{10/21}$, or roughly like $\sqrt{M_{X'}}$, if we keep the annihilation cross section independent of $M_{X'}$; whereas for fixed X' mass, the lower bound on M_ϕ will scale like $(\langle\sigma v\rangle')^{-2/21}$, which explains why the blue region in the last three frames of Fig. 3.10 only grows rather slowly even though the annihilation cross section is reduced by more than 10 orders of magnitude.

3.4 Dependence on Initial Conditions

In the previous Section we had assumed that the radiation and X' densities initially vanish exactly. This is completely realistic only if ϕ is a (weakly coupled) inflaton decaying purely perturbatively into X' particles and/or radiation. In contrast, in moduli cosmology one assumes that inflaton decay first reheats the universe as usual. However, ϕ attains a large value during inflation, so that eventually its density dominates the total energy density. In this case the temperature will not be zero at any time after inflaton decay. Of course, it stands to reason that if the epoch of ϕ domination is sufficiently long, the initial temperature will not matter, so imposing eqs. (3.24) will be a good approximation. In this Section we investigate quantitatively what impact a non–vanishing radiation content can have.

Even if at some sufficiently early time the universe is radiation dominated, $\rho_R > \rho_\phi$, eventually these two densities will become equal if ϕ particles are sufficiently long–lived, since the ratio ρ_ϕ/ρ_R ($\rho_\phi \propto a^{-3}$ and $\rho_R \propto a^{-4}$) increases proportional to the scale factor a. For a short time after this, the total radiation density will still be dominated by the "primordial" component. In this "adiabatic regime" (in the notation of ref. [156]) the temperature $T \propto a^{-1}$ because of entropy conservation. In the subsequent "non–adiabatic regime", most radiation already comes from ϕ decay and $T \propto a^{-3/8}$ as in eq. (3.19). Note that (after inflaton decay) the temperature of the universe never increases in this scenario, as already pointed out in ref. [7].

It would be tempting to simply define our "initial" time, and "initial" scale factor, such that $\rho_{\phi,I} = \rho_{R,I}$. However, the case with initially vanishing radiation density could then not be covered. Moreover, at this initial time our dimensionless scale factor A would usually not be equal to 1. We therefore prefer to define our initial conditions such that $A = 1$, and describe the initial radiation density through the

dimensionless parameter

$$\mu = \frac{\rho_{R,I}}{\rho_{\phi,I}} \,. \tag{3.58}$$

The case covered in the previous Section obviously corresponds to $\mu = 0$, but very large (positive) values of μ are in principle possible which leads to radiation domination. We assume that the energy density of dark matter particles is initially negligible compared to $\rho_\phi + \rho_R$. This should be a good approximation even if the initial temperature $T_I \geq M_{X'}$ and X' particles were in full equilibrium, simply because the total number of relativistic degrees of freedom should be much larger than $\tilde{g}_{X'}$. The initial Hubble parameter is then given by

$$H_I^2 = \frac{8\pi}{3M_{\rm Pl}^2}\left(\rho_{\phi,I} + \rho_{R,I}\right) = \frac{8\pi\Phi_I T_{\rm RH}^4}{3M_{\rm Pl}^2}\,(1+\mu) \,. \tag{3.59}$$

In the second equality of above equation we changed the variables as introduced in eq. (3.10). In our numerical examples we take H_I (in units of Γ_ϕ) and μ as free parameters. The initial co–moving densities of scalar and radiation can then be written as

$$\begin{aligned} \Phi_I &= \frac{3M_{\rm Pl}^2 H_I^2}{8\pi T_{\rm RH}^4\,(1+\mu)} \,, \\ R_I &= \mu\Phi_I \,. \end{aligned} \tag{3.60}$$

So using eq. (3.13) we define the initial temperature as

$$T_I = T_{\rm RH}\left(\frac{30}{\pi^2 g_{\rm eff}(T_I)} R_I\right)^{\frac{1}{4}} \,. \tag{3.61}$$

In our numerical analyses we take $g_{\rm eff}(T_I) = 106.75$ (Table 2.1 of Chapter 2), which is the total number of degrees of freedom in the Standard Model if $T \gg m_t$ (top quark mass).

After the initial time, but before most ϕ particles have decayed, the dimensionless Hubble parameter $\widetilde{H}$ can be estimated as

$$\widetilde{H} \simeq \Phi_I^{\frac{1}{2}}\left(1 + \frac{\mu}{A}\right)^{\frac{1}{2}} \,, \tag{3.62}$$

where we again have neglected the contribution from X' particles. Evidently the second term on the rhs of eq. (3.62) becomes negligible once $A \gg \mu$; in this epoch the universe is again matter dominated. Recall, however, that ϕ particles do eventually decay at $A \simeq A_{\rm decay}$, see eq. (3.26). For $\mu \gtrsim 1$, the ϕ matter dominated epoch therefore occurs for

$$\mu \ll A \lesssim \left(\frac{3}{2}\frac{\gamma}{(1+\mu)^{1/2}} + 1\right)^{2/3} \,, \tag{3.63}$$

where $\gamma = H_I/\Gamma_\phi$, see eq. (3.27). If $\mu > 1$, an extended period of ϕ matter domination therefore requires $\mu^2 \ll \gamma$.

On the other hand, γ cannot be arbitrarily large in the post–inflationary universe. We certainly need $H < M_{\rm Pl}$ in order to treat gravity classically, see e.g. [157]. In inflationary cosmology the smallness of the density perturbations, and the upper bound on primordial gravitational waves, requires $H \lesssim 10^{-5} M_{\rm Pl}$ during inflation [7], and hence also afterwards. We therefore adopt the bound $H_I < 10^{-5} M_{\rm Pl}$, which by

using eqs. (3.4) and (3.27) implies

$$\gamma < \frac{10^{-5}}{\alpha}\left(\frac{M_{\rm Pl}}{M_\phi}\right)^3 . \tag{3.64}$$

The rhs of (3.64) is therefore also an upper bound on μ^2 if the universe is to undergo a ϕ matter dominated epoch.

Since X' production or annihilation has little effect on the thermal plasma, the final radiation density is simply given by

$$R_F \simeq R_I + R_F(\mu = 0)\,, \tag{3.65}$$

where $R_F(\mu = 0)$ has been given in eq. (3.28). If $\mu^2 \ll \gamma$, the first term on the rhs of eq. (3.65) is negligible, i.e. if the universe underwent an extended period of ϕ matter domination, the final radiation density will come mostly from ϕ decays.

However, the initial conditions may affect the final DM relic density even if there is an epoch of ϕ matter domination. So far we have only specified the initial radiation density in terms of μ. In complete generality the initial X' density is another free parameter. However, we wish to avoid the proliferation of parameters, and therefore write the initial (co–moving) X' density as

$$X'_I = \left(\frac{1}{T_{\rm RH}}\right)^3 \frac{g_{X'} T_I {M_{X'}}^2}{2\pi^2} K_2\left(\frac{M_{X'}}{T_I}\right) . \tag{3.66}$$

We use the above equation in our numerical calculation. This is based on the Maxwell–Boltzmann distribution, but it is still a reasonably good approximation for bosons and fermions from relativistic to non–relativistic limits, as long as X' is (approximately) in full thermal equilibrium with the hot plasma. This in turn should be true if $T_I \gtrsim M_{X'}$ unless the X' annihilation cross section is very small: equilibrium should be reached if $n_{X',\rm EQ}(T_I)\langle\sigma v\rangle' \gtrsim H_I$, which by putting $n_{X',\rm EQ}(T_I)$ (the relativistic case is appropriate at T_I) from eq. (3.8) and H_I from eq. (3.59) we have

$$g_{X'}\langle\sigma v\rangle' \gtrsim \left(\frac{4 g_{\rm eff}(T_I)(1+\mu)}{45\mu}\right)^{3/4} \pi^{17/4} \frac{1}{\sqrt{\alpha\gamma M_\phi^3 M_{\rm Pl}}}\,, \tag{3.67}$$

where we used the approximation $\tilde{g}_{X'}\zeta(3) \simeq g_{X'}$. Here we have again considered $H_I = \gamma\Gamma_\phi$ and used eq. (3.4) for Γ_ϕ. The condition (3.67) can only be violated if either μ or $\langle\sigma v\rangle'$ is very small. In the former case eq. (3.66) in any case predicts a very small initial X' density, so it doesn't matter that this small number may not be correct. In the latter case interactions of X' with the thermal plasma will certainly remain negligible at later times, so we can write the final X' as sum of the initial value (which may not be given by eq. (3.66) then) and a possible contribution from direct $\phi \to X'$ decays

$$X'_F \simeq X'_I + X'_{F(,Br)}, \quad \text{with } X'_{F(,Br)} = \frac{B_{X'} T_{\rm RH} \Phi_I}{M_\phi}\,. \tag{3.68}$$

We are now ready to present some numerical results. In Fig. 3.11 we show the final DM relic density for the same ϕ mass and $B_{X'}$ as in Fig. 3.2. We chose two different values of the initial radiation (and X') density, parameterized by μ: $\mu = 10^{-5}$ (left column) and $\mu = 1$ (right column). Moreover, we chose three different values for the initial Hubble parameter, parameterized by γ: $\gamma = 10^{10}$ (first row), $\gamma = 10^{15}$ (second row), and $\gamma = 10^{20}$ (third row). Since $\mu \leq 1$, in all examples the universe is dominated

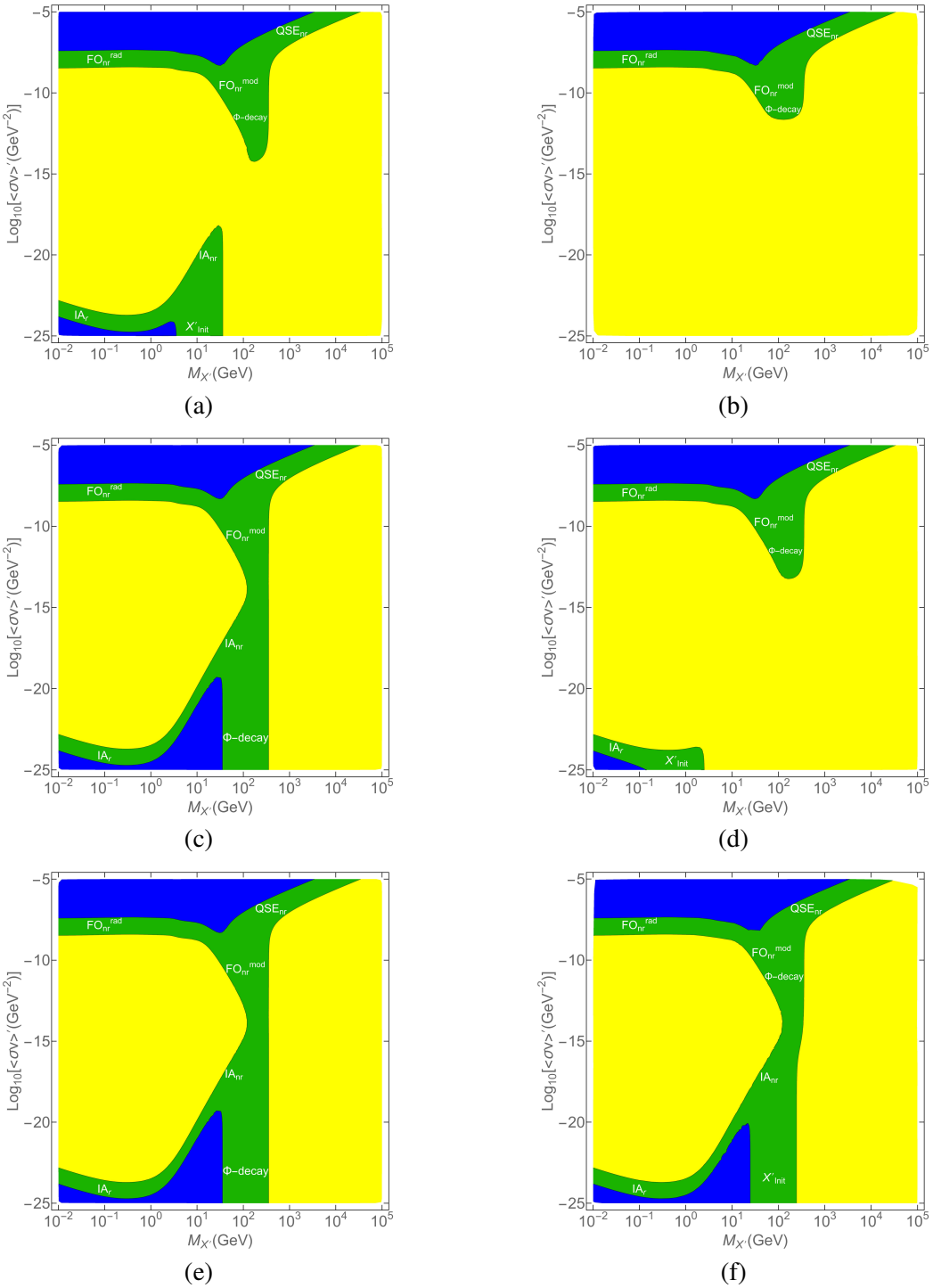

Figure 3.11: Contours of constant relic density for different initial conditions. The meaning of the differently colored regions is as in Fig. 2; note that we only show results where the evolution of the number of degrees of freedom with temperature has been treated carefully. We have taken $M_\phi = 5 \times 10^6$ GeV and $\alpha = 1$, leading to $T_{\rm RH} = 848.5$ MeV, and $B_{X'} = 10^{-5}$. The six frames are for different combinations of γ and μ: (γ, μ) = a) $(10^{10}, 10^{-5})$, b) $(10^{10}, 1)$, c) $(10^{15}, 10^{-5})$, d) $(10^{15}, 1)$, e) $(10^{20}, 10^{-5})$, f) $(10^{20}, 1)$.

by ϕ matter for all A between 1 and $A_{\rm decay}$ defined in eq. (3.26). Note that condition (3.63) is satisfied in all these cases.

We see that the initial conditions do not affect the final DM density if the X' annihilation cross section is sufficiently large. We saw in the previous Section that X' particles then achieve full thermal equilibrium with the hot plasma during the epoch of ϕ matter domination; for sufficiently high $T_{\rm RH}$, X' will drop out of equilibrium only after all ϕ particles have decayed. Adding a non–vanishing initial radiation component increases the temperature relative to the case $\mu = 0$, making it easier for X' to attain thermal equilibrium. Hence any scenario that leads to X' freeze–out for $\mu = 0$ will have X' in thermal equilibrium also for some time during ϕ domination. This period of thermal equilibrium will wipe out any dependence of the final X' density on the initial conditions. For the parameters of Fig. 3.11 this is true for $\langle\sigma v\rangle' \gtrsim 10^{-12}$ GeV^{-2}.

Hence the initial conditions can affect the final DM density only if for $\mu = 0$ the latter is determined by the "inverse annihilation" or "ϕ decay" mechanisms discussed in the previous Section, see eqs. (3.48), (3.56) and (3.57). The results obtained for $\mu = 0$ will then only be approximately correct if the initial value X'_I is much less than the final value of X' produced during the epoch of ϕ matter domination. From these equations and the initial condition (3.66) we find that the initial contribution is negligible if

$$\begin{aligned}
\frac{\mu^{3/4}(1+\mu)^{1/4}}{\gamma^{1/2}} &\ll \kappa_{\phi-{\rm decay}} B_{X'} \left(\frac{\alpha M_\phi}{M_{\rm Pl}}\right)^{1/2} , \\
\kappa_{\phi-{\rm decay}} &\approx \left(\frac{\pi^5 g_{\rm eff}(T_I)^3}{2^6\, 3^2\, 5^3}\right)^{1/4} \frac{\pi^2}{\tilde{g}_{X'}\zeta(3)} ; \qquad (3.69) \\
\frac{\mu^{3/4}(1+\mu)^{1/4}}{\gamma^{1/2}} &\ll \kappa_{IA_{nr}} \frac{\alpha^{1/2} M_\phi^{3/2} M_{\rm Pl}^{1/2} T_{\rm RH}^6 \langle\sigma v\rangle'}{M_{X'}^6} , \\
\kappa_{IA_{nr}} &\approx \left(\frac{\pi^5 g_{\rm eff}(T_I)^3}{2^6\, 3^2\, 5^3}\right)^{1/4} \frac{48\chi g_{X'}^2 g_{\rm eff}(T_{RH})^{3/2}}{5^{3/2}\pi^{11/2}\zeta(3)\tilde{g}_{X'} g_{\rm eff}(T_*)^3} ; \qquad (3.70) \\
\frac{\mu^{3/4}(1+\mu)^{1/4}}{\gamma^{1/2}} &\ll \kappa_{IA_r} \alpha^{1/2} M_\phi^{3/2} M_{\rm Pl}^{1/2} \langle\sigma v\rangle' , \\
\kappa_{IA_r} &\approx \left(\frac{\pi^5 g_{\rm eff}(T_I)^3}{2^6\, 3^2\, 5^3}\right)^{1/4} \frac{2^{11}\zeta(3)\tilde{g}_{X'}}{5^{3/2}\pi^{11/2} g_{\rm eff}(T_{RH})^{3/2}} . \qquad (3.71)
\end{aligned}$$

The inequality in (3.69) applies if X' production in the epoch of ϕ domination is from direct $\phi \to X'$ decays, while the inequalities in (3.70) and (3.71) apply if the main X' production mechanism for $\mu = 0$ is inverse annihilation, with X' being non–relativistic and relativistic, respectively. In these inequalities we have only displayed the dependence on the free parameters; numerical coefficients and degrees of freedom are collected in the κ's. Altogether the initial contribution to the X' density will be negligible if the lhs (left hand side) is (much) less than the largest of the right–hand sides of three inequalities.

When deriving these inequalities we have assumed that the initial temperature is larger than $M_{X'}$, so that $X'_I \propto T_I^3$ is not exponentially suppressed. Moreover, we have assumed that the condition (3.63) is satisfied, so that the universe underwent an extended period of ϕ matter domination. Finally, we have used eq. (3.4) to compute Γ_ϕ; this is needed, since we express the initial Hubble parameter, and hence Φ_I, in terms of γ defined in eq. (3.27).

The inequality in (3.69) is relevant for $M_{X'} \gtrsim 10$ GeV and $\langle\sigma v\rangle' \lesssim 10^{-18}$ GeV^{-2}. For the parameters

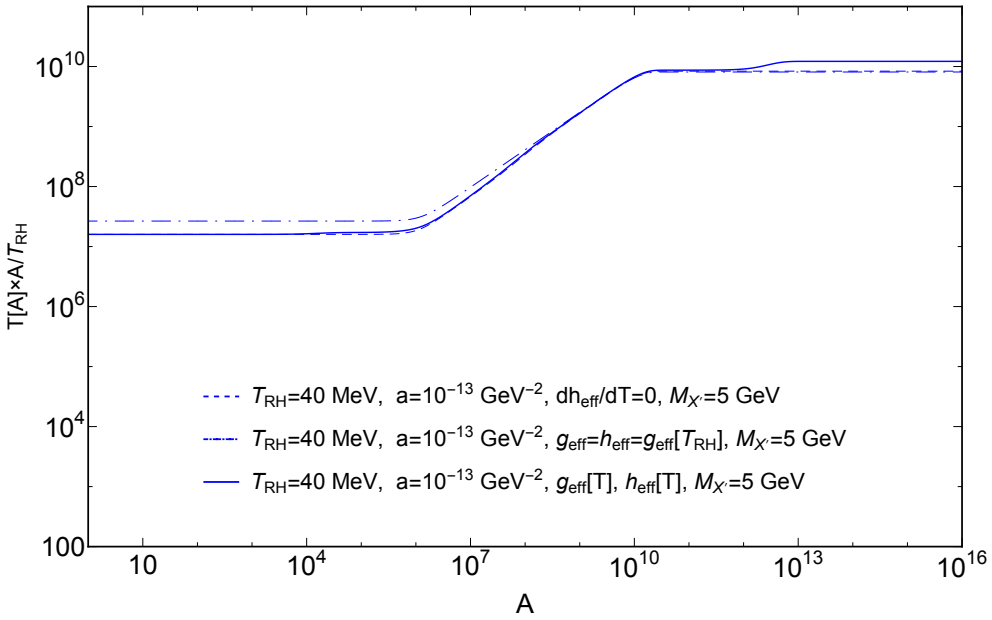

Figure 3.12: Evolution of the scaled temperature with respect to A for non–vanishing dark matter and radiation densities with $\mu = 1$ and $\gamma = 10^{15}$.

used in Figs. 3.11 the rhs amounts to about 3×10^{-10}. The values of the lhs in the six frames are almost of order 2×10^{-9} in (a), 10^{-5} in (b), 6×10^{-12} in (c), 4×10^{-8} in (d), 2×10^{-14} in (e), and 10^{-10} in (f). Correspondingly in the lower–right parts of the plane shown in Fig. 3.11 the initial contribution X'_I dominates in (a), completely dominates in (b) and (d), is subdominant but not completely negligible in (f) (in this case the rhs of the inequality of (3.69) is larger than the lhs but not much larger than that) and can be neglected in (c) and (e). The regions with approximately correct final DM density which is dominated by X'_I are labeled as $X'_{\rm Init}$ in Figs. 3.11.

The situation is a bit more complicated in the part of parameter space where X' production is dominated by inverse annihilation if $\mu = 0$, since the rhs of the inequalities in (3.70) and (3.71) explicitly depend on the annihilation cross section and – for the inequality in (3.71) – the mass of the DM particle. Let us focus on the region near the center of the plots, with $M_{X'} \simeq 50$ GeV and $\langle\sigma v\rangle' \simeq 10^{-17}$ GeV^{-2}, where the inverse annihilation process produces approximately the correct relic density for $\mu = 0$, with the DM particles being non–relativistic already at production. The rhs of the inequality in (3.70) is of order 4×10^{-10} here. The lhs are like the ones explained in previous paragraph. Correspondingly in this central part of the parameter plane X'_I to some extent dominates in (a) (again in this case the rhs of the inequality of (3.70) is larger than the lhs but not much larger than that), completely dominates in frames (b) and (d), is negligible in (c) and (e), and contributes about equally in (f).

To verify the inequality of (3.71) in the relativistic inverse annihilation case we consider $\langle\sigma v\rangle' \simeq 10^{-24}$ GeV^{-2}. We do not need to consider the DM mass, since the rhs of this inequality (3.71) does not depend on it. Using this thermally averaged cross section the rhs is of order 3×10^{-7}. This value causes the left lower part of Fig. 3.11 which corresponds to IA_r dominates in all frames except in frame (b) where the value of lhs of inequality (3.71) is of order 10^{-5}.

We thus see that for small DM annihilation cross section, one may need $\gamma > 10^{20}$ in order to be independent of the initial conditions, even if we require the initial radiation density to be not larger than the initial ϕ mass density. In contrast, for $\mu = 0$ the final DM relic density is independent of γ once $\gamma \gtrsim 10^7$. Note that for $\mu = 1$, $T_I \sim \sqrt{\gamma} T_{\rm RH}$. Since BBN constraints imply $T_{\rm RH} \geq 4$ MeV and T_I

should be smaller than the reheat temperature after inflation, the latter would have to be at least 10^8 GeV if $\gamma \sim 10^{20}$. For the parameters of Fig. 3.11, $\gamma > 10^{20}$ with $\mu = 1$ implies $T_I \gtrsim 10^{10}$ GeV. Note, however, that possible problems from a high post–inflationary reheat temperature, e.g. overproduction of gravitinos, are alleviated by the huge amount of entropy produced during the very long epoch of ϕ matter domination and out–of–equilibrium decay of ϕ particles.

Finally, we should mention that considering the evolution of degrees of freedom is also important for non–vanishing initial DM and radiation densities in an early matter matter dominated epoch. This case is shown in Fig. 3.12, where the initial DM and radiation densities are equal ($\mu = 1$ and $\gamma = 10^{15}$), with three approaches to the treatment of degrees of freedom of SM. These cases are $g_{\rm eff} = g_{\rm eff}(T_{RH}) = h_{\rm eff}(T_{RH})$ (dashed dotted line); $g_{\rm eff}(T)$, $h_{\rm eff}(T)$ and $dh_{\rm eff}/dT = 0$ (dashed line); $g_{\rm eff}(T)$ and $h_{\rm eff}(T)$ (solid line). The plot of Fig. 3.12 shows $T[A]A/T_{RH}$ versus A. For scale factors $A \lesssim 10^6$ and $A \gtrsim 10^{10}$ the universe is radiation dominated; however, for $10^6 \lesssim A \lesssim 10^{10}$ is matter dominated. As Fig. 3.12 shows $T[A]A/T_{RH}$ is almost constant in radiation domination and $T[A]A \propto A^{5/8}$ in matter domination. In Fig. 3.12 in contrast to Fig. 3.8 the diagram passes the QCD transition only once; due to this fact the effect we showed in Fig. 3.8 for very tiny scale factors is not present here. However, consideration of the evolution of degrees of freedom represents itself in Fig. 3.12 at very large scale factors for the three cases we mentioned.

3.5 Summary and Conclusions

In this Chapter which is based on our paper [38], we studied the production of DM particles in non–thermal cosmological scenarios with an early matter dominated era. Such scenarios can naturally occur in inflationary cosmology when a UV–complete theory contains a scalar particle ϕ (modulus) with mass smaller than the Hubble scale during inflation. This scalar is heavy with respect to SM particles and long–lived due to greatly suppressed couplings, coming from the presence of Planck mass squared in the denominator of its decay width, to SM particles. We used the evolution of relativistic degrees of freedom for energy and entropy density ($g_{\rm eff}$ in eq. (3.2) and $h_{\rm eff}$ in (3.15)) with respect to temperature, to improve previous analyses of this non–thermal DM production scenario. We calculated these degrees of freedom in Chapter 2. Moreover, we have investigated the effect of a non–vanishing initial radiation and DM density.

Our study shows that a careful treatment of the temperature dependence of $h_{\rm eff}$ is very important for different DM production mechanisms over large regions of parameter space as it can be seen in Figs. 3.2, 3.3, 3.4, and 3.5. In fact, this generally contradicts with the usual WIMP freeze–out scenario in standard cosmology. In such case the evolution of entropy degrees of freedom $h_{\rm eff}$ is only important when the temperature changes rapidly around the decoupling temperature. Even then, the effect does not exceed the 10% difference in relic density for S–wave annihilation cross section (Fig. 2.5 of Chapter 2). The main reason is that we always normalize the DM density to the radiation density, or equivalently to the entropy density. In the absence of any phase transition or heavy particle decay the co–moving entropy density of the universe in the standard cosmology is constant after inflationary period. However, in the scenarios we considered in this Chapter this is not true, where the decay of ϕ particles have produced almost all of the entropy density. This fact causes a significant error in the predicted final DM relic density. In addition, the sensitivity of different production mechanisms with respect to various treatments of degrees of freedom variates. Especially relativistic and non–relativistic "inverse annihilation" in ref. [38, 146] are more sensitive than others.

We mentioned earlier in the non–thermal scenario that we consider here the final relic density variates with respect to standard cosmology, depending on the choice of different free parameters. As we

know WIMPs with annihilation cross section lower than the required value of the thermal production are overabundant. However, our results in Fig. 3.10 represents if DM particles are produced non–thermally with annihilation cross section below the canonical value for WIMPs, the relic density is too high except for the cases where the branching ratio of direct decay of modulus to DM ($\phi \to X'$) is below $10^{-4}(M_{X'}/100\ \text{GeV})$, and the ϕ particles are not too heavy, $M_\phi \lesssim 10^7\ \text{GeV}(M_{X'}/100\ \text{GeV})^{2/3}$. Remembering eq. (3.4) the moduli decay width is suppressed by M_{Pl}^{-2}, it is the case in almost all moduli or Polonyi models, then $M_\phi < 10^7$ GeV implies a reheat temperature much lower than 1 GeV ($T_{\text{RH}} \lesssim 1$). We can avoid this bound only if the DM annihilation cross section is more than 10 orders of magnitude below the cross section of thermal WIMPs. In such a case the current DM searches (direct, indirect and at colliders) can not probably find a signal of DM particles. We found this bound by assuming that the initial radiation and DM abundance are negligible. Avoiding this assumption only affects the final relic density of DM so this bound will be valid in general.

Moreover, we studied the effect of non–vanishing initial radiation and DM density. The ratio of initial radiation and ϕ matter (modulus) densities are parameterized by μ . Also, we argued that due to high temperatures at early times the initial density of DM particles is non–zero and we can estimate it from the equilibrium number density of DM (eq. 3.8). If the DM annihilation cross section is (very) large so that DM particles reached thermal equilibrium during modulus domination epoch and possibly afterwards, the initial radiation density does not affect the final relic density. However, for small DM annihilation cross section a small non–zero value of μ parameter can influence the relic abundance significantly, in case the ϕ matter dominated era does not last very long. The interval of early matter domination is parameterized by the ratio γ of initial Hubble rate to the total decay width of modulus ϕ (eq. 3.27). Finally, we find that only if $\gamma > 10^{20}\mu^{3/2}\sqrt{1+\mu}(10^{-5}/B_{X'})^2(10^7\ \text{GeV}/M_\phi)$ (Fig. 3.11), where $B_{X'}$ is the branching ratio for direct decays of modulus ϕ to DM particles X', the final relic density of DM does not depend on μ values. Besides, a long enough period of modulus domination occurs only if $\gamma \gg \max(1, \mu^2)$.

On scales smaller than the Hubble scale density perturbations will increase linearly with the scale factor during the early period of ϕ matter (modulus) domination [7]. In fact, this improves the perturbation spectrum at very small scales relative to radiation domination era in standard cosmology. Even though, in most cases we studied here for non–thermally produced DM particles, they will quickly thermalize with SM particles to reach the kinetic equilibrium. This leads to the fact that their free–streaming length becomes much larger than the size of the density perturbations that are enhanced during the time of early matter domination, this phenomenon causes the effective erasure of these perturbations again. Similar consequence occurs for very weakly coupled DM particles that did not thermalize after being produced. They would have to be produced predominantly directly from ϕ decay. Except for DM particles that are produced non–relativistically, e.g. DM mass of the order $M_{X'} \simeq M_\phi/2$ from direct modulus decay $\phi \to X'X'$, the free–streaming length of X' particles are too large for the early "minihaloes" to form and survive [158, 159]. Consequently, the framework we studied in this Chapter in almost all production mechanisms replicates the predictions of standard cold dark matter regarding structure formation issues.

As we noted earlier, the presence of an early period of matter domination by a heavy scalar with Planck suppressed decay rate can yield the correct relic abundance for different regions of DM mass and annihilation cross section parameter space. These sets of valid $\langle\sigma v\rangle'$ can be smaller or larger than that required for thermal WIMPs produced in a radiation dominated era. Essentially, we can determine the annihilation cross section of DM particles by their annihilation in today's universe; this is possible when we can quantify the density of DM (knowing the parameters) in the location of annihilation event. In addition, we can measure the coupling the DM particles from collider physics experiments [160–162]. By having the couplings one can calculate the annihilation cross section and check if it is in agreement with the thermal WIMP scenario, or if it has smaller or larger value than the WIMP one which we studied in our non–thermal cosmology framework. Eventually, we should emphasize that since the ϕ modulus

particle are significantly heavy, and feebly coupled, we will not be able to directly observe them in the foreseeable future.

In our (to some extent) simple scenario for non–thermal production of DM we had to solve the set of Friedmann–Boltzmann differential equations numerically for modulus (ϕ matter), radiation, and DM. This calculation is done over a large range of Hubble parameter, time, or scale factors which is computationally rather expensive[11]. Consequently, in this Chapter (based on ref. [38]) we chose the thermally averaged annihilation cross section of DM particles to be constant in most cases; which is the simplest approximation.

In the next Chapter we intend to use the results of this Chapter on DM production in an early matter (ϕ) dominated epoch, including the full energy (or temperature) dependence of the annihilation cross section, along with the numerical values of evolving degrees of freedom, from Chapter 2 to study the production of the well–motivated DM candidate particle i.e. neutralino in non–thermal scenarios with low reheating temperatures.

[11] The calculation is done on the "BAF" cluster of Physikalisches Institut. We used `Mathematica` program to do the scan over the parameter space of DM mass and cross section (colourful figures) for about 50000 points in each figure.

CHAPTER 4

Neutralino Dark Matter in Low Reheating Scenarios

4.1 Introduction

Neutralino as a weakly interacting massive particle (WIMP), and the most favourable supersymmetric DM candidate has been widely studied in the last years [163, 164]. However, recent direct [24–29], indirect [19–23] and collider searches [30–35] have not found any evidence for it assuming it is produced thermally in the early universe i.e. a thermal WIMP.

TeV scale supersymmetry until the second run of large hadron collider (LHC) was the most well–motivated theory to explain DM, hierarchy problem, gauge unification, etc [17, 118]. Since no new physics signal have been found yet, it might seem that SUSY is becoming less attractive among phenomenologists. However, it is still possible to have a slightly fine–tuned SUSY theory with masses heavier than TeV scale [165]. Also, if one should sacrifice the TeV scale SUSY as a natural solution to hierarchy problem and naturalness, there is still hope to have DM and grand unification in a supersymmetric theory assuming the mass of scalar partners is split from fermion partners at lower energy scale [129, 130].

One alternative solution to have a viable DM candidate in a SUSY theory may be to relax the condition on the required relic abundance for WIMP DM and to go beyond the thermal WIMP assumption [16]. This can happen by considering SUSY as an effective theory of a UV-complete one like superstring theory or its supergravity version [131, 143, 144]. This can be one of the correct ways to look at DM paradigm and beyond the standard model physics. In such a scenario the early moments of cosmology between the inflationary era and BBN can be different from the standard approach where only radiation dominates the universe.

In the standard cosmology when the temperature of the universe goes below 5% of WIMP mass the freeze–out happens [163, 164]. However, this scenario can change in the presence of an early epoch of matter domination. It is also quite possible that due to lack of our knowledge about the pre big bang nucleosynthesis (BBN) era of cosmology the production mechanism of dark matter (DM) can be different from that of the thermal WIMP. UV-complete theories like superstring theory propose the presence of some heavy long–lived scalar fields (due to Planck suppression in their decay width) i.e. moduli which dominate the energy density of the universe [109–114, 122–125]. The decay of these fields can affect the thermal history after inflation by producing radiation and DM [38, 146]. However, the reheating temperature at the time of their decay should be higher than 4 MeV not to spoil the success of BBN [121, 126–128].

Different types of neutralino DM in low reheating scenarios are studied in the literature [108, 131, 132,

138, 166–169]. However, the details of Friedmann–Boltzmann equations are not considered in [107, 170, 171]. In [166] the effects of degrees of freedom are not included properly due to neglecting the equation regarding entropy production. Moreover, different regions with correc relic density are not illustrated. In [168] different production mechanisms and the effects of initial dark matter and radiation densities are not discussed. Also, the degrees of freedom used in the calculation have not treated the QCD effects properly.

In this Chapter which is based on paper [39] we study the production of neutralino DM in scenarios with low reheating temperature with considering the properties which are ignored in the previous studies. In Sec. 4.2, we illustrate the minimal supersymmetric standard model (MSSM) and consider neutralino DM in such context. Afterwards, we illustrate our set of Friedman–Boltzmann equations in a universe dominated by a heavy scalar field (which we studied in Chapter 3) to compute the DM relic density (Sec. 4.3). Then, we briefly review neutralino properties in thermal scenario (Sec. 4.4). Moreover, we show the regions where different neutralino types can be produced non–thermally to match the observed DM yield (Sec. 4.5). By using the modified version of `micrOMEGAs` code [172] we compute its relic abundance in different SUSY scenarios. In Sec. 4.6 we discuss experimental constraints on neutralino DM and different low reheating scenarios which can yield the correct relic density for neutralino. These scenarios match with the ones shown in Sec. 4.5 for various choices of moduli masses and branching ratios. Finally, we summarise our results in Sec. 4.7.

4.2 Minimal Supersymmetric Standard Model

Since the details of derivation of SUSY Lagrangian is beyond the scope of this thesis and is already widely studied in the literature [17, 115–120], we will only mention the superpotential and soft breaking terms which are relevant for our discussion. The superpotential for the MSSM which respects gauge symmetry, renormalizability, and R–parity conservation is given by [17]

$$W_{\rm MSSM} = \mathbf{y_u}\bar{u}H_u \cdot Q - \mathbf{y_d}\bar{d}H_d \cdot Q - \mathbf{y_e}\bar{e}H_d \cdot L + \mu H_u \cdot H_d \,, \tag{4.1}$$

where "$\cdot$" means $i\sigma_2$ and σ_2 is the second Pauli matrix. Also, Yukawa matrices are shown by $\mathbf{y}$'s. The chiral superfields for Higgses, left and right (up and down) handed quarks, left and right handed leptons are denoted by H_u and H_d, Q and $\bar{u}$ and $\bar{d}$, L and $\bar{e}$, respectively. SUSY should be broken at some scale, since we do not see any SUSY particle around with a mass similar to its SM partner. Consequently, we mention the "Soft SUSY breaking terms" which are added to the SUSY Lagrangian to prevent the appearance of quadratic divergences [17] in the following

$$\begin{aligned} L_{\rm soft} \;=\; & -\frac{1}{2}\left(M_3\widetilde{g}\widetilde{g} + M_2\widetilde{W}\widetilde{W} + M_1\widetilde{B}\widetilde{B} + c.c.\right) \\ & -\left(\mathbf{a_u}\widetilde{\bar{u}}^{\dagger}H_u\widetilde{Q} + \mathbf{a_d}\widetilde{\bar{d}}^{\dagger}H_d\widetilde{Q} + \mathbf{a_e}\widetilde{\bar{e}}^{\dagger}H_u\widetilde{L} + c.c.\right) \\ & -\left(\widetilde{Q}^{\dagger}\mathbf{m^2_{\tilde{Q}}}\widetilde{Q} + \widetilde{L}^{\dagger}\mathbf{m^2_{\tilde{L}}}\widetilde{L} + \widetilde{\bar{u}}^{\dagger}\mathbf{m^2_{\tilde{\bar{u}}}}\widetilde{\bar{u}} + \widetilde{\bar{d}}^{\dagger}\mathbf{m^2_{\tilde{\bar{d}}}}\widetilde{\bar{d}} + \widetilde{\bar{e}}^{\dagger}\mathbf{m^2_{\tilde{\bar{e}}}}\widetilde{\bar{e}} + m^2_{H_u}H^*_uH_u + m^2_{H_d}H^*_dH_d\right) \\ & -\left(B\mu H_u \cdot H_d + c.c.\right) . \end{aligned} \tag{4.2}$$

In $W_{\rm MSSM}$ and $L_{\rm soft}$ we consider all three generations of fermions [1]. In eq. 4.2, the terms include M_3, M_2, and M_1 denote gluino, wino, and bino mass terms, respectively. The parameters $\mathbf{a_u}$, $\mathbf{a_d}$, and $\mathbf{a_e}$ are complex 3×3 matrices in family space for trilinear couplings. Sfermions mass 3×3 matrices are shown

[1] Here *c.c.* means the complex conjugate of previous terms in the parantheses.

by $\mathbf{m}^2_{\widetilde{\mathbf{Q}}}$, $\mathbf{m}^2_{\widetilde{\mathbf{L}}}$, $\mathbf{m}^2_{\widetilde{\bar{\mathbf{u}}}}$, $\mathbf{m}^2_{\widetilde{\bar{\mathbf{d}}}}$, and $\mathbf{m}^2_{\widetilde{\bar{\mathbf{e}}}}$. The doublets of left handed squarks and sleptons by $\widetilde{Q}$ and $\widetilde{L}$, and singlets of handed up and down–type squarks, and sleptons by $\widetilde{\bar{u}}$, $\widetilde{\bar{d}}$, and $\widetilde{\bar{e}}$ are shown, respectively. Masses, $m^2_{H_u}$ and $m^2_{H_d}$, and bilinear terms, $B\mu$, are for the up and down Higgs doublets.

In MSSM with R–parity conservation the lightest supersymmetric particle (LSP) can be neutralino (as a Majorana fermion) which may also be the DM candidate [18]. The neutralino mass matrix in the flavor basis can be written as [17]

$$\mathbf{M}_{\widetilde{\chi}} = \begin{pmatrix} M_1 & 0 & -\cos\beta\,\sin\theta_W\, m_Z & \sin\beta\,\sin\theta_W\, m_Z \\ 0 & M_2 & \cos\beta\,\cos\theta_W\, m_Z & -\sin\beta\,\cos\theta_W\, m_Z \\ -\cos\beta\,\sin\theta_W\, m_Z & \cos\beta\,\cos\theta_W\, m_Z & 0 & -\mu \\ \sin\beta\,\sin\theta_W\, m_Z & -\sin\beta\,\cos\theta_W\, m_Z & -\mu & 0 \end{pmatrix}. \tag{4.3}$$

The mass matrix can be diagonalized with a matrix $\mathbf{N}$ in the following way to get the mass eigenvalues [17]

$$\widetilde{\chi}_i = \mathbf{N}_{ij}\psi^0_j\,, \quad \sum_{j=1}^{4} N^2_{ij} = 1\,. \tag{4.4}$$

Neutralino mass matrix is a combination of bino, wino, and higgsinos, i.e. $\widetilde{\chi}_i = N_{i1}\widetilde{B} + N_{i2}\widetilde{W}^0 + N_{i3}\widetilde{H}^0_1 + N_{i4}\widetilde{H}^0_2$ [17]. We have the masses of different neutralinos in the following [17]

$$\mathbf{N}^*\mathbf{M}_{\widetilde{\chi}}\mathbf{N}^{-1} = \begin{pmatrix} m_{\widetilde{\chi}_1} & 0 & 0 & 0 \\ 0 & m_{\widetilde{\chi}_2} & 0 & 0 \\ 0 & 0 & m_{\widetilde{\chi}_3} & 0 \\ 0 & 0 & 0 & m_{\widetilde{\chi}_4} \end{pmatrix}. \tag{4.5}$$

In the following limit

$$m_Z \ll |\mu \pm M_1|,\, |\mu \pm M_2|, \tag{4.6}$$

the mass eigenstates of neutralino can be considered as a "bino–like" $\widetilde{\chi}_1 \approx \widetilde{B}$, a "wino–like" $\widetilde{\chi}_2 \approx \widetilde{W}^0$, and "higgsino–like" $\widetilde{\chi}_3, \widetilde{\chi}_4 \approx \left(\widetilde{H}^0_u \pm \widetilde{H}^0_d\right)/\sqrt{2}$, where the mass eigenvalues are given by [17]

$$m_{\widetilde{\chi}_1} = M_1 - \frac{m^2_Z \sin^2\theta_W(M_1 + \mu\sin 2\beta)}{\mu^2 - M^2_1} + \dots\,, \tag{4.7}$$

$$m_{\widetilde{\chi}_2} = M_2 - \frac{m^2_W(M_2 + \mu\sin 2\beta)}{\mu^2 - M^2_2} + \dots\,, \tag{4.8}$$

$$m_{\widetilde{\chi}_3}, m_{\widetilde{\chi}_4} = |\mu| + \frac{m^2_Z(I - \sin 2\beta)(\mu + M_1\cos^2\theta_W + M_2\sin^2\theta_W)}{2(\mu + M_1)(\mu + M_2)} + \dots\,, \tag{4.9}$$

$$|\mu| + \frac{m^2_Z(I + \sin 2\beta)(\mu - M_1\cos^2\theta_W - M_2\sin^2\theta_W)}{2(\mu - M_1)(\mu - M_2)} + \dots\,, \tag{4.10}$$

where $I = \pm 1$ denotes the sign of μ parameter. After diagonalising the neutralino mass matrix depending on the values of M_1, M_2 and μ different types of neutralino can be dominant in every four mass eigenstates. However, the lightest neutralino will play the role of DM [17].

The MSSM formalism given by eqs. (4.1) and (4.2) has 105 free parameters in addition to 19 free parameters of SM. To be consistent with the phenomenological observations at the weak scale, no flavor changing neutral current, no new source of CP–violation, and universality in first and second generations

can be assumed [173]. Using these assumptions the number of SUSY parameters can be reduced to 19 parameters as inputs for further studies of this kind of model. This model is called phenomenological MSSM (pMSSM) with the set of parameters given below [173]

$\tan\beta$: the ratio of the vev of the two–Higgs doublet fields,

M_A: the mass of the pseudoscalar Higgs boson,

μ: the Higgs–higgsino mass parameter,

M_1, M_2, M_3: the bino, wino and gluino mass parameters,

$m_{\tilde{q}}$, $m_{\tilde{u}_R}$, $m_{\tilde{d}_R}$, $m_{\tilde{l}}$, $m_{\tilde{e}_R}$: first/second generation sfermion masses,

$m_{\tilde{Q}}$, $m_{\tilde{t}_R}$, $m_{\tilde{b}_R}$, $m_{\tilde{L}}$, $m_{\tilde{\tau}_R}$: third generation sfermion masses,

A_t, A_b, A_τ : third generation trilinear couplings.

Also, we will use the above parameters at the weak scale to do the phenomenological study of SUSY in pMSSM. In such case the LSP can be any of neutralino types i.e. bino, wino, and higgsinos.

In minimal supergravity (mSUGRA) or constrained MSSM (CMSSM) gaugino masses unify at the GUT (grand unified theory) scale, $M_{GUT} = 1.5 \times 10^{16}$ GeV, so we can have the following prediction at the weak scale [17, 117]

$$M_3 \ : \ M_2 \ : \ M_1 \ \simeq \ 7 \ : \ 2 \ : \ 1 \, . \tag{4.11}$$

In mSUGRA or CMSSM to find the SUSY spectra of masses at the weak scale we also require to assume the following set of boundry conditions at GUT scale for gaugino masses, sfermion masses, Higgs masses, and trilinear couplings [17, 117].

$$M_3 = M_2 = M_1 = m_{1/2} \, , \tag{4.12}$$

$$\mathbf{m}^{\mathbf{2}}_{\tilde{\mathbf{Q}}} = \mathbf{m}^{\mathbf{2}}_{\tilde{\mathbf{u}}} = \mathbf{m}^{\mathbf{2}}_{\tilde{\mathbf{d}}} = \mathbf{m}^{\mathbf{2}}_{\tilde{\mathbf{L}}} = \mathbf{m}^{\mathbf{2}}_{\tilde{\mathbf{e}}} = m_0^2 \mathbf{1} \, , \tag{4.13}$$

where $\mathbf{1}$ shows unit matrix,

$$m^2_{H_u} = m^2_{H_d} = m_0^2 \, , \tag{4.14}$$

$$\mathbf{a_u} = A_0 \mathbf{y_u}, \ \ \mathbf{a_d} = A_0 \mathbf{y_d}, \ \ \mathbf{a_e} = A_0 \mathbf{y_e} \, , \tag{4.15}$$

$\mathbf{a}$'s and $\mathbf{y}$'s are 3×3 matrices for trilinear couplings and Yukawa's.

Generally, we can parameterize the above universal soft terms at the GUT scale as scalar mass m, gaugino mass M, the trilinear coupling A, and the bilinear Higgs mixing B. Radiative electroweak symmetry breaking (REWSB) condition imposes the following initial parameters at the GUT scale to be sufficient for finding SUSY spectra at the weak scale [17, 118]

$$tan\,\beta, \ \ m_0, \ \ m_{1/2}, \ \ A_0, \ \ sign(\mu) \, , \tag{4.16}$$

where the ratio of vacuum expectation values of up and down neutral Higgses is given by $\tan\beta = \langle H_u \rangle / \langle H_d \rangle$ and the sign of μ parameter is shown by $sign(\mu)$. As a consequence, using the above parameters we can do the scan over CMSSM/mSUGRA parameter space. In such scenarios the lightest

neutralino is bino or higgsino [117]. We will study MSSM approaches explained in this Section in low reheating scenarios in the next Sections.

4.3 Neutralino Relic density in an Early Matter Dominated Epoch

To compute the final DM relic density in an early matter dominated era we use the result of [38], which was also the subject of previous Chapter to have a correct estimation which is more precise than earlier results. To do an accurate calculation of relic density the result of [37] for precise evolution of degrees of freedom is used.

The set of Friedmann–Boltzmann equations in the early stages of the universe dominated by a modulus field ϕ with energy density ρ_ϕ can be written as follows (like eq. (3.5))

$$\frac{d\rho_\phi}{dt} + 3H\rho_\phi = -\Gamma_\phi \rho_\phi \,, \tag{4.17}$$

$$\frac{d\,s_R}{dt} + 3Hs_R = \frac{1}{T}\left[(1-\bar{B})\Gamma_\phi\rho_\phi + 2\,\langle E\rangle_{\rm eff}\,\langle\sigma v\rangle_{\rm eff}\left(n^2 - {n_{\rm eq}}^2\right)\right] , \tag{4.18}$$

$$\frac{d\,n}{dt} + 3Hn = \frac{B_\chi}{M_\phi}\Gamma_\phi\rho_\phi - \langle\sigma v\rangle_{\rm eff}\left(n^2 - {n_{\rm eq}}^2\right) . \tag{4.19}$$

The radiation energy density of thermal bath is given by

$$\rho_R(T) = \frac{\pi^2}{30} g_{\rm eff}(T) T^4 \,, \tag{4.20}$$

and $g_{\rm eff}$ is the relativistic energy density degrees of freedom (DoF). The entropy density for radiation comes from

$$s_R(T) = \frac{\rho_R(T) + p_R(T)}{T} = \frac{2\pi^2}{45} h_{\rm eff}(T) T^3 \,, \tag{4.21}$$

where $h_{\rm eff}$ is the entropy DoF. We use the result of Chapter 2 for $h_{\rm eff}$ and $g_{\rm eff}$. The part of energy due to DM branching from modulus is

$$\bar{B} = \frac{\langle E\rangle_{\rm eff}\, B_\chi}{M_\phi} \,. \tag{4.22}$$

The number density of the odd sector (SUSY) particles are shown as n where $n = \sum_i n_i$ and $n_{\rm eq} = \sum_i n_{{\rm eq},i}$ is the number density in equilibrium. Then, the thermally averaged cross section and the portion of energy injected to the thermal bath by the annihilation of SUSY particles can be written as [50, 166]

$$\langle\sigma v\rangle_{\rm eff} = \sum_{i=1}^{N}\sum_{j=1}^{N} \langle\sigma_{ij} v_{ij}\rangle \frac{n_{{\rm eq},i}}{n_{\rm eq}} \frac{n_{{\rm eq},j}}{n_{\rm eq}}, \tag{4.23}$$

$$\langle E\rangle_{\rm eff}\,\langle\sigma v\rangle_{\rm eff} = \sum_{i=1}\sum_{j=1} \left(\langle E_i\rangle + \langle E_j\rangle\right)\langle\sigma_{ij} v_{ij}\rangle \frac{n_{{\rm eq},i}}{n_{\rm eq}} \frac{n_{{\rm eq},j}}{n_{\rm eq}} \,. \tag{4.24}$$

The relative velocity of i and j particles with mass $M_{i,j}$, momentum $p_{i,j}$ and energy $E_{i,j}$ can be obtained from

$$v_{ij} = \frac{\sqrt{\left(p_i \cdot p_j\right)^2 - M_i^2 M_j^2}}{E_i E_j} \,. \tag{4.25}$$

The total annihilation rate of $\chi_i\chi_j$ is given by

$$\sigma_{ij} = \sum_X \sigma(\chi_i\chi_j \to X)\,, \tag{4.26}$$

where X is the set of standard model particles [15, 50]. The thermally averaged cross section is defined by

$$\left\langle \sigma_{ij} v_{ij} \right\rangle = \frac{\int d^3p_i d^3p_j f_i f_j \sigma_{ij} v_{ij}}{\int d^3p_i d^3p_j f_i f_j}\,, \tag{4.27}$$

here f_i's are approximated by Maxwell–Boltzmann distribution [50].

At reheat temperature the energy density of the universe becomes equal to the Hubble rate of a radiation dominated universe

$$T_{\rm RH} = \sqrt{\Gamma_\phi M_{\rm Pl}} \left(\frac{45}{4\pi^3 g_{\rm eff}(T_{\rm RH})} \right)^{1/4}\,. \tag{4.28}$$

The decay width of a long–lived modulus field Γ_ϕ coming from a supergravity theory is given by

$$\Gamma_\phi = \alpha \frac{M_\phi^3}{M_{\rm Pl}^2}\,,\quad \alpha = \frac{C}{8\pi} = \text{ constant}\,, \tag{4.29}$$

where C is a constant depending on the final products of scalar decay. All the parameters we did not explain here are defined the previous Chapter. In the rest of this Chapter we assume $\alpha = 1$. To find the numerical value of relic abundance we use the following changes of variables for densities to work in the comoving frame

$$\Phi \equiv \frac{\rho_\phi A^3}{T_{\rm RH}^4}\,,\ R \equiv \rho_R \frac{A^4}{T_{\rm RH}^4}\,,\ X \equiv n_\chi \frac{A^3}{T_{\rm RH}^3}\,,\ A \equiv a T_{\rm RH}\,, \tag{4.30}$$

here n_χ is the neutralino number density. As the temperature reduces n will be equivalent to n_χ, since all SUSY particles finally decay to LSP that is neutralino in our study. Then, the Hubble variable can be written as

$$H = \widetilde{H} T_{\rm RH}^2 A^{-3/2} c_1^{-1/2} M_{\rm Pl}^{-1}\,, \tag{4.31}$$

where $c_1 = \frac{3}{8\pi}$ and the Hubble rate in the comoving volume $\widetilde{H}$ is

$$\widetilde{H} \equiv \left(\Phi + \frac{R}{A} + \frac{\langle E \rangle_{\rm eff} X}{T_{\rm RH}} \right)^{1/2}\,. \tag{4.32}$$

By changing the variables according to eq. (4.30), we will have the Friedmann equations for evolving degrees of freedom in the comoving frame [38]

$$\widetilde{H} \frac{d\Phi}{dA} = -\, c_\rho^{1/2} A^{1/2} \Phi\,, \tag{4.33}$$

$$\begin{aligned} \frac{dT}{dA} = \left(1 + \frac{T}{3h_{\rm eff}} \frac{dh_{\rm eff}}{dT} \right)^{-1} \Bigg[& -\frac{T}{A} + \frac{15 T_{\rm RH}^6}{2\pi^2 c_1^{1/2} M_{\rm Pl} H T^3 h_{\rm eff} A^{\frac{11}{2}}} \Big(c_\rho^{1/2} A^{3/2} (1-\bar{B}) \Phi \\ & + c_1^{1/2} M_{\rm pl} \frac{2 \langle E \rangle_{\rm eff} \langle \sigma v \rangle_{\rm eff}}{A^{3/2}} \left(X^2 - {X_{\rm eq}}^2 \right) \Big) \Bigg]\,, \end{aligned} \tag{4.34}$$

$$\widetilde{H}\frac{dX}{dA} = \frac{c_\rho^{1/2} T_{\rm RH} B_\chi}{M_\phi} A^{1/2}\Phi + c_1^{1/2}\, M_{\rm pl} T_{\rm RH} A^{-5/2} \langle\sigma v\rangle_{\rm eff} \left({X_{\rm eq}}^2 - X^2\right). \tag{4.35}$$

In the above differential equations we have $c_\rho = \frac{\pi^2 g_{\rm eff}(T_{RH})}{30}$. We solve the above set of differential equations with the following initial conditions [38, 134, 146]

$$X_I = 0,\;\; R_I = 0,\;\; \Phi_I = \frac{3H_I^2 M_{Pl}^2}{8\pi T_{RH}^4},\;\; H_I = \gamma {\Gamma_\phi}^2. \tag{4.36}$$

The case of considering non–vanishing initial densities for DM and radiation are studied in [38]. Also, we discussed it in Chapter 3 and the outcome will be similar for neutralino so we will not mention it in this Chapter.

To compute the final numerical value of relic abundance, we use the following relation for relic density in a non–thermal cosmology as mentioned in [38]

$$\begin{aligned}\Omega_\chi h^2 &= \frac{\rho_\chi(T_{\rm now})}{\rho_\gamma(T_{\rm now})}\Omega_\gamma h^2 = \frac{\rho_\chi(T_F)}{2\rho_R(T_F)}\frac{g_{\rm eff}(T_F)h_{\rm eff}(T_{\rm now})}{h_{\rm eff}(T_F)}\frac{T_F}{T_{\rm now}}\Omega_\gamma h^2 \\ &= M_\chi \frac{X(T_F)}{R(T_F)}\frac{A_F T_F g_{\rm eff}(T_F) h_{\rm eff}(T_{\rm now})}{2T_{\rm now} T_{\rm RH} h_{\rm eff}(T_F)}\Omega_\gamma h^2\,,\end{aligned} \tag{4.37}$$

where $T_{\rm now}$ and $\Omega_\gamma h^2$ are the current temperature of cosmic microwave background (CMB) photons and radiation density of CMB. As provided by Particle Data Group[42], they take the following numerical values

$$\Omega_\gamma h^2 = 2.473 \times 10^{-5}\,,\; T_{now} = 2.7255\; K = 2.35 \times 10^{-13} GeV. \tag{4.38}$$

The present relic density of DM is also determined by current observations[42]

$$\Omega_{DM} h^2 = 0.1186 \pm 0.002. \tag{4.39}$$

In this analysis the details of thermalization process [149–151] which may affect the thermal production of neutralino from SM particles are not considered. We may consider such effects in the future studies. Also, we do not consider the production of neutralino from energetic thermal bath particles [148], since it is important only for neutralino mass near the modulus mass which is not the case in our setup. Since all SUSY particles ultimately decay to the LSP, n will reduce to n_χ and $\langle E\rangle_{\rm eff}$ will be equivalent to $\langle E\rangle_{\rm eff} \approx \sqrt{M_\chi^2 + 3T^2}$. Also, from our previous result [38] we know that the effect of DM annihilation to radiation is negligible on the final radiation density and thus the term containing this effect can be ignored. Additionally, we should mention that the $\langle\sigma v\rangle_{\rm eff}$ reduces to $\langle\sigma v\rangle$ for the lightest neutralino. Moreover, in `MicrOMEGAs` the thermally averaged cross section is a function of temperature T. This function can be efficiently calculated at temperatures much lower than M_χ. In our numerical calculation we assume $\langle\sigma v\rangle(T \geq M_\chi/13) = \langle\sigma v\rangle(T = M_\chi/13)$ and $\langle\sigma v\rangle(T < M_\chi/13) = \langle\sigma v\rangle(T)$ which helps to increase the speed of calculation without losing the accuracy in the final result [3].

[2] In the rest of this Chapter, we consider $\gamma = 10^{15}$ for our numerical calculations.

[3] To solve eqs. (4.33), (4.34), and (4.35) we used `CVODE` package to change the routine in `micrOMEGAs` for solving Boltzmann equation and computing relic density.

4.4 Relic Density of Thermally Produced Neutralino Dark matter

In this section we briefly mention the cross section and the approximate relic density of thermally produced neutralino. If $M_1 \ll M_2, \mu$ then LSP will be bino. Its approximate cross section and thermal relic density come from [18, 174]

$$\langle \sigma_{\widetilde{B}} v \rangle = \frac{3g^4 \tan^4 \theta_W r(1+r^2)}{2\pi m^2_{\widetilde{l}_R} x(1+r)^4}, \quad x \equiv \frac{M_1}{T}, \quad r \equiv \frac{M_1^2}{m^2_{\widetilde{l}_R}}, \tag{4.40}$$

$$\Omega_{\widetilde{B}} h^2 \propto \frac{m^4_{\widetilde{l}_R}}{M_1^2}\,, \tag{4.41}$$

where as it is shown they depend on the mass of right handed sleptons $m_{\widetilde{l}_R}$,which are almost mass degenerate [18]. Here θ_W is the weak mixing angle and g is the electroweak coupling of $SU(2)_L$ gauge group. In case $\mu \ll M_1, M_2$ the LSP is higgsino–like and by neglecting the terms including M_W (the mass of W boson) and considering the coannihilation effects from higgsino like charginos [64, 104, 175], since their mass can be close to neutralinos, we have thermally averaged cross section and thermal relic density as [174]

$$\langle \sigma_{\widetilde{H}} v \rangle = \frac{g^4}{512\pi\mu^2}\left(21 + 3\tan^2\theta_W + 11\tan^4\theta_W\right), \tag{4.42}$$

$$\Omega_{\widetilde{H}} h^2 \propto \mu^2\,. \tag{4.43}$$

Bino and higgsino like neutralinos can appear in mSUGRA (CMSSM) where SUSY is broken by gravity mediation effects [18].

Wino–like neutralino is possible in anomaly mediation SUSY breaking [155]. In this case $M_2 \ll M_1, \mu$. Considering the limit $M_2 \gg M_W$ and the coannihilation effects from wino–like charginos [64, 104, 176] the thermally averaged cross section and thermal abundance are given by [174]

$$\langle \sigma_{\widetilde{W}} v \rangle = \frac{3g^4}{16\pi M_2^2}, \tag{4.44}$$

$$\Omega_{\widetilde{W}} h^2 \propto M_2^2\,. \tag{4.45}$$

4.5 Neutralino Production in a Non–thermal Cosmology

We are interested in neutralinos with thermally averaged cross section smaller or larger than thermal WIMP, since interesting regions which satisfy thermal relic density are excluded already or will be probed by ongoing experiments. This can be satisfied by different production mechanisms with smaller cross sections which are shown in [38, 146] i.e. for modified non–relativistic freeze–out (FO^{mod}_{nr}), non–relativistic inverse annihilation (IA_{nr}) [4], relativistic inverse annihilation (IA_r) [5] , and from modulus branching ratio (Φ–decay). The quasi static equilibrium (QSE_{nr}) and Φ–decay regions can give the relic density for neutralinos with $\langle \sigma v \rangle$ larger than thermal WIMP [38, 146].

[4] This scenario is like freeze-in DM (the so called FIMP) which is first mentioned in [145]. For a review on FIMP models and constraints look at [154].

[5] This mechanism is not interesting for neutralino DM case since it will not be relativistic in the low reheating scenarios that we consider here.

Assuming the massless limit of final states of neutralino thermal annihilation leads to eqs (4.40), (4.42), and (4.44) for thermally averaged cross section of bino–, higgsino–, and wino– like neutralino DM, respectively. Depending on the mass and cross section of DM which can be determined by the type of neutralino, different production mechanisms in low reheating temperature scenarios can yield the final abundance of DM to satisfy the observed value i.e. $\Omega_\chi h^2 \simeq 0.12$ [42].

Quasi static equilibrium (QSE) mechanism happens when the terms correspond to DM from branching ratio of moduli and annihilation of SM particles cancel out each other (on the right hand side of eq. (4.19)). Then the relic density (from eq. (3.43)) will be [38]

$$\Omega_\chi h^2[\mathrm{QSE_{nr}}] \approx \frac{120\,\Gamma\left(\frac{5}{3}\right)^{3/2}}{\pi}\frac{M_\chi M_\phi}{\lambda^3 L^{3/4} g_{\rm eff}(T_{\rm RH}) B_\chi M_{\rm Pl}^2 \langle\sigma v\rangle^2 T_{\rm RH}^3}\frac{g_{\rm eff}(T_F)h_{\rm eff}(T_{\rm now})}{2T_{\rm now}h_{\rm eff}(T_F)}\Omega_\gamma h^2\,, \tag{4.46}$$

where $\lambda \approx 2$ in eq. (3.38) and L is a constant depending on branching ratio of DM, modulus mass, and reheating temperature, and given by [38, 146]

$$L \equiv (1 - B_{\rm eff})\Gamma\left(\frac{5}{3}\right)\left(\frac{3}{2}\right)^{2/3}\,, \quad B_{\rm eff} \equiv \frac{B_\chi\left(M_\chi^2 + 3T_{RH}^2\right)^{1/2}}{M_\phi}\,, \tag{4.47}$$

where $B_{\rm eff}$ is a very small number since M_ϕ should be larger than the order of 100 TeV to avoid the BBN bound, and M_χ is relatively smaller than modulus mass.

The usual non-relativistic freeze–out during radiation dominated era occurs also for DM masses with the freeze-out temperature below the reheat temperature and following relic density (like eq. (3.44))

$$\Omega_\chi h^2[\mathrm{FO}_{\rm nr}^{\rm rad}] \approx \frac{4\sqrt{5}}{\sqrt{\pi}}\frac{\hat{x}_{\rm FO}}{g_{\rm eff}(\hat{T}_{\rm FO})^{1/2} M_{\rm Pl}\langle\sigma v\rangle}\frac{g_{\rm eff}(T_F)h_{\rm eff}(T_{\rm now})}{2T_{\rm now}h_{\rm eff}(T_F)}\Omega_\gamma h^2\,, \quad \text{with } \hat{x}_{\rm FO} = \frac{M_\chi}{\hat{T}_{\rm FO}}\,. \tag{4.48}$$

If the $\langle\sigma v\rangle < \langle\sigma v\rangle_{crit}$ (c.f. [38, 146] and eq. (3.36)) then the relic abundance will be given by the sum of the contribution of branching from moduli and production mechanisms in the inefficient annihilation regime [38, 146]

$$\Omega_\chi h^2 \approx \Omega_{\chi,\rm ann} h^2 + \Omega_{\chi,\rm decay} h^2\,. \tag{4.49}$$

The contribution $\Omega_{\chi,\rm decay}h^2$ comes from ϕ decays and obeys [38, 146] (like eq.(3.48))

$$\Omega_{\chi,\rm decay} h^2 \approx \frac{B_\chi T_{\rm RH} M_\chi}{L^{3/4} M_\phi}\frac{g_{\rm eff}(T_F)h_{\rm eff}(T_{\rm now})}{2T_{\rm now}h_{\rm eff}(T_F)}\Omega_\gamma h^2\,, \tag{4.50}$$

The relic abundance for non–relativistic freeze–out during modulus domination (FO_{nr}^{mod}) is given by [38, 146] (like eq.(3.49))

$$\Omega_{\chi,\rm ann} h^2[\mathrm{FO}_{\rm nr}^{\rm mod}] \approx \frac{8}{\sqrt{5\pi}}\frac{g_{\rm eff}(T_{\rm RH})^{1/2}}{L^{3/4} g_{\rm eff}(T_{\rm FO})}\frac{T_{\rm RH}^3 {x_{FO}}^4}{{M_\chi}^3 M_{\rm Pl}\langle\sigma v\rangle}\frac{g_{\rm eff}(T_F)h_{\rm eff}(T_{\rm now})}{2T_{\rm now}h_{\rm eff}(T_F)}\Omega_\gamma h^2\,, \quad \text{with } x_{FO} = \frac{M_\chi}{T_{FO}}\,. \tag{4.51}$$

The relic density of DM in non–relativistic inverse annihilation scenario which can be relevant to neutralino DM is [38, 146] (like eq.(3.56))

$$\Omega_{\chi,\rm ann} h^2[\mathrm{IA_{nr}}] \approx \frac{48\,\chi\, g_\chi^2}{5^{3/2}\pi^{15/2}L^{3/4}}\frac{g_{\rm eff}(T_{RH})^{3/2} T_{\rm RH}^7 M_{\rm Pl}\langle\sigma v\rangle}{g_{\rm eff}(T_*)^3 {M_\chi}^5}\frac{g_{\rm eff}(T_F)h_{\rm eff}(T_{\rm now})}{2T_{\rm now}h_{\rm eff}(T_F)}\Omega_\gamma h^2\,, \tag{4.52}$$

where for neutralino (a Majorana fermion) we consider $g_\chi = 2$. The factor χ is a numerical factor which is around 292 (computed in eq. (3.54)), $T_* \approx 0.28 M_\chi$ for $M_\chi \lesssim T_{RH}$, and $T_* \approx T_{RH}/2$ for $M_\chi \gtrsim T_{RH}$ [38, 146].

In these calculations we assumed the rapid thermalisation process of decay products of modulus ϕ which causes the DM particles reach equilibrium fast. In the regime $M_\chi \ll M_\phi$ the approximation of instantaneous thermalisation can be ideally considered [38].

4.5.1 Parameter Regions with Correct Relic Abundance

If the freeze–out of neutralino happens before reheating, cross sections less or greater than typical WIMP can accomplish the valid relic density. In such a case (i.e. $\hat{T}_{FO} \gtrsim T_{RH}$) DM with $\langle\sigma v\rangle \gtrsim 10^{-8}\text{GeV}^{-2}$ can be produced from Φ–decay or QSE_{nr} to satisfy the relic abundance bound. However, for $\langle\sigma v\rangle \lesssim 10^{-8}\text{GeV}^{-2}$ the valid range of relic abundance can be satisfied by Φ–decay, FO^{mod}_{nr}, IA_{nr}.

To find the regions that match well with the observed value for relic density, i.e. $\Omega_\chi h^2 \approx 0.12$ [42], we require to illustrate the boundaries of different DM production mechanisms shown in Fig. 3.2. This helps to have an analytical understanding of which mechanism can give the suitable relic density for a specific kind of neutralino in case of a low reheating temperature.

The two freeze–out mechanisms in radiation and matter dominated era can meet each other for tiny B_χ ($\ll 10^{-7}$ based on our analysis in Chapter 3 and Figs. 3.2 and 3.10) at a specific mass or freeze-out temperature which comes from

$$\frac{\widetilde{\widetilde{T_{FO}}}}{T_{RH}} \approx \left(\frac{2}{5}\right)^{1/3} \frac{1}{L^{1/4}} \left(\frac{g_{\text{eff}}(T_{RH})}{g_{\text{eff}}(\widetilde{\widetilde{T_{FO}}})}\right)^{1/6} , \tag{4.53}$$

where we used eqs. (4.48) and (4.51). Also, we assumed $T_{FO} \approx \hat{T}_{FO}$ to find $\widetilde{\widetilde{T_{FO}}}$. If we consider $\widetilde{\widetilde{T_{FO}}} \approx \widetilde{\widetilde{M_\chi}}/20$, then for different moduli $M_\phi \approx 5\times10^5, 5\times10^6, 5\times10^7$ GeV the specific DM mass $\widetilde{\widetilde{M_\chi}} \approx 5.8\times10^{-1}, 1.2\times10^{1}, 3.6\times10^{2}$ GeV. For very small B_χ ($\ll 10^{-7}$) the modified freeze–out and the inverse annihilation regions (eqs. (4.51) and (4.52)) can coincide for a mass fixed by relic density i.e. $\widetilde{M_\chi}$ given by

$$\langle\sigma v\rangle_{FOIA} \approx \left(\frac{5}{3\chi}\right)^{1/2} \frac{(2\pi)^{7/2}}{g_\chi} \frac{g_{\text{eff}}(\widetilde{M_\chi}/4)}{g_{\text{eff}}(T_{RH})^{1/2}} \frac{\widetilde{M_\chi}}{T_{RH}^2 M_{Pl}} , \tag{4.54}$$

where we used $T_* \approx T_{FO}$ which is a very good approximation for masses around $\widetilde{M_\chi}$ in FO^{mod}_{nr} scenario. For different set of moduli masses $M_\phi \approx 5\times10^5, 5\times10^6, 5\times10^7$ GeV ($T_{RH} \approx 4.068\times10^1, 8.486\times10^2, 2.549\times10^4$ MeV), there are $\langle\sigma v\rangle_{FOIA} \approx 10^{-13}, 10^{-14}, 10^{-15}$ GeV^{-2} , and $\widetilde{M_\chi} \approx 3.5$ GeV, 100 GeV, 3 TeV, respectively.

For tiny B_χ ($\ll 10^{-7}$) if the thermally averaged cross section can satisfy the following inequality

$$\langle\sigma v\rangle < \langle\sigma v\rangle_{FOIA} , \tag{4.55}$$

which shows values lower than WIMP range and FO^{mod}_{nr}, then neutralino is produced in non–relativistic inverse annihilation IA_{nr} scenario. Moreover, for $B_\chi \ll 10^{-7}$ if the neutralino cross section is smaller than the required value for WIMP but larger than $\langle\sigma v\rangle_{FOIA}$, the dominant mechanism is the modified freeze–out.

In addition, if we consider for $\widetilde{M_\chi}$ the branching of scalar to DM gives the correct relic density, we can

find that specific branching ratio from eq. (4.50) which we call $\widetilde{B_\chi}$. Then we have these values of $\widetilde{B_\chi} \approx 4.5 \times 10^{-3}, 7.6 \times 10^{-5}, 8.5 \times 10^{-7}$ for moduli masses $M_\phi \approx 5 \times 10^5, 5 \times 10^6, 5 \times 10^7$ GeV, respectively. Moreover, IA_{nr} and Φ–decay regions will match to each other when B_χ is larger than $\widetilde{B_\chi}$. Consequently, using eqs. (4.52) and (4.50) for cross sections lower than the following one

$$\langle \sigma v \rangle_{IA\Phi} \approx \frac{5^{3/2}\pi^{15/2}}{48 g_\chi^2 \chi} \frac{g_{\rm eff}(M_\chi/4)^3}{g_{\rm eff}(T_{RH})^{3/2}} \frac{B_\chi M_\chi^6}{T_{RH}^6 M_{Pl} M_\Phi} \,, \tag{4.56}$$

where the DM production will happen in IA_{nr} or Φ–decay mechanisms, for the second one the relic abundance is independent of $\langle \sigma v \rangle$. For a fixed neutralino mass if the cross section is smaller than $\langle \sigma v \rangle_{IA\Phi}$ then the correct relic density will be satisfied by Φ–decay scenario.

If B_χ is smaller than $\widetilde{B_\chi}$ then the equality between the regions of correct relic density for QSE_{nr} and Φ–decay production mechanisms (eqs. (4.46) and (4.50)) occurs. So we gain the following cross section

$$\langle \sigma v \rangle_{QSE\Phi} \approx \frac{3^{1/2}5^{1/2}\Gamma\left(\frac{5}{3}\right)^{3/4}}{\pi^{1/2}} \frac{M_\phi}{B_\chi g_{\rm eff}(T_{RH})^{1/2} T_{RH}^2 M_{Pl}} \,, \tag{4.57}$$

which shows that if the thermally averaged cross section is larger than that DM can be produced in QSE_{nr} region. However, if $\langle \sigma v \rangle_{WIMP} \lesssim \langle \sigma v \rangle \lesssim \langle \sigma v \rangle_{QSE\Phi}$ it can be produced via Φ–decay. For $B_\chi > \widetilde{B_\chi}$ and $\langle \sigma v \rangle > \langle \sigma v \rangle_{WIMP}$ DM should be produced via QSE_{nr} to satisfy the correct yield. In Sec. 4.6 and plots of Figs. 4.1, 4.2, 4.3, and 4.4 we see how the mentioned parameter regions in this section give correct relic density to bino, higgsino, and wino DM in a non–thermal cosmology.

4.5.2 The Scan over SUSY Parameter Space

The scan in pMSSM [173] is done over the p10MSSM parameter space (based on [166]) shown in table 4.1 [6]. In pMSSM the SUSY parameters are considered at TeV scale. In such a case all three different types of neutralinos appear in the final result.

We also have done another scan over the parameter space of CMSSM where the universal gaugino and scalar masses, trilinear couplings, and ratio of vacuum expectation values of Higgs doublets are considered at GUT scale, where the gauge forces unify [7]. In such scenario the neutralino can be bino or higgsino like [18]. The range of parameters we used are shown in the table 4.2.

To calculate the relic density, direct detection (DD) and indirect detection (ID) cross sections of neutralinos we use `MicrOMEGAs v4.3.5` [172]. We apply `SuSpect v2.41` [177] as a SUSY spectrum generator which computes SUSY parameters (masses and couplings, etc.) at weak scale with the initial values at a given scale using renormalisation group equations (RGEs). We do not discuss the details of RGEs for SUSY here, since it is beyond the scope of this thesis. Interested reader should look at ref. [17]. To do the scan we used `T3PS v1.0` program where the computation can be performed faster by using the parallel processing in it [178]. The only constraint we used in our scan is the nuisance parameter for the 125 GeV Higgs mass i.e 122 $GeV \leq m_h \leq$ 128 GeV [179, 180]. This constraint is sufficient for our purpose, since we basically require to produce some valid points in the SUSY parameter space and study the production of neutralino in low reheating scenarios.

The relic abundance of bino–like DM depends not only on (bino–like) neutralino mass but also on sfermion masses (also chargino's and sfermion's in case of coannihilation) as it is shown in eq. (4.41)

[6] The number of random points for our scan in pMSSM is 4000. The number of points that satisfy the Higgs mass range are around 800.

[7] Our scan CMSSM is done over 2000 points. After imposing the Higgs mass constraint around 700 points are left.

[18, 181, 182]. So for a specific M_χ there is a degeneracy in the thermal relic density of bino DM. This shows itself in the red points in Fig. 4.1 (a) (4.3 (a)) for relic density versus neutralino mass in pMSSM (CMSSM) scan. Due to different initial parameters in random scan, sfermion and chargino masses derived by RGEs do not follow a specific pattern which shows itself in the scattered shape of points in Figs. 4.1 (a) (4.3 (a)) and 4.5 (b) (4.6 (b)) for the thermal relic density and velocity independent thermally averaged cross section of bino–like neutralino. However, the relic density of higgsino–like and wino–like neutralinos are scaled by the squared of their masses i.e. μ and M_2 as eqs. (4.43) and (4.45) show. These are displayed by green and blue points in Fig. 4.1 (a) (Fig. 4.3 (a)).

In our numerical calculation we do not consider the effect of Sommerfeld enhancement since it mostly affects winos with large masses due to the appearance of Yukawa–like potential via the exchange of weak gauge bosons in their massless limit [183, 184]. However, we included coannihilation effects [64, 104] in our scan using the relevant features in `micrOMEGAs`[8]. Our focus is mostly on the dilution or concentration of neutralino DM in the low reheating scenario where its effect can be sizeable in comparison to coannihilation and Sommerfeld enhancement contributions.

Lightest neutralinos with $M_\chi \lesssim 100$ GeV are severely constrained from the large electron–positron collider (LEP). Consequently, we represent the result of our scan only for $M_\chi \gtrsim 100$ GeV. This constraint is considered in our calculation using `micrOMEGAs` [172]. Also, the result of large hadron collider (LHC) searches mostly satisfy this constraint [30–35].

Parameter	Range
bino mass	$0.1 < M_1 < 5$
wino mass	$0.1 < M_2 < 6$
gluino mass	$0.7 < M_3 < 10$
stop trilinear coupling	$-12 < A_t < 12$
stau trilinear coupling	$-12 < A_\tau < 12$
sbottom trilinear coupling	$A_b = -0.5$
pseudoscalar mass	$0.2 < m_A < 10$
μ parameter	$0.1 < \mu < 6$
3rd generation soft squark mass	$0.1 < m_{\widetilde{Q}_3} < 15$
3rd generation soft slepton mass	$0.1 < m_{\widetilde{L}_3} < 15$
1st/2nd generation soft squark mass	$m_{\widetilde{Q}_{1,2}} = M_1 + 100$ GeV
1st/2nd generation soft slepton mass	$m_{\widetilde{L}_{1,2}} = m_{\widetilde{Q}_3} + 1$ TeV
ratio of Higgs doublet VEVs	$2 < \tan\beta < 62$

Table 4.1: The parameters of the p10MSSM and their ranges used in our scan. All masses and trilinear couplings are given in TeV, unless indicated otherwise. All the parameters of the model are given at the SUSY breaking scale. The range of parameters in this Table are similar to Table 1 of ref. [166].

[8] The coannihilation effects can be quantified using the following parameter [172]

$$B_{FO} = \frac{K_1\left(\frac{M_i+M_j}{\hat{T}_{FO}}\right)}{K_1\left(\frac{2M_\chi}{\hat{T}_{FO}}\right)} \approx e^{\frac{\hat{X}_{FO}\left(M_i+M_j-2M_\chi\right)}{M_\chi}}, \tag{4.58}$$

where i and j denote the particles with closest mass to lightest neutralino (like charginos or sfermions in some scenarios [175, 181, 182, 185]) . For $\hat{X}_{FO} = M_\chi/\hat{T}_{FO} \sim 25$ if we choose $B_{FO} \sim 10^{-5}$, then it implies $M_i + M_j \lesssim 2.46\, M_\chi$. In `micrOMEGAs`, B_ϵ parameter is a limit defined by user to consider coannihilation channels in WIMP annihilation. It means that in computing the relic density the channels with B_{FO} smaller than B_ϵ will be included. As B_ϵ is smaller the contribution of coannihilations are calculated more precisely. For $B_\epsilon = 1$ there would not be any coannihilation assumption. Here we choose $B_\epsilon = 10^{-5}$ in our calculations.

Parameter	Range
scalar mass	$0.1 < m_0 < 6$
gaugino mass	$0.1 < m_{1/2} < 6$
trilinear coupling	$-12 < A_0 < 12$
ratio of Higgs doublet VEVs	$1 < \tan\beta < 60$
sign of μ parameter	$\mu > 0$

Table 4.2: The range of CMSSM parameters we used in our scan are given at GUT scale. The unit for masses and trilinear couplings is TeV.

4.6 Experimental Constraints and Motivation for Non–thermally Produced Neutralino

In indirect direction, thermally averaged cross section $\langle\sigma v\rangle$ appears in computing the flux of DM annihilation products (Appendix B.1). Since the intergalactic medium can resemble the thermal bath of the early universe due to high density and pressure, DM particles can meet each other with higher probability than any other place. So the possibility of DM annihilation to SM particles is more than any where else. The exclusion bounds on the $\langle\sigma v\rangle$ (up to 95% limit) provided by the combined analysis of MAGIC and FermiLAT results [21] on dwarf satellite galaxies for annihilation cross section of DM particles to W^+W^-, b^+b^-, $\tau^+\tau^-$, and $\mu^+\mu^-$ pairs are shown in frame (b) of Fig. 4.5 (4.6) for pMSSM (CMSSM) scan. As the cyan line in these frames represents winos with masses lower than 800 GeV, which annihilate dominantly to W^+W^- final state, are excluded by indirect detection [21]. Also, the dominant annihilation channel of higgsino–like neutralino is W^+W^- (also $Z\bar{Z}$) which based on frame (b) of Fig. 4.5 (4.6) should be heavier than 350 GeV. This range encompasses a considerable range of thermally produced higgso–like and wino–like neutralino DM in pMSSM scan (only higgsino–like in CMSSM) which could approximately match with the thermal WIMP, shown in Fig. 4.1 (a) (4.3 (a)), and different non–thermal production scenarios shown Figs. 4.1 and 4.2 (Figs. 4.3 and 4.4). As Fig. 4.5 (b) (4.6 (b)) shows bino–like neutralinos evade the constraints on annihilation to $f\bar{f}$ shown by yellow, pink, and light green lines, and respectively for b^+b^-, $\tau^+\tau^-$, and $\mu^+\mu^-$ final states [21]. This happens, since their thermally averaged cross section is below the canonical value $\sim 3\times10^{-26}\ cm^3/s$ for WIMP and follows the pattern of eq. (4.40).

In direct detection experiments the detector measures the recoil energy of nuclei of heavy stable elements when possible DM particles interact with them (Appendix B.2). These experiments provide some exclusion curves for the plane of DM mass and spin independent cross section of their interaction with detectors protons in the nuclei (σ_p^{SI}). The cross sections above these curves are excluded with the probability of 90% confidence level. The elastic scattering of nucleon with DM ($\chi\ N \to \chi\ N$) can be explained by the spin independent four fermion term $\bar{\chi}\chi\bar{N}N$ in the effective interaction Lagrangian. The dominant mediator for such interaction can be the Higgses or squarks. The σ_p^{SI} will depend on the type of mediator, neutralino and N_{1i}'s [184, 186, 187]. We will not discuss the details of such interactions here; they are extensively studied in the literature for different types of neutralinos [186, 188–191]. We have only computed them numerically using `micrOMEGAs` to verify the current limits of neutralino in the DD expeiments. Fig. 4.5 (a) (Fig. 4.6 (a)) is the plot for spin independent cross section of neutralino and nucleon in direct detection experiments with respect to DM mass in pMSSM (CMSSM) scan, respectively. It includes all three kind of neutralino (only bino and higgsino in CMSSM). The constraints provided by XENON1T [28] and PandaX–II [29] experiments are shown in Figs. 4.5 (a) (4.6 (a)) by solid black

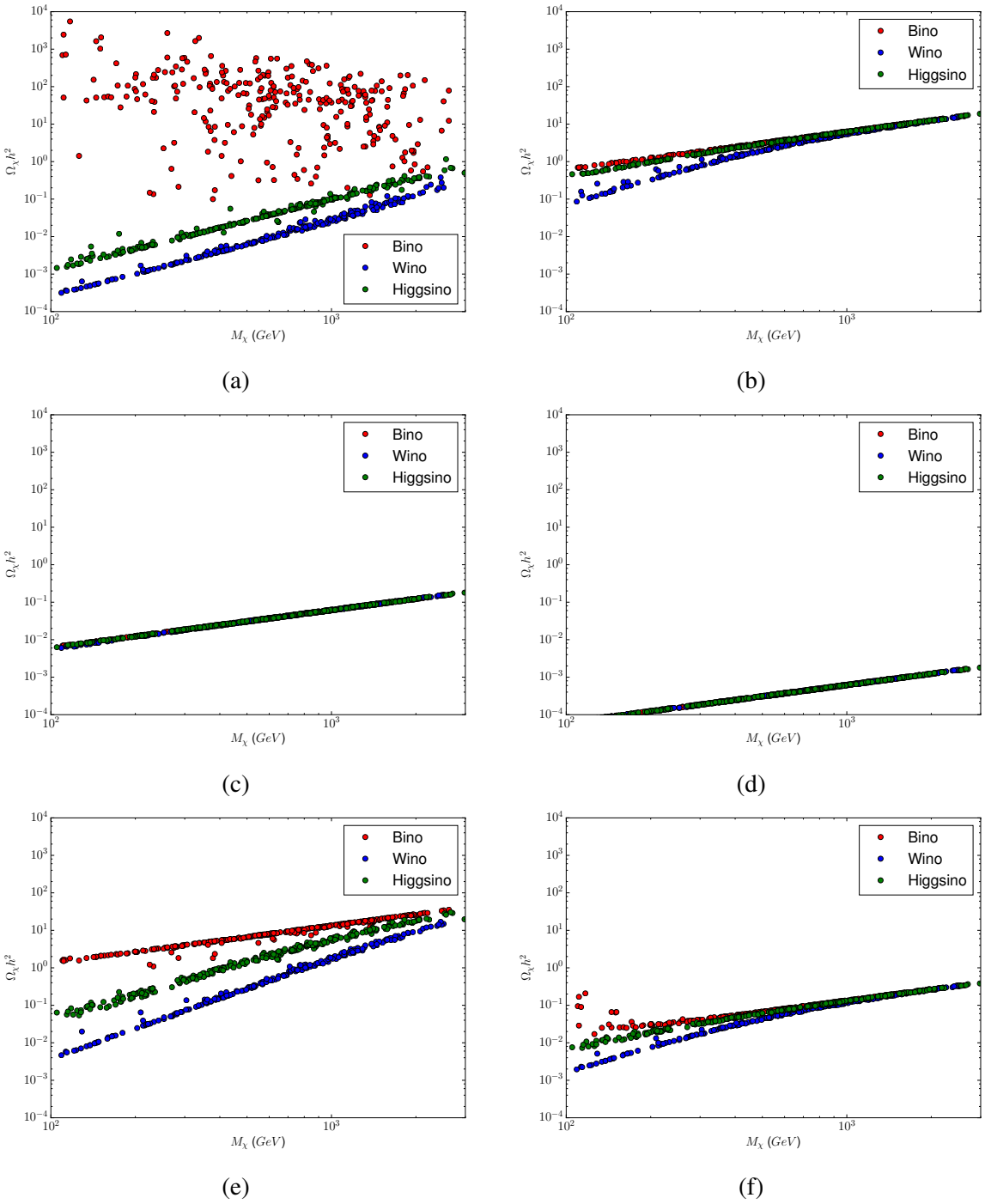

Figure 4.1: The plots of relic density $\Omega_\chi h^2$ versus DM mass M_χ based on the scan over pMSSM parameter space (Table 4.1) in different cosmological scenarios before radiation domination are shown above. The first top left figure (a) is for the relic density of thermally produced DM. The rests are for different low reheating setups with moduli masses M_ϕ and branching ratios B_χ, (M_ϕ, B_χ): b) (5×10^5 GeV, 10^{-3}), c) (5×10^5 GeV, 10^{-5}), d) (5×10^5 GeV, 10^{-7}), e) (5×10^6 GeV, 10^{-3}), f) (5×10^6 GeV, 10^{-5}).

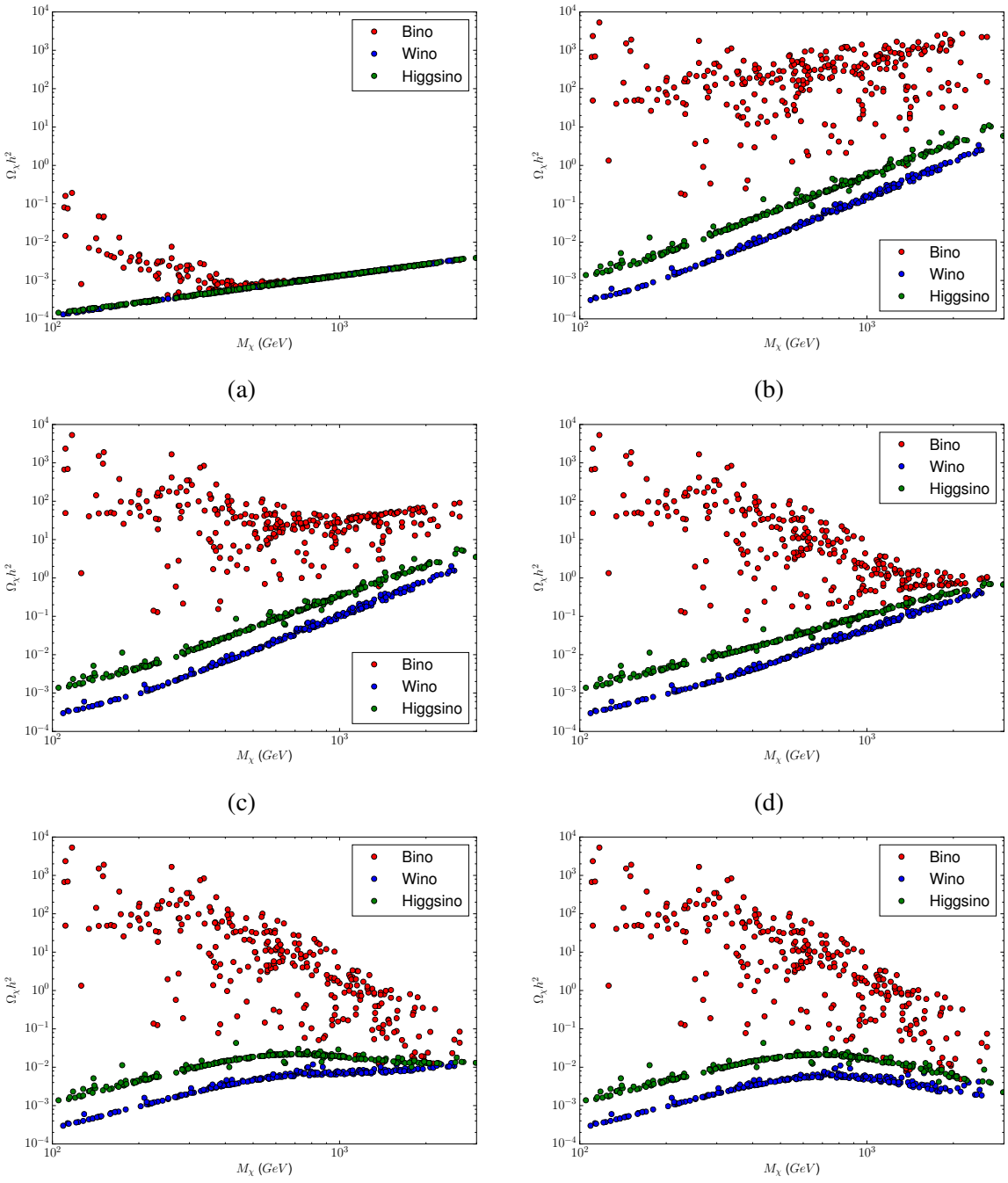

Figure 4.2: These plots also like the last 5 plots of Fig. (4.1) are for different (M_ϕ, B_χ): a) (5×10^6 GeV, 10^{-7}), b) (5×10^7 GeV, 10^{-1}), c) (5×10^7 GeV,10^{-3}), d) (5×10^7 GeV, 10^{-5}), e) (5×10^7 GeV, 10^{-7}), f) (5×10^7 GeV, 10^{-9}).

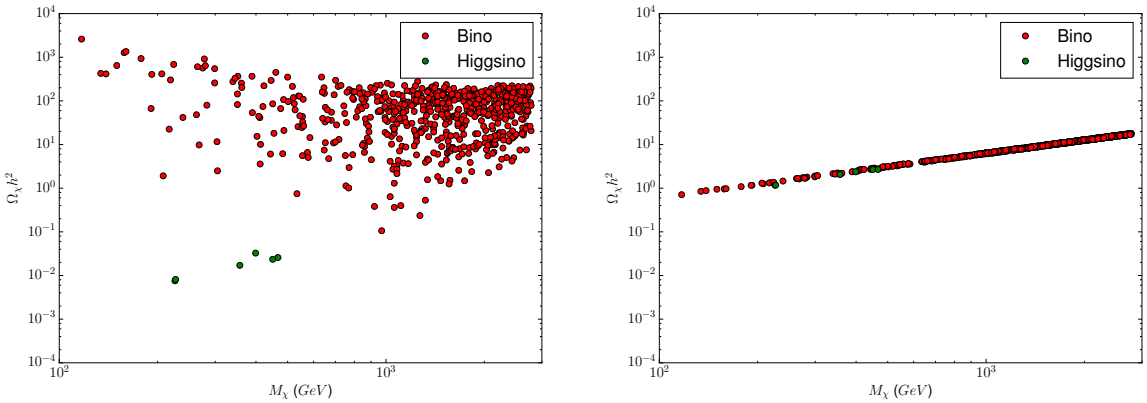

(a)

(b)

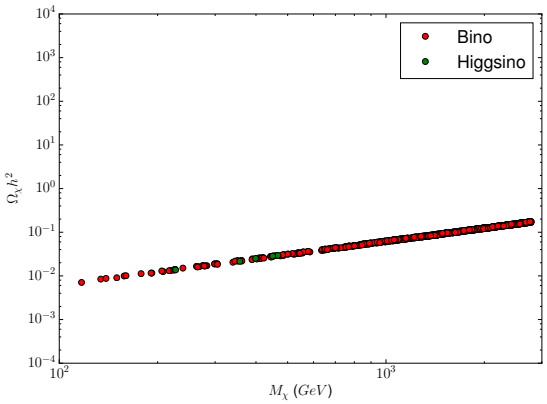

(c)

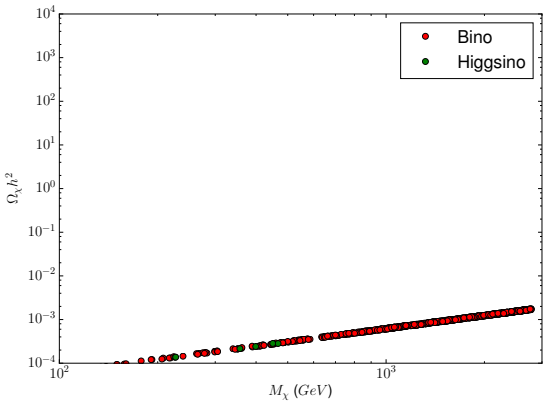

(d)

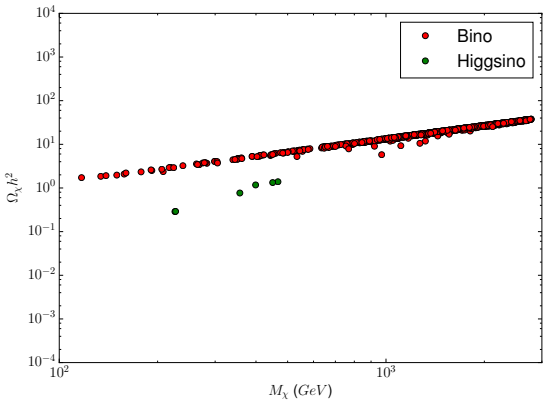

(e)

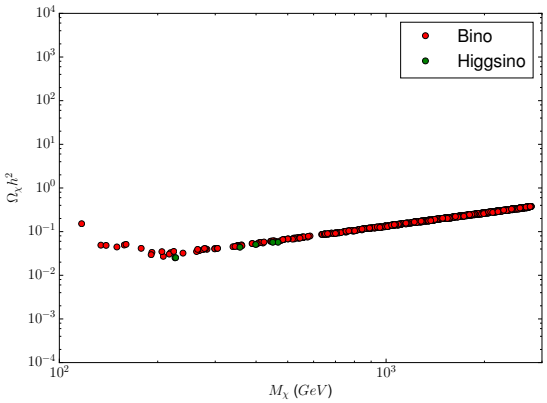

(f)

Figure 4.3: The plots of relic density $\Omega_\chi h^2$ versus DM mass M_χ based on the scan over CMSSM parameter space (Table 4.2) in different cosmological scenarios before radiation domination are shown above. The first top left figure (a) is for the relic density of thermally produced DM. The rests are for different low reheating setups with moduli masses M_ϕ and branching ratios B_χ, (M_ϕ, B_χ): b) (5×10^5 GeV, 10^{-3}), c) (5×10^5 GeV, 10^{-5}), d) (5×10^5 GeV, 10^{-7}), e) (5×10^6 GeV, 10^{-3}), f) (5×10^6 GeV, 10^{-5}).

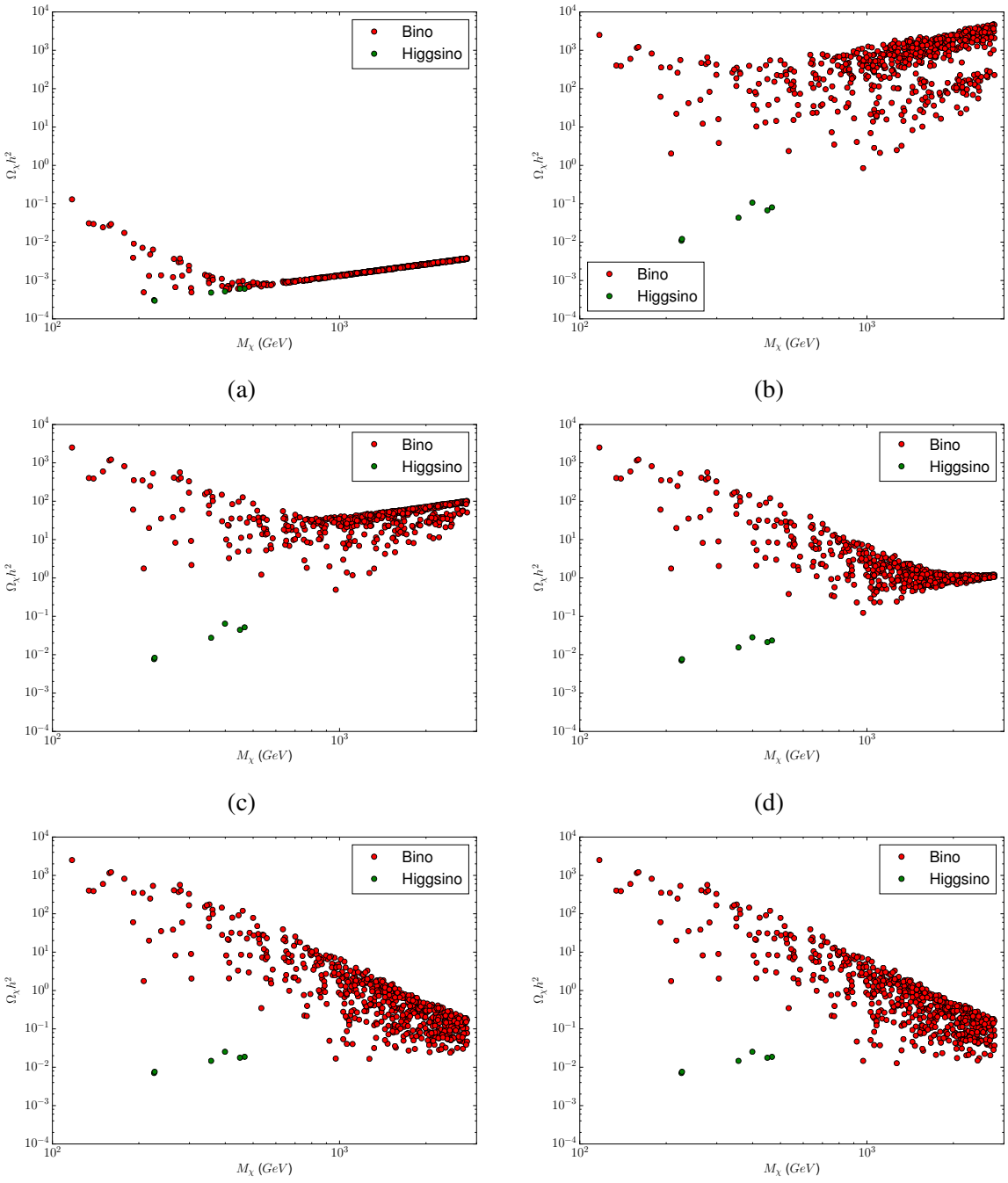

Figure 4.4: These plots also like the last 5 plots of Fig. (4.3) are for different (M_ϕ, B_χ): a) (5×10^6 GeV, 10^{-7}), b) (5×10^7 GeV, 10^{-1}), c) (5×10^7 GeV,10^{-3}), d) (5×10^7 GeV, 10^{-5}), e) (5×10^7 GeV, 10^{-7}), f) (5×10^7 GeV, 10^{-9}).

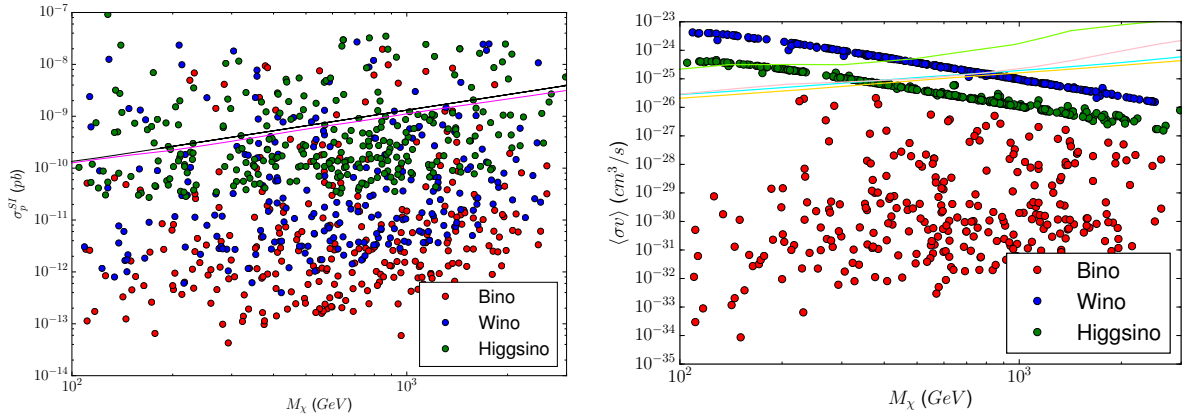

(a) (b)

Figure 4.5: In the left panel spin–independent cross section for proton and neutralino σ_p^{SI} is shown for different neutralinos with mass M_χ. The magenta line is for PandaX–II exclusion limit [29]. However, the exclusion limit from XENON1T experiment is shown via black line [28]. The right panel represents the s–wave thermally averaged cross section $\langle\sigma v\rangle$ for various neutralino masses M_χ. The lines with colors cyan, yellow, pink, and light green are the constraints from the combination of MAGIC and FermiLAT results for the annihilation of a pair of Majorana DM to W^+W^-, b^+b^-, $\tau^+\tau^-$, and $\mu^+\mu^-$ final states [21]. The scan is done in pMSSM based on the parameters of Table (4.1).

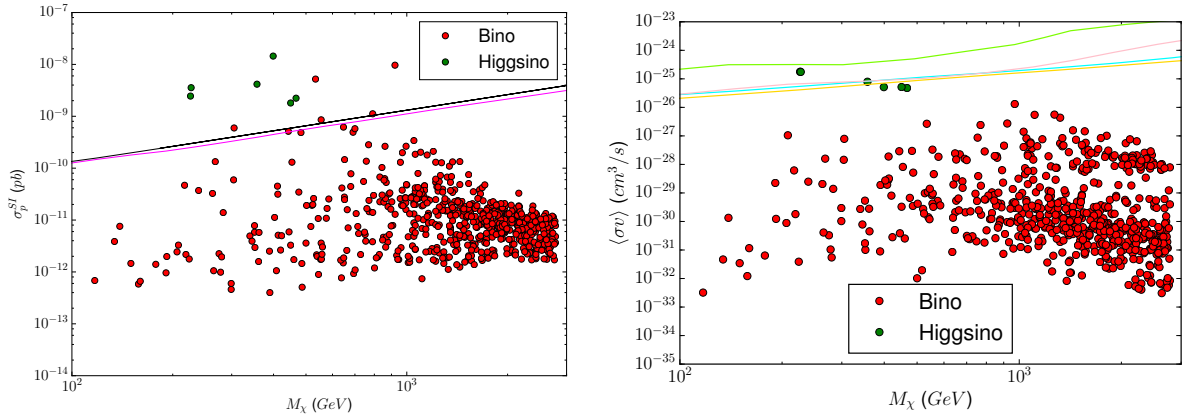

(a) (b)

Figure 4.6: In the left panel spin–independent cross section for proton and neutralino σ_p^{SI} is shown for different neutralinos with mass M_χ. The magenta line is for PandaX–II exclusion limit [29]. However, the exclusion limit from XENON1T experiment is shown via black line [28]. The right panel represents the s–wave thermally averaged cross section $\langle\sigma v\rangle$ for various neutralino masses M_χ. The lines with colors cyan, yellow, pink, and light green are the constraints from the combination of MAGIC and FermiLAT results for the annihilation of a pair of Majorana DM to W^+W^-, b^+b^-, $\tau^+\tau^-$, and $\mu^+\mu^-$ final states [21]. The scan is done in CMSSM based on the parameters of Table (4.2).

and magenta curves, respectively. These curves exclude DM particles with spin independent cross sections larger than 10^{-10} pb for mass 100 GeV and 2.5×10^{-9} pb for mass 3 TeV. It includes a considerable amount of higgsinos. However, a large portion of binos and winos are below this limit.

Adding the result of ID and DD in previous paragraphs generally yields binos still considerably having the chance to play the role of neutralino DM. However, their thermal relic density is much above the observational value $\Omega h^2 \simeq 0.12$ [42] which can cause the overclosure of the universe. This problem can be solved by assuming the production of neutralinos in an early matter dominated epoch which is explained in Sec. 4.5. In such a case to achieve the correct relic density of binos, FO_{nr}^{mod}, IA_{nr}, and Φ–decay production mechanisms can help. Moreover, there are regions of parameter space for winos and higgsinos which are not excluded by ID and DD constraints. However, in these regions they have a thermal relic density different from observational one, they can gain the correct relic via the presence of modulus dominated era. Since for them $\langle\sigma v\rangle$ is larger than the thermal WIMP, production mechanisms that efficiently produce the sufficient DM abundance are QSE_{nr} and Φ–decay. In Figs. 4.1, 4.2, 4.3, and 4.3 we have considered three different reheating models with moduli masses 5×10^5, 5×10^6, 5×10^7 GeV, and reheating temperatures 4.068×10^1, 8.486×10^2, 2.549×10^4 MeV, repectively to depict our results.

The regions where neutralino in pMSSM is produced by Φ–decay are in Figs. 4.1 (b) (all binos, higgsinos and winos with $M_\chi \gtrsim 200$ GeV), 4.1 (c), 4.1 (d), 4.1 (e) (almost all binos; higgsinos and winos with $M_\chi \gtrsim 2.5$ TeV), 4.1 (f) (bino and higgsinos with $M_\chi \gtrsim 200$ GeV, and winos with $M_\chi \gtrsim 400$ GeV), 4.2 (a) (all winos and higgsinos; binos heavier than 400 GeV), 4.2 (b) (all higgsinos and winos; binos with $M_\chi \gtrsim 400$ GeV).

Quasi static equilibrium production mechanism is efficient for winos and higgsinos, due to the fact that their $\langle\sigma v\rangle$ is larger than the thermal WIMP, in Figs. 4.1 (b) ($M_\chi \lesssim 200$ GeV), 4.1 (e) ($M_\chi \lesssim 2.5$ TeV), 4.1 (f) (higgsinos with $M_\chi \lesssim 200$ GeV and winos with $M_\chi \lesssim 400$ GeV), 4.2 (b) (with $M_\chi \gtrsim 200$ GeV), and 4.2 (c) (with $M_\chi \gtrsim 200$ GeV). Also, in Fig. 4.2 (d) for $M_\chi \gtrsim 400$ GeV the sum of Φ–decay and QSE_{nr} mechanisms gives the final relic density for higssinos and winos.

Modified non–relativistic freezeout occurs mostly in Fig. 4.2 (b) (binos with $200\ GeV \lesssim M_\chi \lesssim 400$ GeV), and in Figs. 4.2 (c), 4.2 (d), 4.2 (e), 4.2 (f) (binos with $M_\chi \gtrsim 200$ GeV).

The production of DM via IA_{nr} is dominant in Figs. 4.1 (f) (binos with $M_\chi \lesssim 100$ GeV), 4.2 (a) (binos with $100\ GeV \lesssim M_\chi \lesssim 200$ GeV).

One should note that in Figs. 4.2 (e) and 4.2 (f) since the branching ratio is very small, the QSE_{nr} is not efficient. Then the production of winos and higgsinos heavier than 500 GeV will be diluted with respect to their thermal relic abundance. The above results match with the approximate analytical equations in Sec. 4.5.1.

The discussion we have done in the last five paragraphs for the range of DM mass and different production mechanisms is also true for neutralino in CMSSM except there is not any wino–like neutralino in such a scenario. The frames in Figs. 4.3 and 4.4 have similar results to Figs. 4.1 and 4.2 for the same set of branching ratios and modulus masses.

There is one more issue regarding bino–like neutralino production in a non–thermal scenario. Non–thermally produced DM particles with cross sections lower than WIMP which satisfy the relic abundance can enhance the growth of structures. This shows itself by boosting the formation of microhalos due to the linear growth of perturbations during early matter domination rather than logarithmic growth in radiation domination [36, 159]. These micro halos can compensate for the low annihilation rate of DM, here bino dark matter, by increasing its self-annihilation (enhancing the J–factor (B.4)) which is invisible to the current direct detection experiments [158, 192, 193] (the cross section is close or below the neutrino floor [194]). However, this kind of DM is potentially observable in indirect detection experiment like future probes of FermiLAT.

4.7 Summary and Conclusions

In this Chapter, we studied the production of neutralino DM in a non–thermal cosmological model dominated by a heavy long lived scalar field i.e. modulus. According to previous studies [38, 146], such a scenario provides different possible production mechanisms for DM particles (Sec. 4.5). In the SUSY context with R–parity conservation the lightest neutralino can play the role of DM (Sec. 4.4). However, since a neutralino is a mixture of bino, higgsino, and wino in the SUSY parameter space, the real nature of it can be dominated by any of these three types depending on SUSY breaking scenario. Particularly, this causes the under–abundance or over–abundance of a specific kind of neutralino DM (Fig. 4.1 (a)). Considering the domination of the universe by a modulus before BBN can compensate the difference between the observed relic density of DM and theoretically predicted one for neutralino DM (Sec. 4.5.1).

We studied SUSY parameter space by scanning over it in two versions of MSSM: pMSSM and CMSSM. This produced different neutralino masses and cross sections which necessarily do not give correct thermal relic density (Sec. 4.5.2). Also, the low mass regions of higgsino and wino like neutralino are constrained by different DM experiments (Sec. 4.6). Higgsinos lighter than 350 GeV and winos lighter than 800 GeV are constrained by ID experiment. Moreover, the DM cross section with $\sigma_p^{SI} \gtrsim 5\times10^{-10}$ pb are excluded via PandaX–II [29] and Xenon1T [28] experiments. Then, we investigated the non–thermal production in a modulus dominated era where radiation and neutralino can be produced from scalar decay parameterized in eqs. (4.17) – (4.19). The plots of relic density with respect to DM mass for different moduli masses and branching ratios are shown in Figs. 4.1 (b)–4.2 (f) (pMSSM) and 4.3 (b)–4.4 (f) (CMSSM). In Sec. 4.6 we discussed the different production mechanisms i.e. QSE_{nr}, FO_{nr}^{mod}, IA_{nr}, Φ–decay that appear in these non–thermal plots. We also found analytical expressions for the boundaries of different production mechanisms, where the values of two of them become equal. These boundaries can be exploited to show through which mechanism a given DM particle could be non–thermally produced to gain the observed relic density, as we explained in Sec. 4.5.1. The regions of parameter space for winos and higgsinos which are not excluded by ID and DD experiments and underproduced in thermal production, it can gain the correct relic abundance in branching from modulus and quasi static equilibrium case. The bino–like neutralino due to its small $\langle\sigma v\rangle$ (smaller than the canonical value) is not constrained by ID. However, it is overproduced in the thermal WIMP scenario. Even in DD the σ_p^{SI} of binos on average is lower the PandaX–II and Xenon1T limits (more close to neutrino floor [194] or below it) as Figs. 4.5 (a) and 4.6 (a) show. If bino is produced in an early matter dominated epoch can gain the correct relic density through branching from the scalar field, inverse annihilation, or freeze–out in matter dominated era. Since the bino is less constrained by experiments among other types of neutralino and its overproduction can be explained in a universe dominated by a heavy modulus, it is still a suitable DM candidate.

If we find the neutralino DM as a best motivated DM candidate in the ongoing or future experiments, in case its thermally averaged cross section do not match with the thermal WIMP, assuming its production in a non–thermal scenario will be an appropriate explanation. Also, this will give us more information about the early universe cosmology through determining the correct mass for modulus and its branching ratio to DM and other particles (based on our discussion in Sec. 4.5.1).

CHAPTER 5

Conclusions and Outlook

We are convinced by the results of cosmological and astrophysical observations that dark matter (DM) should undoubtedly exist in the universe. This issue has led to an outburst of interest among theoretical and experimental physicists. Many attempts on both theory and experiment sides are currently being made to understand the real nature of dark matter. In this thesis, we studied the production of dark matter in the early universe especially in the scenarios with low reheating temperature.

In Chapter 2, we used the result of lattice quantum chromodynamics (QCD) for the equation of state of up, down, charm, and strange quarks and gluons that matches the result of hadron resonance gas model around QCD transition temperature. We also considered the effect of neutrino decoupling on radiation energy and entropy densities. This led to the precise calculation of degrees of freedom (DoF) of standard model. The effect of our precise treatment of DoF on the relic density of WIMP (weakly interacting massive particle) DM is up to around 10% difference for DM masses between 3 to 15 GeV with respect to previous studies for both S–wave and P–wave cross sections.

In Chapter 3 we studied the production of DM in an early matter dominated epoch with low reheating temperature using our treatment of DoF in Chapter 2. The scenarios with early matter domination can happen after the inflationary reheating and before the domination of the universe by a radiation component. These types of models are motivated by unified theories like superstring theory, so that after the compactification of extra dimensions some new scalar fields (moduli) appear that can gain mass through Higgs–like mechanisms. These fields can couple to standard model particles and dark matter. Due to their longevity via the Planck mass suppression in their decay width, they can dominate the early moments of the universe after inflation until their decay at reheating time, where they can produce radiation and dark matter. This kind of scenario leads to new production mechanisms beyond the thermal WIMP; particularly for DM candidates with thermally averaged cross section smaller than WIMP. We showed that a precise treatment of the evolution of DoF improves the estimation of DM relic density, in such scenarios, by several hundred percent. We have also found an upper bound on the modulus mass in case thermally averaged cross section is smaller than the canonical value for WIMP. The lower bound on modulus mass comes from the lowest reheating temperature which is around 4MeV not to spoil the success of big bang nucleosynthesis (BBN); that imposes $M_\phi \gtrsim 100$TeV. Moreover, we investigated the effect of initially vanishing and non–vanishing DM and radiation densities on the non–thermal production mechanisms. Depending on initial conditions and parameters, non–vanishing initial densities can cause the DM relic density to exceed the observed value of $\Omega_{DM}h^2 \simeq 0.12$ in non–thermally produced regions of parameter space with the previously correct relic abundance; something that would not have happened with initially vanishing densities.

Supersymmetry (SUSY) is an appropriate candidate for beyond the standard model physics, since

it solves various problems like DM, hierarchy in the electroweak sector, gauge unification, etc. in one framework. Moreover, it can be the low energy limit of a unified theory like superstring theory. SUSY has been widely studied in the literature and probed in different experiments; however, without any empirical evidence. Neutralino as the most popular candidate for WIMP in supersymmetric models is constrained severely by the experiments. The relic density for neutralinos in regions of SUSY parameter space avoiding the constraints, does not match the thermal WIMP prediction. This can be solved in low reheating scenarios. In Chapter 4 we considered neutralino production in a period of modulus domination which can give the correct relic density to different types of neutralinos via new production mechanisms mentioned in Chapter 3.

Direct detection experiments like Xenon1T, PandaX–II, and SuperCDMS are approaching the regions of cross section (σ_p^{SI}) smaller than $\sim 10^{-10}$ pb. Below and near this region the effect of neutrino background appears which makes the detection very difficult. Direct detection probes may in the future overcome this problem for such low σ_p^{SI} to probe the DM candidates that are produced non–thermally e.g. bino–like neutralino in supersymmetry.

Current indirect detection experiments can probe thermally averaged cross sections around the canonical value for thermal WIMPs ($3 \times 10^{-26} cm^3/s$), but have not given any confirmed evidence yet. Assuming non–thermal production of DM particles to satisfy the relic density, leads to cross sections smaller or larger than that of the thermal WIMP. These new cross sections can be probed or ruled out by experiments like FermiLAT, HESS, AMS–02, and DAMPE. As we explained at the end of Sec. 4.6, the production of DM during modulus domination can enhance the growth of perturbations linearly instead of the logarithmic growth in a radiation dominated era. This in turn increases the production of micro halos after the time DM particles are kinetically decoupled during matter domination. These micro halos can elevate the self interaction rate of DM particles, that avoid the present experimental limit by indirect detection experiments via increasing the chance of detectability of DM with small annihilation cross section. This is another reason that makes DM production in an early matter dominated epoch phenomenologically motivating, especially for DM particles with cross sections lower than the thermal WIMP.

Producing and measuring the properties of a very massive moduli–like particle is not accessible in future colliders (at least in the current century), since their mass should be larger than $\sim$ 100 TeV to avoid the conflict with BBN constraints. But current and future gravitational wave and cosmic microwave background (CMB) experiments, in case of having an adequate level of precision, may measure the possible effects of an early matter domination in the universe, and the consequent decay of a heavy long–lived particle to DM and SM particles. Even though we can not produce such heavy particles, which could dominate the universe at early times, it is in principle possible to produce and search for the trace of non–thermally produced DM particles with tiny couplings to SM at the Large Hadron Collider or future colliders like the International Linear Collider, Future Circular Collider, Compact Linear Collider, etc.

Finally, I hope that my attempts during my PhD and in this thesis have been a small step toward unraveling the mysteries of dark matter and the cosmos.

APPENDIX A

Thermodynamics and Lattice Quantum Chromodynamics

Quantum chromodynamics is the fundamental theory of strong interactions and nuclear matter. In quantum field theory (QFT) we can illustrate the thermodynamics of a system using grand canonical ensemble. This ensemble is defined by the density operator and partition functions [195, 196].

$$\rho = e^{-\frac{1}{T}(H-\mu_i N_i)}\,,\;\; Z = \hat{T}r\rho\,,\;\; \hat{T}r(...) = \sum_n \langle n|(...)|n\rangle\;. \tag{A.1}$$

Then all other thermodynamic variables are computed from the partition function. In QFT the partition function can be computed from the path integral of that specific QFT (here QCD).

In lattice quantum chromodynamics (LQCD) the thermodynamic variables are calculated using the discretization of the space–time to a hyper cubic lattice with volume $N_s^3 \times N_\tau$ where $L = aN_s$ and $T^{-1} = aN_\tau$ are spatial and temporal length of lattice, respectively. The methods and numerical details of LQCD is beyond the scope of this thesis. Interested reader should look at these references [195, 196]. However, we briefly explain the thermodynamic equations that are connected to the result of LQCD and their relation with QCD field theory.

Using the partition function we can drive the free energy and entropy of a thermal system.

$$F = -T\log Z\,, p = \frac{\partial(T\log Z)}{\partial V}\,, S = \frac{\partial(T\log Z)}{\partial T}\,. \tag{A.2}$$

Also we can write the second law of thermodynamics using the number of similar particles in each energy state ($\bar{N}_i$) as follows

$$\bar{N}_i = -\frac{\partial(T\log Z)}{\mu_i}\,,\qquad E = -pV + TS + \mu_i\bar{N}_i\,. \tag{A.3}$$

The following quantities are extensive and we are interested in the thermodynamic limit of them. Then we consider them in the unit of volume

$$f = \frac{F}{V}\,,\qquad s = \frac{S}{V}\,,\quad n_i = \frac{\bar{N}_i}{V}\,,\quad \rho = \frac{E}{V}\,, \tag{A.4}$$

where by using eq. (A.2) we obtain

$$p = -f\,,\quad \rho = \frac{T^2}{V}\frac{\partial\log Z}{\partial T} = -\frac{1}{V}\frac{\partial\log Z}{\partial T^{-1}}\,. \tag{A.5}$$

Energy momentum tensor of a relativistic system of fluid is given by

$$T^{\mu\nu} = (p+\rho)u^{\mu}u^{\nu} - pg^{\mu\nu}\,, \tag{A.6}$$

where $g^{\mu\nu}$ is the Minkowski metric with diagonal components $(1,-1,-1,-1)$. The unit four vector of velocity in that fluid rest frame is

$$u^{\mu} = (1,0,0,0)\,. \tag{A.7}$$

Another quantity which has a great interest in LQCD and thermal field theory studies is trace anomaly

$$I(T) \equiv T^{\mu\mu}(T) = T^5 \frac{\partial}{\partial T}\frac{p(T)}{T^4}\,, \tag{A.8}$$

where Einstein summation rule is used in above. There are the following relations between above quantities

$$I = \rho - 3p\,, \quad s = \frac{\rho+p}{T}\,, \quad c_s^2 = \frac{dp}{d\rho}\,, \tag{A.9}$$

and c_s is the sound speed in the fluid. When a system is in thermal equilibrium the relation between different thermodynamic variables is called the equation of state,

$$f(p,V,T,\mu_i) = 0\,, \tag{A.10}$$

which provides the information to study that system further.

The grand canonical ensemble of QCD can be quantified by the partition function which is widely studied in the literature [195, 196]. This partition function is

$$Z(V,\mu_f,T;g,m_f) = \bar{T}r\left(e^{-(H-\mu_f Q_f)/T}\right) = \int DAD\bar{\psi}D\psi e^{-S_{g_s}[A_\mu]}e^{S_f[\bar{\psi},\psi,A_\mu]}\,, \tag{A.11}$$

where the Euclidean [1] action for gauge bosons and fermions are denoted by

$$S_{g_s}[A_\mu] = \int_0^{1/T} d\tau \int_V d^3x \frac{1}{2} TrF_{\mu\nu}(x)F_{\mu\nu}(x)\,,$$

$$S_f[\bar{\psi},\psi,A_\mu] = \int_0^{1/T} d\tau \int_V d^3x \sum_{f=1}^{N_f} \bar{\psi}_f(x)\left(\gamma_\mu D_\mu + m_f - \mu_f\gamma_0\right)\psi_f(x)\,,$$

$$D_\mu = (\partial_\mu - \mathrm{ig_s A_\mu}), \quad \mathrm{A_\mu = T^a A^a_\mu(x)}, \quad \mathrm{a = 1,...,N^2-1}\,, \quad \mathrm{F_{\mu\nu}(x) = \frac{i}{g_s}[D_\mu, D_\nu]}\,, \tag{A.12}$$

By considering the infinity limit of spatial volume $V \to \infty$ the thermodynamic limit in the above integrals can be obtained. The following quantity shows the conserved quark numbers operator for the relevant chemical potential μ_f defined as

$$Q_f = \bar{\psi}_f\gamma_0\psi_f\,. \tag{A.13}$$

The dependency on thermodynamic variables i.e. μ_f, V and T appears in the eq. (A.11) for partition function. Also, it depends on quark mass (m_f) and strong coupling constant (g_s). In the last line of

[1] It refers to considering the imaginary time ($\tau \to$ i t) in field theory which causes similarity between time and spatial coordinates.

eq. (A.12) N shows the order of $SU(N)$ gauge group. For QCD $N = 3$ and $a = 1, ..., 8$ denotes the index of group generators T^a.

The limit $T \to 0$ of above equations corresponds to the vacuum QCD in infinite four dimentional spacetime volume. In lattice gauge theory considering Bose–Einstein statistics for bosons and Fermi–Dirac for fermions (including Pauli exclusion principle) the following boundary conditions can be used

$$A_\mu(\tau, \mathbf{x}) = A_\mu(\tau + 1/T, \mathbf{x}), \qquad \psi(\tau, \mathbf{x}) = -\psi(\tau + 1/T, \mathbf{x}), \tag{A.14}$$

for bosons and fermions, respectively [195, 196].

In QCD studies N_f shows the number of quark flavors. In case it is an explicit sum of numbers, it represents that the masses are different. For example, $N_f = 2 + 1$ denotes the up and down quark masses (m_u and m_d) are equal but not with the strange quark mass (m_s). If it is written as a single number, it means that the masses of all quarks are equal (e.g. $N_f = 3$ i.e. $m_u = m_d = m_s$) [195, 196].

APPENDIX B

Indirect and Direct Detection Experiments

B.1 Indirect Detection

The center of our galaxy as the closest dense region with high probability of accumulation of dark matter (DM) particles due to large gravitational effects is one of the most interesting regions for indirect searches. One way to observe the annihilation of dark matter particles indirectly is through the detection of gamma rays from the center of our galaxy [15, 105, 187, 197]. These gamma rays can be from the annihilation of a pair of dark matter particles

$$\chi\chi \rightarrow \gamma\gamma\,, \tag{B.1}$$

or from annihilation of their charged products

$$\chi\chi \rightarrow \mu^+\mu^-, \tau^+\tau^-, b\bar{b}, W^+W^- \rightarrow \gamma + \dots\,. \tag{B.2}$$

The flux of such events per energy bin can be calculated from the following formula [15, 105, 187, 197]

$$\frac{d\Phi_\gamma}{dE_\gamma} = \frac{\langle\sigma v\rangle}{8\pi m_\chi^2}\frac{dN_\gamma}{dE_\gamma}\int_{\Delta\Omega} d\Omega \int_{\text{line of sight}} ds\,\rho^2(r)\,, \quad r = \sqrt{s^2 + d^2 - 2sd\cos\theta}\,, \tag{B.3}$$

where the distance from Earth to the center of the source is denoted by d. The $\rho(r)$, N_γ and m_χ are the local density of DM at source place, number of detected photons and DM mass, respectively. Also, r shows the distance from the location of annihilation to the Earth. The so called J–factor is given by

$$J = \frac{1}{8\pi}\int_{\Delta\Omega} d\Omega \int_{\text{line of sight}} ds\,\rho^2(r)\,. \tag{B.4}$$

There are several DM density profiles [198–200] based on simulation of the distribution of matter in the galaxy which are generally parameterized as

$$\rho(r) = \frac{\rho_0}{\left(\frac{r}{R}\right)^\gamma\left[1+\left(\frac{r}{R}\right)^\alpha\right]^{\frac{\beta-\gamma}{\alpha}}}\,, \tag{B.5}$$

where α, β, and γ can be specified for each profile. The characteristic length for each profile is denoted by R [198–200]. As a consequence, the computation of flux is model dependent. There are some experiments to measure such gamma ray events like FermiLAT [19–23, 57, 58], etc. These experiments can probe different regions of m_χ and $\langle\sigma v\rangle$ parameter space to detect events like what are shown in (B.1) and (B.2)

or provide some exclusion curves where the regions above them are mostly excluded at 95% confidence level.

B.2 Direct Detection

In direct detection experiment the event rate of DM interaction with the nuclei in the detector is given by [15, 105]

$$R \approx \frac{\rho_{\chi_\odot} \sigma_{\chi,\mathrm{N}} \langle v_\chi \rangle}{m_\chi m_N}\,, \tag{B.6}$$

where $\rho_{\chi_\odot}$ is the local energy density of DM near our solar system in the galaxy and $\sigma_{\chi,\mathrm{N}}$ is the elastic scattering cross section of DM and nucleon. The average velocity of DM (χ) with respect to target nuclei (N) is denoted by $\langle v_\chi \rangle$. The mass of DM and nuclei are written as m_χ and m_N, respectively. If the distribution of speed of dark matter is purely Maxwellian the event rate can be approximated as follows [1]

$$R \propto \frac{\rho_{\chi_\odot} \sigma_{\chi,\mathrm{N}}}{m_\chi m_N} v_\odot \exp\left(-\frac{E_T m_N}{2\mu^2}\right), \tag{B.7}$$

where the circular speed of the Sun around the Milky Way center is denoted by $v_\odot = 220\ \mathrm{km{\cdot}s^{-1}}$. E_T is the threshold of the recoil energy that can be measured by the detector and the reduced mass of nucleon and DM system is defined by $1/\mu = 1/m_\chi + 1/m_N$ [15, 105]. If a direct detection experiment puts an upper limit on the event rate then we can interpret it as an upper limit on $\rho_{\chi_\odot}$ and/or $\sigma_{\chi,\mathrm{N}}$ which behaves like [187]

$$m_\chi \exp\left(\frac{E_T m_N}{2\mu^2}\right), \tag{B.8}$$

so that at small m_χ it behaves exponentially and at large DM mass it increases linearly. This leads to the known exclusion curves over the parameter space of cross section and dark matter mass; provided by direct detection experiments like Xenon1T [28], PandaX–II [29], etc. These curves exclude the regions above them at 90% confidence level.

[1] The details of derivation are beyond the scope of this thesis. Interested reader should look at [105].

Bibliography

[1] G. Bertone and D. Hooper, *A History of Dark Matter*, Submitted to: Rev. Mod. Phys. (2016), arXiv: 1605.04909 [astro-ph.CO] (cit. on p. 2).

[2] V. C. Rubin, N. Thonnard and W. K. Ford Jr., *Rotational properties of 21 SC galaxies with a large range of luminosities and radii, from NGC 4605 /R = 4kpc/ to UGC 2885 /R = 122 kpc/*, Astrophys. J. **238** (1980) 471 (cit. on p. 2).

[3] F. Zwicky, *Die Rotverschiebung von extragalaktischen Nebeln*, Helv. Phys. Acta **6** (1933) 110, [Gen. Rel. Grav.41,207(2009)] (cit. on p. 2).

[4] W. Hu and S. Dodelson, *Cosmic microwave background anisotropies*, Ann. Rev. Astron. Astrophys. **40** (2002) 171, arXiv: astro-ph/0110414 [astro-ph] (cit. on p. 2).

[5] P. A. R. Ade et al., *Planck 2015 results. XIII. Cosmological parameters*, Astron. Astrophys. **594** (2016) A13, arXiv: 1502.01589 [astro-ph.CO] (cit. on pp. 2, 3, 20, 23).

[6] P. A. R. Ade et al., *Planck 2013 results. XVI. Cosmological parameters*, Astron. Astrophys. **571** (2014) A16, arXiv: 1303.5076 [astro-ph.CO] (cit. on pp. 2, 5).

[7] E. W. Kolb and M. S. Turner, *The Early Universe*, Front. Phys. **69** (1990) 1 (cit. on pp. 2, 5, 6, 9, 19, 30, 32, 33, 39, 50, 51, 57).

[8] M. Markevitch et al., *Direct constraints on the dark matter self-interaction cross-section from the merging galaxy cluster 1E0657-56*, Astrophys. J. **606** (2004) 819, arXiv: astro-ph/0309303 [astro-ph] (cit. on p. 2).

[9] D. Clowe, A. Gonzalez and M. Markevitch, *Weak lensing mass reconstruction of the interacting cluster 1E0657-558: Direct evidence for the existence of dark matter*, Astrophys. J. **604** (2004) 596, arXiv: astro-ph/0312273 [astro-ph] (cit. on p. 2).

[10] R. Massey et al., *The behaviour of dark matter associated with four bright cluster galaxies in the 10 kpc core of Abell 3827*, Mon. Not. Roy. Astron. Soc. **449**.4 (2015) 3393, arXiv: 1504.03388 [astro-ph.CO] (cit. on p. 2).

[11] F. Kahlhoefer et al., *On the interpretation of dark matter self-interactions in Abell 3827*, Mon. Not. Roy. Astron. Soc. **452**.1 (2015) L54, arXiv: 1504.06576 [astro-ph.CO] (cit. on p. 2).

[12] J. D. Bekenstein, *Relativistic gravitation theory for the MOND paradigm*, Phys. Rev. **D70** (2004) 083509, [Erratum: Phys. Rev.D71,069901(2005)], arXiv: astro-ph/0403694 [astro-ph] (cit. on p. 2).

[13] V. Sahni, *Dark matter and dark energy*, Lect. Notes Phys. **653** (2004) 141, [,141(2004)], arXiv: astro-ph/0403324 [astro-ph] (cit. on p. 2).

[14] R. H. Sanders and S. S. McGaugh,
Modified Newtonian dynamics as an alternative to dark matter,
Ann. Rev. Astron. Astrophys. **40** (2002) 263, arXiv: astro-ph/0204521 [astro-ph]
(cit. on p. 2).

[15] G. Bertone, D. Hooper and J. Silk, *Particle dark matter: Evidence, candidates and constraints*,
Phys. Rept. **405** (2005) 279, arXiv: hep-ph/0404175 [hep-ph] (cit. on pp. 2, 27, 64, 85, 86).

[16] H. Baer et al.,
Dark matter production in the early Universe: beyond the thermal WIMP paradigm,
Phys. Rept. **555** (2015) 1, arXiv: 1407.0017 [hep-ph] (cit. on pp. 2, 3, 59).

[17] S. P. Martin, *A Supersymmetry primer*
(1997) 1, [Adv. Ser. Direct. High Energy Phys.18,1(1998)], arXiv: hep-ph/9709356 [hep-ph]
(cit. on pp. 2, 28, 59–62, 69).

[18] M. Drees and M. M. Nojiri, *The Neutralino relic density in minimal $N = 1$ supergravity*,
Phys. Rev. **D47** (1993) 376, arXiv: hep-ph/9207234 [hep-ph] (cit. on pp. 2, 61, 66, 69, 70).

[19] M. Ackermann et al., *Searching for Dark Matter Annihilation from Milky Way Dwarf Spheroidal Galaxies with Six Years of Fermi Large Area Telescope Data*,
Phys. Rev. Lett. **115**.23 (2015) 231301, arXiv: 1503.02641 [astro-ph.HE]
(cit. on pp. 2, 5, 22, 23, 27, 59, 85).

[20] A. Albert et al., *Searching for Dark Matter Annihilation in Recently Discovered Milky Way Satellites with Fermi-LAT*, Astrophys. J. **834**.2 (2017) 110,
arXiv: 1611.03184 [astro-ph.HE] (cit. on pp. 2, 27, 59, 85).

[21] M. L. Ahnen et al., *Limits to dark matter annihilation cross-section from a combined analysis of MAGIC and Fermi-LAT observations of dwarf satellite galaxies*, JCAP **1602**.02 (2016) 039,
arXiv: 1601.06590 [astro-ph.HE] (cit. on pp. 2, 27, 59, 71, 76, 85).

[22] E. Charles et al.,
Sensitivity Projections for Dark Matter Searches with the Fermi Large Area Telescope,
Phys. Rept. **636** (2016) 1, arXiv: 1605.02016 [astro-ph.HE] (cit. on pp. 2, 59, 85).

[23] M. Ackermann et al., *The Fermi Galactic Center GeV Excess and Implications for Dark Matter*,
Astrophys. J. **840**.1 (2017) 43, arXiv: 1704.03910 [astro-ph.HE] (cit. on pp. 2, 59, 85).

[24] G. Angloher et al.,
Results on light dark matter particles with a low-threshold CRESST-II detector,
Eur. Phys. J. **C76**.1 (2016) 25, arXiv: 1509.01515 [astro-ph.CO] (cit. on pp. 2, 27, 59).

[25] R. Agnese et al., *New Results from the Search for Low-Mass Weakly Interacting Massive Particles with the CDMS Low Ionization Threshold Experiment*,
Phys. Rev. Lett. **116**.7 (2016) 071301, arXiv: 1509.02448 [astro-ph.CO]
(cit. on pp. 2, 27, 59).

[26] D. S. Akerib et al., *Results from a search for dark matter in the complete LUX exposure*,
Phys. Rev. Lett. **118**.2 (2017) 021303, arXiv: 1608.07648 [astro-ph.CO]
(cit. on pp. 2, 27, 59).

[27] D. S. Akerib et al., *Limits on spin-dependent WIMP-nucleon cross section obtained from the complete LUX exposure*, Phys. Rev. Lett. **118**.25 (2017) 251302,
arXiv: 1705.03380 [astro-ph.CO] (cit. on pp. 2, 59).

[28] E. Aprile et al., *First Dark Matter Search Results from the XENON1T Experiment*, Phys. Rev. Lett. **119**.18 (2017) 181301, arXiv: 1705.06655 [astro-ph.CO] (cit. on pp. 2, 59, 71, 76, 78, 86).

[29] X. Cui et al., *Dark Matter Results From 54-Ton-Day Exposure of PandaX-II Experiment*, Phys. Rev. Lett. **119**.18 (2017) 181302, arXiv: 1708.06917 [astro-ph.CO] (cit. on pp. 2, 59, 71, 76, 78, 86).

[30] S. Chatrchyan et al., *Search for new physics in the multijet and missing transverse momentum final state in proton-proton collisions at* $\sqrt{s} = 7$ *TeV*, Phys. Rev. Lett. **109** (2012) 171803, arXiv: 1207.1898 [hep-ex] (cit. on pp. 2, 59, 70).

[31] G. Aad et al., *Hunt for new phenomena using large jet multiplicities and missing transverse momentum with ATLAS in 4.7* fb^{-1} *of* $\sqrt{s} = 7$ *TeV proton-proton collisions*, JHEP **07** (2012) 167, arXiv: 1206.1760 [hep-ex] (cit. on pp. 2, 59, 70).

[32] G. Aad et al., *Search for direct production of charginos, neutralinos and sleptons in final states with two leptons and missing transverse momentum in pp collisions at* $\sqrt{s} = 8$ *TeV with the ATLAS detector*, JHEP **05** (2014) 071, arXiv: 1403.5294 [hep-ex] (cit. on pp. 2, 59, 70).

[33] V. Khachatryan et al., *Searches for electroweak production of charginos, neutralinos, and sleptons decaying to leptons and W, Z, and Higgs bosons in pp collisions at 8 TeV*, Eur. Phys. J. **C74**.9 (2014) 3036, arXiv: 1405.7570 [hep-ex] (cit. on pp. 2, 59, 70).

[34] A. M. Sirunyan et al., *Combined search for electroweak production of charginos and neutralinos in proton-proton collisions at* $\sqrt{s} = 13$ *TeV*, JHEP **03** (2018) 160, arXiv: 1801.03957 [hep-ex] (cit. on pp. 2, 59, 70).

[35] M. Aaboud et al., *Search for electroweak production of supersymmetric particles in final states with two or three leptons at* $\sqrt{s} = 13$ *TeV with the ATLAS detector* (2018), arXiv: 1803.02762 [hep-ex] (cit. on pp. 2, 59, 70).

[36] G. Kane, K. Sinha and S. Watson, *Cosmological Moduli and the Post-Inflationary Universe: A Critical Review*, Int. J. Mod. Phys. **D24**.08 (2015) 1530022, arXiv: 1502.07746 [hep-th] (cit. on pp. 3, 30, 77).

[37] M. Drees, F. Hajkarim and E. R. Schmitz, *The Effects of QCD Equation of State on the Relic Density of WIMP Dark Matter*, JCAP **1506**.06 (2015) 025, arXiv: 1503.03513 [hep-ph] (cit. on pp. 3, 4, 6, 24, 25, 29, 30, 34, 63).

[38] M. Drees and F. Hajkarim, *Dark Matter Production in an Early Matter Dominated Era*, JCAP **1802**.02 (2018) 057, arXiv: 1711.05007 [hep-ph] (cit. on pp. 3, 4, 28, 29, 36, 37, 39–41, 56, 58, 59, 63–68, 78).

[39] M. Drees and F. Hajkarim, *Neutralino Dark Matter in Low Reheating Scenarios* (), arXiv: 180X.XXXXX (cit. on pp. 4, 60).

[40] M. Davis et al., *The Evolution of Large Scale Structure in a Universe Dominated by Cold Dark Matter*, Astrophys. J. **292** (1985) 371 (cit. on p. 5).

[41] C. L. Bennett et al., *Nine-Year Wilkinson Microwave Anisotropy Probe (WMAP) Observations: Final Maps and Results*, Astrophys. J. Suppl. **208** (2013) 20, arXiv: 1212.5225 [astro-ph.CO] (cit. on p. 5).

[42] K. A. Olive et al., *Review of Particle Physics*, Chin. Phys. **C38** (2014) 090001 (cit. on pp. 5, 9, 12, 13, 17, 36, 65, 67, 68, 77).

[43] Y. B. Zel'dovich, *Magnetic model of universe*, Zh. Eksp. Teor. Fiz **48** (1965) 986 (cit. on p. 5).

[44] Y. B. Zel'dovich, L. B. Okun' and S. Pikel'ner, *Quarks: astrophysical and physicochemical aspects*, Physics-Uspekhi **8**.5 (1966) 702 (cit. on p. 5).

[45] H.-Y. Chiu, *Symmetry between particle and anti-particle populations in the universe*, Phys. Rev. Lett. **17** (1966) 712 (cit. on p. 5).

[46] B. W. Lee and S. Weinberg, *Cosmological Lower Bound on Heavy Neutrino Masses*, Phys. Rev. Lett. **39** (1977) 165 (cit. on p. 5).

[47] G. Steigman, *Cosmology Confronts Particle Physics*, Ann. Rev. Nucl. Part. Sci. **29** (1979) 313 (cit. on p. 5).

[48] J. R. Ellis et al., *Supersymmetric Relics from the Big Bang*, Nucl. Phys. **B238** (1984) 453 (cit. on pp. 5, 6).

[49] G. L. Kane et al., *Study of constrained minimal supersymmetry*, Phys. Rev. **D49** (1994) 6173, arXiv: hep-ph/9312272 [hep-ph] (cit. on p. 5).

[50] J. Edsjo and P. Gondolo, *Neutralino relic density including coannihilations*, Phys. Rev. **D56** (1997) 1879, arXiv: hep-ph/9704361 [hep-ph] (cit. on pp. 5, 63, 64).

[51] A. Birkedal et al., *Little Higgs dark matter*, Phys. Rev. **D74** (2006) 035002, arXiv: hep-ph/0603077 [hep-ph] (cit. on p. 5).

[52] V. Barger et al., *Complex Singlet Extension of the Standard Model*, Phys. Rev. **D79** (2009) 015018, arXiv: 0811.0393 [hep-ph] (cit. on p. 5).

[53] E. Aprile et al., *Dark Matter Results from 225 Live Days of XENON100 Data*, Phys. Rev. Lett. **109** (2012) 181301, arXiv: 1207.5988 [astro-ph.CO] (cit. on p. 5).

[54] R. Agnese et al., *Search for Low-Mass Weakly Interacting Massive Particles Using Voltage-Assisted Calorimetric Ionization Detection in the SuperCDMS Experiment*, Phys. Rev. Lett. **112**.4 (2014) 041302, arXiv: 1309.3259 [physics.ins-det] (cit. on p. 5).

[55] D. S. Akerib et al., *First results from the LUX dark matter experiment at the Sanford Underground Research Facility*, Phys. Rev. Lett. **112** (2014) 091303, arXiv: 1310.8214 [astro-ph.CO] (cit. on p. 5).

[56] A. Geringer-Sameth and S. M. Koushiappas, *Exclusion of canonical WIMPs by the joint analysis of Milky Way dwarfs with Fermi*, Phys. Rev. Lett. **107** (2011) 241303, arXiv: 1108.2914 [astro-ph.CO] (cit. on pp. 5, 6, 22, 24).

[57] M. Ackermann et al., *Constraining Dark Matter Models from a Combined Analysis of Milky Way Satellites with the Fermi Large Area Telescope*, Phys. Rev. Lett. **107** (2011) 241302, arXiv: 1108.3546 [astro-ph.HE] (cit. on pp. 5, 6, 22, 85).

[58] M. Ackermann et al., *Dark matter constraints from observations of 25 Milky Way satellite galaxies with the Fermi Large Area Telescope*, Phys. Rev. **D89** (2014) 042001, arXiv: 1310.0828 [astro-ph.HE] (cit. on pp. 5, 6, 22, 85).

[59] S. Galli et al., *Updated CMB constraints on Dark Matter annihilation cross-sections*, Phys. Rev. **D84** (2011) 027302, arXiv: 1106.1528 [astro-ph.CO] (cit. on pp. 5, 23).

[60] M. Hindmarsh and O. Philipsen, *WIMP dark matter and the QCD equation of state*, Phys. Rev. **D71** (2005) 087302, arXiv: hep-ph/0501232 [hep-ph] (cit. on pp. 6, 10, 13–15, 20).

[61] M. Laine and Y. Schroder, *Quark mass thresholds in QCD thermodynamics*, Phys. Rev. **D73** (2006) 085009, arXiv: hep-ph/0603048 [hep-ph] (cit. on pp. 6, 10, 11, 13–15, 20, 22).

[62] A. Bazavov et al., *Equation of state in (2+1)-flavor QCD*, Phys. Rev. **D90** (2014) 094503, arXiv: 1407.6387 [hep-lat] (cit. on pp. 6, 10–12, 14, 16, 17, 19, 20, 29, 30).

[63] P. Huovinen and P. Petreczky, *QCD Equation of State and Hadron Resonance Gas*, Nucl. Phys. **A837** (2010) 26, arXiv: 0912.2541 [hep-ph] (cit. on pp. 6, 12, 29).

[64] P. Gondolo and G. Gelmini, *Cosmic abundances of stable particles: Improved analysis*, Nucl. Phys. **B360** (1991) 145 (cit. on pp. 6, 10, 13–15, 19, 20, 35, 66, 70).

[65] G. Steigman, B. Dasgupta and J. F. Beacom, *Precise Relic WIMP Abundance and its Impact on Searches for Dark Matter Annihilation*, Phys. Rev. **D86** (2012) 023506, arXiv: 1204.3622 [hep-ph] (cit. on pp. 6, 13, 20–22, 24).

[66] P. Gondolo et al., *DarkSUSY: Computing supersymmetric dark matter properties numerically*, JCAP **0407** (2004) 008, arXiv: astro-ph/0406204 [astro-ph] (cit. on pp. 9, 13, 24).

[67] G. Belanger et al., *micrOMEGAs$_3$: A program for calculating dark matter observables*, Comput. Phys. Commun. **185** (2014) 960, arXiv: 1305.0237 [hep-ph] (cit. on pp. 9, 15, 24).

[68] A. Arbey and F. Mahmoudi, *SuperIso Relic v3.0: A program for calculating relic density and flavour physics observables: Extension to NMSSM*, Comput. Phys. Commun. **182** (2011) 1582 (cit. on pp. 9, 24).

[69] K. A. Olive, *The Thermodynamics of the Quark - Hadron Phase Transition in the Early Universe*, Nucl. Phys. **B190** (1981) 483 (cit. on pp. 10, 12).

[70] K. A. Olive, D. N. Schramm and G. Steigman, *Limits on New Superweakly Interacting Particles from Primordial Nucleosynthesis*, Nucl. Phys. **B180** (1981) 497 (cit. on pp. 10, 12).

[71] M. Srednicki, R. Watkins and K. A. Olive, *Calculations of Relic Densities in the Early Universe*, Nucl. Phys. **B310** (1988) 693 (cit. on pp. 10, 14, 15).

[72] F. Karsch, E. Laermann and A. Peikert, *The Pressure in two flavor, (2+1)-flavor and three flavor QCD*, Phys. Lett. **B478** (2000) 447, arXiv: hep-lat/0002003 [hep-lat] (cit. on p. 10).

[73] K. Kajantie et al., *The Pressure of hot QCD up to g6 ln(1/g)*, Phys. Rev. **D67** (2003) 105008, arXiv: hep-ph/0211321 [hep-ph] (cit. on p. 10).

[74] G. Boyd et al., *Thermodynamics of SU(3) lattice gauge theory*, Nucl. Phys. **B469** (1996) 419, arXiv: hep-lat/9602007 [hep-lat] (cit. on p. 10).

[75] B. Beinlich et al., *String tension and thermodynamics with tree level and tadpole improved actions*, Eur. Phys. J. **C6** (1999) 133, arXiv: hep-lat/9707023 [hep-lat] (cit. on p. 10).

[76] M. Okamoto et al.,
Equation of state for pure SU(3) gauge theory with renormalization group improved action,
Phys. Rev. **D60** (1999) 094510, arXiv: hep-lat/9905005 [hep-lat] (cit. on p. 10).

[77] Y. Namekawa et al., *Thermodynamics of SU(3) gauge theory on anisotropic lattices*,
Phys. Rev. **D64** (2001) 074507, arXiv: hep-lat/0105012 [hep-lat] (cit. on p. 10).

[78] R. V. Gavai, S. Gupta and S. Mukherjee, *The Speed of sound and specific heat in the QCD plasma: Hydrodynamics, fluctuations and conformal symmetry*, Phys. Rev. **D71** (2005) 074013, arXiv: hep-lat/0412036 [hep-lat] (cit. on p. 10).

[79] K. Kajantie et al., *Is there a hot electroweak phase transition at m(H) larger or equal to m(W)?*,
Phys. Rev. Lett. **77** (1996) 2887, arXiv: hep-ph/9605288 [hep-ph] (cit. on pp. 10, 29).

[80] F. Csikor, Z. Fodor and J. Heitger, *Endpoint of the hot electroweak phase transition*,
Phys. Rev. Lett. **82** (1999) 21, arXiv: hep-ph/9809291 [hep-ph] (cit. on pp. 10, 29).

[81] Z. Fodor, *Electroweak phase transitions*, Nucl. Phys. Proc. Suppl. **83** (2000) 121,
arXiv: hep-lat/9909162 [hep-lat] (cit. on pp. 10, 29).

[82] Y. Aoki et al., *The Order of the quantum chromodynamics transition predicted by the standard model of particle physics*, Nature **443** (2006) 675, arXiv: hep-lat/0611014 [hep-lat]
(cit. on p. 10).

[83] S. Borsanyi et al., *Full result for the QCD equation of state with 2+1 flavors*,
Phys. Lett. **B730** (2014) 99, arXiv: 1309.5258 [hep-lat] (cit. on p. 10).

[84] S. Borsanyi et al., *The QCD equation of state with dynamical quarks*, JHEP **11** (2010) 077,
arXiv: 1007.2580 [hep-lat] (cit. on pp. 11, 12, 14, 16, 17, 19).

[85] C. T. H. Davies et al.,
Precise Charm to Strange Mass Ratio and Light Quark Masses from Full Lattice QCD,
Phys. Rev. Lett. **104** (2010) 132003, arXiv: 0910.3102 [hep-ph] (cit. on p. 11).

[86] G. Mangano et al., *Relic neutrino decoupling including flavor oscillations*,
Nucl. Phys. **B729** (2005) 221, arXiv: hep-ph/0506164 [hep-ph] (cit. on p. 13).

[87] J. Lesgourgues and S. Pastor, *Neutrino mass from Cosmology*,
Adv. High Energy Phys. **2012** (2012) 608515, arXiv: 1212.6154 [hep-ph] (cit. on pp. 13, 29).

[88] K. Griest and M. Kamionkowski,
Unitarity Limits on the Mass and Radius of Dark Matter Particles,
Phys. Rev. Lett. **64** (1990) 615 (cit. on p. 21).

[89] L. Goodenough and D. Hooper, *Possible Evidence For Dark Matter Annihilation In The Inner Milky Way From The Fermi Gamma Ray Space Telescope* (2009), arXiv: 0910.2998 [hep-ph]
(cit. on p. 22).

[90] D. Hooper and L. Goodenough, *Dark Matter Annihilation in The Galactic Center As Seen by the Fermi Gamma Ray Space Telescope*, Phys. Lett. **B697** (2011) 412, arXiv: 1010.2752 [hep-ph]
(cit. on p. 22).

[91] T. Daylan et al., *The characterization of the gamma-ray signal from the central Milky Way: A case for annihilating dark matter*, Phys. Dark Univ. **12** (2016) 1,
arXiv: 1402.6703 [astro-ph.HE] (cit. on p. 22).

[92] F. Calore et al., *A Tale of Tails: Dark Matter Interpretations of the Fermi GeV Excess in Light of Background Model Systematics*, Phys. Rev. **D91**.6 (2015) 063003, arXiv: 1411.4647 [hep-ph] (cit. on p. 22).

[93] Q. Yuan and B. Zhang,
Millisecond pulsar interpretation of the Galactic center gamma-ray excess, JHEAp **3-4** (2014) 1, arXiv: 1404.2318 [astro-ph.HE] (cit. on p. 22).

[94] E. Carlson and S. Profumo,
Cosmic Ray Protons in the Inner Galaxy and the Galactic Center Gamma-Ray Excess,
Phys. Rev. **D90**.2 (2014) 023015, arXiv: 1405.7685 [astro-ph.HE] (cit. on p. 22).

[95] N. Mirabal, *Annihilating dark matter or noise?: A statistical examination of the Fermi GeV excess around the Galactic Centre* (2014), arXiv: 1411.7410 [astro-ph.HE] (cit. on p. 22).

[96] X.-L. Chen and M. Kamionkowski, *Particle decays during the cosmic dark ages*,
Phys. Rev. **D70** (2004) 043502, arXiv: astro-ph/0310473 [astro-ph] (cit. on p. 23).

[97] N. Padmanabhan and D. P. Finkbeiner, *Detecting dark matter annihilation with CMB polarization: Signatures and experimental prospects*, Phys. Rev. **D72** (2005) 023508,
arXiv: astro-ph/0503486 [astro-ph] (cit. on p. 23).

[98] M. S. Madhavacheril, N. Sehgal and T. R. Slatyer,
Current Dark Matter Annihilation Constraints from CMB and Low-Redshift Data,
Phys. Rev. **D89** (2014) 103508, arXiv: 1310.3815 [astro-ph.CO] (cit. on p. 23).

[99] T. R. Slatyer, N. Padmanabhan and D. P. Finkbeiner,
CMB Constraints on WIMP Annihilation: Energy Absorption During the Recombination Epoch,
Phys. Rev. **D80** (2009) 043526, arXiv: 0906.1197 [astro-ph.CO] (cit. on p. 23).

[100] G. Steigman, *CMB Constraints On The Thermal WIMP Mass And Annihilation Cross Section*,
Phys. Rev. **D91**.8 (2015) 083538, arXiv: 1502.01884 [astro-ph.CO] (cit. on p. 23).

[101] J. F. Beacom, N. F. Bell and G. D. Mack,
General Upper Bound on the Dark Matter Total Annihilation Cross Section,
Phys. Rev. Lett. **99** (2007) 231301, arXiv: astro-ph/0608090 [astro-ph] (cit. on p. 25).

[102] H. Yuksel et al., *Neutrino Constraints on the Dark Matter Total Annihilation Cross Section*,
Phys. Rev. **D76** (2007) 123506, arXiv: 0707.0196 [astro-ph] (cit. on p. 25).

[103] Q. Yuan et al., *Gamma rays and neutrinos from dark matter annihilation in galaxy clusters*,
Phys. Rev. **D82** (2010) 023506, arXiv: 1002.0197 [astro-ph.HE] (cit. on p. 25).

[104] K. Griest and D. Seckel, *Three exceptions in the calculation of relic abundances*,
Phys. Rev. **D43** (1991) 3191 (cit. on pp. 25, 66, 70).

[105] G. Jungman, M. Kamionkowski and K. Griest, *Supersymmetric dark matter*,
Phys. Rept. **267** (1996) 195, arXiv: hep-ph/9506380 [hep-ph] (cit. on pp. 27, 85, 86).

[106] A. Tan et al., *Dark Matter Results from First 98.7 Days of Data from the PandaX-II Experiment*,
Phys. Rev. Lett. **117**.12 (2016) 121303, arXiv: 1607.07400 [hep-ex] (cit. on p. 27).

[107] R. Easther et al., *Supersymmetry, Nonthermal Dark Matter and Precision Cosmology*,
Phys. Rev. **D89**.2 (2014) 023522, arXiv: 1307.2453 [hep-ph] (cit. on pp. 27, 60).

[108] G. Arcadi and P. Ullio, *Accurate estimate of the relic density and the kinetic decoupling in non-thermal dark matter models*, Phys. Rev. **D84** (2011) 043520, arXiv: 1104.3591 [hep-ph]
(cit. on pp. 27, 30, 32, 59).

[109] J. Polonyi, *Generalization of the Massive Scalar Multiplet Coupling to the Supergravity* (1977) (cit. on pp. 27, 59).

[110] A. Vilenkin and L. H. Ford, *Gravitational Effects upon Cosmological Phase Transitions*, Phys. Rev. **D26** (1982) 1231 (cit. on pp. 28, 59).

[111] A. D. Linde,
Scalar Field Fluctuations in Expanding Universe and the New Inflationary Universe Scenario, Phys. Lett. **116B** (1982) 335 (cit. on pp. 28, 59).

[112] A. A. Starobinsky, *Dynamics of Phase Transition in the New Inflationary Universe Scenario and Generation of Perturbations*, Phys. Lett. **117B** (1982) 175 (cit. on pp. 28, 59).

[113] A. S. Goncharov, A. D. Linde and M. I. Vysotsky,
COSMOLOGICAL PROBLEMS FOR SPONTANEOUSLY BROKEN SUPERGRAVITY, Phys. Lett. **147B** (1984) 279 (cit. on pp. 28, 59).

[114] M. Dine, L. Randall and S. D. Thomas, *Supersymmetry breaking in the early universe*, Phys. Rev. Lett. **75** (1995) 398, arXiv: hep-ph/9503303 [hep-ph] (cit. on pp. 28, 59).

[115] H. P. Nilles, *Supersymmetry, Supergravity and Particle Physics*, Phys. Rept. **110** (1984) 1 (cit. on pp. 28, 60).

[116] H. E. Haber and G. L. Kane,
The Search for Supersymmetry: Probing Physics Beyond the Standard Model, Phys. Rept. **117** (1985) 75 (cit. on pp. 28, 60).

[117] M. Drees, "An Introduction to supersymmetry",
Current topics in physics. Proceedings, Inauguration Conference of the Asia-Pacific Center for Theoretical Physics (APCTP), Seoul, Korea, June 4-10, 1996. Vol. 1, 2, 1996,
arXiv: hep-ph/9611409 [hep-ph] (cit. on pp. 28, 60, 62, 63).

[118] M. Drees, R. Godbole and P. Roy, *Theory and phenomenology of sparticles: An account of four-dimensional N=1 supersymmetry in high energy physics*, 2004
(cit. on pp. 28, 35, 59, 60, 62).

[119] H. K. Dreiner, H. E. Haber and S. P. Martin, *Two-component spinor techniques and Feynman rules for quantum field theory and supersymmetry*, Phys. Rept. **494** (2010) 1,
arXiv: 0812.1594 [hep-ph] (cit. on pp. 28, 60).

[120] L. E. Ibanez and A. M. Uranga,
String theory and particle physics: An introduction to string phenomenology,
Cambridge University Press, 2012, ISBN: 9780521517522, 9781139227421, URL: http://www.cambridge.org/de/knowledge/isbn/item6563092/?site_locale=de_DE
(cit. on pp. 28, 60).

[121] A. Polnarev and M. Y. Khlopov,
Era of superheavy-particle dominance and big bang nucleosynthesis,
Sov. Astron.(Engl. Transl.);(United States) **26**.1 (1982) (cit. on pp. 28, 59).

[122] G. D. Coughlan et al., *Cosmological Problems for the Polonyi Potential*,
Phys. Lett. **131B** (1983) 59 (cit. on pp. 28, 59).

[123] B. de Carlos et al., *Model independent properties and cosmological implications of the dilaton and moduli sectors of 4-d strings*, Phys. Lett. **B318** (1993) 447,
arXiv: hep-ph/9308325 [hep-ph] (cit. on pp. 28, 59).

[124] T. Banks, D. B. Kaplan and A. E. Nelson,
Cosmological implications of dynamical supersymmetry breaking, Phys. Rev. **D49** (1994) 779, arXiv: hep-ph/9308292 [hep-ph] (cit. on pp. 28, 59).

[125] J. R. Ellis, D. V. Nanopoulos and M. Quiros, *On the Axion, Dilaton, Polonyi, Gravitino and Shadow Matter Problems in Supergravity and Superstring Models*, Phys. Lett. **B174** (1986) 176 (cit. on pp. 28, 59).

[126] M. Kawasaki, K. Kohri and N. Sugiyama,
MeV scale reheating temperature and thermalization of neutrino background,
Phys. Rev. **D62** (2000) 023506, arXiv: astro-ph/0002127 [astro-ph]
(cit. on pp. 28, 30, 59).

[127] S. Hannestad, *What is the lowest possible reheating temperature?*,
Phys. Rev. **D70** (2004) 043506, arXiv: astro-ph/0403291 [astro-ph]
(cit. on pp. 28, 30, 59).

[128] P. F. de Salas et al., *Bounds on very low reheating scenarios after Planck*,
Phys. Rev. **D92**.12 (2015) 123534, arXiv: 1511.00672 [astro-ph.CO] (cit. on pp. 28, 30, 59).

[129] J. D. Wells,
"Implications of supersymmetry breaking with a little hierarchy between gauginos and scalars",
11th International Conference on Supersymmetry and the Unification of Fundamental Interactions (SUSY 2003) Tucson, Arizona, June 5-10, 2003, 2003,
arXiv: hep-ph/0306127 [hep-ph] (cit. on pp. 28, 59).

[130] G. F. Giudice and A. Romanino, *Split supersymmetry*,
Nucl. Phys. **B699** (2004) 65, [Erratum: Nucl. Phys.B706,487(2005)],
arXiv: hep-ph/0406088 [hep-ph] (cit. on pp. 28, 59).

[131] B. S. Acharya et al., *A Non-thermal WIMP Miracle*, Phys. Rev. **D80** (2009) 083529,
arXiv: 0908.2430 [astro-ph.CO] (cit. on pp. 28, 59).

[132] G. B. Gelmini and P. Gondolo,
Neutralino with the right cold dark matter abundance in (almost) any supersymmetric model,
Phys. Rev. **D74** (2006) 023510, arXiv: hep-ph/0602230 [hep-ph] (cit. on pp. 28, 59).

[133] D. J. H. Chung, E. W. Kolb and A. Riotto, *Production of massive particles during reheating*,
Phys. Rev. **D60** (1999) 063504, arXiv: hep-ph/9809453 [hep-ph] (cit. on pp. 28, 30).

[134] G. F. Giudice, E. W. Kolb and A. Riotto,
Largest temperature of the radiation era and its cosmological implications,
Phys. Rev. **D64** (2001) 023508, arXiv: hep-ph/0005123 [hep-ph] (cit. on pp. 28, 30, 34, 65).

[135] R. Allahverdi and M. Drees, *Production of massive stable particles in inflaton decay*,
Phys. Rev. Lett. **89** (2002) 091302, arXiv: hep-ph/0203118 [hep-ph] (cit. on p. 28).

[136] C. Pallis, *Massive particle decay and cold dark matter abundance*,
Astropart. Phys. **21** (2004) 689, arXiv: hep-ph/0402033 [hep-ph] (cit. on pp. 28, 30).

[137] P. S. Bhupal Dev, A. Mazumdar and S. Qutub,
Constraining Non-thermal and Thermal properties of Dark Matter, Front.in Phys. **2** (2014) 26,
arXiv: 1311.5297 [hep-ph] (cit. on p. 28).

[138] R. Allahverdi et al., *Nonthermal dark matter in string compactifications*,
Phys. Rev. **D88**.9 (2013) 095015, arXiv: 1307.5086 [hep-ph] (cit. on pp. 28, 59).

[139] S. Nakamura and M. Yamaguchi,
Gravitino production from heavy moduli decay and cosmological moduli problem revived,
Phys. Lett. **B638** (2006) 389, arXiv: hep-ph/0602081 [hep-ph] (cit. on p. 28).

[140] T. Asaka, S. Nakamura and M. Yamaguchi, *Gravitinos from heavy scalar decay*,
Phys. Rev. **D74** (2006) 023520, arXiv: hep-ph/0604132 [hep-ph] (cit. on p. 28).

[141] J. L. Feng, S. Su and F. Takayama, *Supergravity with a gravitino LSP*,
Phys. Rev. **D70** (2004) 075019, arXiv: hep-ph/0404231 [hep-ph] (cit. on p. 28).

[142] M. Endo, K. Hamaguchi and F. Takahashi, *Moduli-induced gravitino problem*,
Phys. Rev. Lett. **96** (2006) 211301, arXiv: hep-ph/0602061 [hep-ph] (cit. on p. 28).

[143] R. Blumenhagen et al., *SUSY Breaking in Local String/F-Theory Models*, JHEP **09** (2009) 007,
arXiv: 0906.3297 [hep-th] (cit. on pp. 28, 59).

[144] L. Aparicio et al., *Sequestered de Sitter String Scenarios: Soft-terms*, JHEP **11** (2014) 071,
arXiv: 1409.1931 [hep-th] (cit. on pp. 28, 59).

[145] L. J. Hall et al., *Freeze-In Production of FIMP Dark Matter*, JHEP **03** (2010) 080,
arXiv: 0911.1120 [hep-ph] (cit. on pp. 28, 42, 66).

[146] G. L. Kane et al.,
Dark matter production mechanisms with a nonthermal cosmological history: A classification,
Phys. Rev. **D93**.6 (2016) 063527, arXiv: 1502.05406 [hep-ph]
(cit. on pp. 28–31, 35–41, 43, 48, 56, 59, 65–68, 78).

[147] R. M. Barnett, J. F. Gunion and H. E. Haber, *Gluino Decay Patterns and Signatures*,
Phys. Rev. **D37** (1988) 1892 (cit. on p. 31).

[148] R. Allahverdi and M. Drees,
Thermalization after inflation and production of massive stable particles,
Phys. Rev. **D66** (2002) 063513, arXiv: hep-ph/0205246 [hep-ph] (cit. on pp. 31, 50, 65).

[149] K. Harigaya and K. Mukaida, *Thermalization after/during Reheating*, JHEP **05** (2014) 006,
arXiv: 1312.3097 [hep-ph] (cit. on pp. 31, 65).

[150] K. Harigaya et al., *Dark Matter Production in Late Time Reheating*,
Phys. Rev. **D89**.8 (2014) 083532, arXiv: 1402.2846 [hep-ph] (cit. on pp. 31, 65).

[151] K. Mukaida and M. Yamada,
Thermalization Process after Inflation and Effective Potential of Scalar Field,
JCAP **1602**.02 (2016) 003, arXiv: 1506.07661 [hep-ph] (cit. on pp. 31, 65).

[152] S. Hamdan and J. Unwin, *Dark Matter Freeze-out During Matter Domination* (2017),
arXiv: 1710.03758 [hep-ph] (cit. on p. 40).

[153] M. Drees, H. Iminniyaz and M. Kakizaki,
Abundance of cosmological relics in low-temperature scenarios, Phys. Rev. **D73** (2006) 123502,
arXiv: hep-ph/0603165 [hep-ph] (cit. on p. 41).

[154] N. Bernal et al., *The Dawn of FIMP Dark Matter: A Review of Models and Constraints*,
Int. J. Mod. Phys. **A32**.27 (2017) 1730023, arXiv: 1706.07442 [hep-ph] (cit. on pp. 42, 66).

[155] T. Moroi and L. Randall, *Wino cold dark matter from anomaly mediated SUSY breaking*,
Nucl. Phys. **B570** (2000) 455, arXiv: hep-ph/9906527 [hep-ph] (cit. on pp. 43, 66).

[156] R. T. Co et al., *Freeze-In Dark Matter with Displaced Signatures at Colliders*,
JCAP **1512**.12 (2015) 024, arXiv: 1506.07532 [hep-ph] (cit. on p. 50).

[157] A. D. Linde, *Chaotic Inflation*, Phys. Lett. **129B** (1983) 177 (cit. on p. 51).

[158] A. L. Erickcek and K. Sigurdson,
Reheating Effects in the Matter Power Spectrum and Implications for Substructure,
Phys. Rev. **D84** (2011) 083503, arXiv: 1106.0536 [astro-ph.CO] (cit. on pp. 57, 77).

[159] *Nonthermal histories and implications for structure formation*, Phys. Rev. **D90**.4 (2014) 043536,
arXiv: 1405.7373 [hep-ph] (cit. on pp. 57, 77).

[160] M. Brhlik, D. J. H. Chung and G. L. Kane,
Weighing the universe with accelerators and detectors, Int. J. Mod. Phys. **D10** (2001) 367,
arXiv: hep-ph/0005158 [hep-ph] (cit. on p. 57).

[161] M. Drees et al., *Scrutinizing LSP dark matter at the CERN LHC*, Phys. Rev. **D63** (2001) 035008,
arXiv: hep-ph/0007202 [hep-ph] (cit. on p. 57).

[162] V. A. Mitsou, *Shedding Light on Dark Matter at Colliders*,
Int. J. Mod. Phys. **A28** (2013) 1330052, arXiv: 1310.1072 [hep-ex] (cit. on p. 57).

[163] L. Roszkowski, E. M. Sessolo and S. Trojanowski,
WIMP dark matter candidates and searches?current status and future prospects,
Rept. Prog. Phys. **81**.6 (2018) 066201, arXiv: 1707.06277 [hep-ph] (cit. on p. 59).

[164] G. Arcadi et al., *The waning of the WIMP? A review of models, searches, and constraints*,
Eur. Phys. J. **C78**.3 (2018) 203, arXiv: 1703.07364 [hep-ph] (cit. on p. 59).

[165] H. Baer et al., *SUSY models under siege: LHC constraints and electroweak fine-tuning*,
Phys. Rev. **D89**.11 (2014) 115019, arXiv: 1404.2277 [hep-ph] (cit. on p. 59).

[166] L. Roszkowski, S. Trojanowski and K. Turzy?ski,
Neutralino and gravitino dark matter with low reheating temperature, JHEP **11** (2014) 146,
arXiv: 1406.0012 [hep-ph] (cit. on pp. 60, 63, 69, 70).

[167] L. Roszkowski, S. Trojanowski and K. Turzynski, *Towards understanding thermal history of the Universe through direct and indirect detection of dark matter*, JCAP **1710**.10 (2017) 005,
arXiv: 1703.00841 [hep-ph] (cit. on p. 60).

[168] G. Gelmini et al., *The Effect of a late decaying scalar on the neutralino relic density*,
Phys. Rev. **D74** (2006) 083514, arXiv: hep-ph/0605016 [hep-ph] (cit. on p. 60).

[169] A. Arbey et al., *Dark Matter Casts Light on the Early Universe* (2018),
arXiv: 1807.00554 [hep-ph] (cit. on p. 60).

[170] L. Aparicio et al., *Light Higgsino Dark Matter from Non-thermal Cosmology*,
JHEP **11** (2016) 038, arXiv: 1607.00004 [hep-ph] (cit. on p. 60).

[171] L. Aparicio et al., *Non-thermal CMSSM with a 125 GeV Higgs*, JHEP **05** (2015) 098,
arXiv: 1502.05672 [hep-ph] (cit. on p. 60).

[172] G. Belanger et al., *MicrOMEGAs: A Program for calculating the relic density in the MSSM*,
Comput. Phys. Commun. **149** (2002) 103, arXiv: hep-ph/0112278 [hep-ph]
(cit. on pp. 60, 69, 70).

[173] A. Djouadi et al., "The Minimal supersymmetric standard model: Group summary report",
GDR (Groupement De Recherche) - Supersymetrie Montpellier, France, April 15-17, 1998, 1998,
arXiv: hep-ph/9901246 [hep-ph],
URL: http://inspirehep.net/record/481987/files/arXiv:hep-ph_9901246.pdf
(cit. on pp. 62, 69).

[174] N. Arkani-Hamed, A. Delgado and G. F. Giudice, *The Well-tempered neutralino*, Nucl. Phys. **B741** (2006) 108, arXiv: hep-ph/0601041 [hep-ph] (cit. on p. 66).

[175] S. Mizuta and M. Yamaguchi, *Coannihilation effects and relic abundance of Higgsino dominant LSP(s)*, Phys. Lett. **B298** (1993) 120, arXiv: hep-ph/9208251 [hep-ph] (cit. on pp. 66, 70).

[176] C. H. Chen, M. Drees and J. F. Gunion, *A Nonstandard string / SUSY scenario and its phenomenological implications*, Phys. Rev. **D55** (1997) 330, [Erratum: Phys. Rev.D60,039901(1999)], arXiv: hep-ph/9607421 [hep-ph] (cit. on p. 66).

[177] A. Djouadi, J.-L. Kneur and G. Moultaka, *SuSpect: A Fortran code for the supersymmetric and Higgs particle spectrum in the MSSM*, Comput. Phys. Commun. **176** (2007) 426, arXiv: hep-ph/0211331 [hep-ph] (cit. on p. 69).

[178] V. Maurer, *T3PS v1.0: Tool for Parallel Processing in Parameter Scans*, Comput. Phys. Commun. **198** (2016) 195, arXiv: 1503.01073 [cs.MS] (cit. on p. 69).

[179] G. Aad et al., *Observation of a new particle in the search for the Standard Model Higgs boson with the ATLAS detector at the LHC*, Phys. Lett. **B716** (2012) 1, arXiv: 1207.7214 [hep-ex] (cit. on p. 69).

[180] S. Chatrchyan et al., *Observation of a new boson at a mass of 125 GeV with the CMS experiment at the LHC*, Phys. Lett. **B716** (2012) 30, arXiv: 1207.7235 [hep-ex] (cit. on p. 69).

[181] J. R. Ellis, T. Falk and K. A. Olive, *Neutralino - Stau coannihilation and the cosmological upper limit on the mass of the lightest supersymmetric particle*, Phys. Lett. **B444** (1998) 367, arXiv: hep-ph/9810360 [hep-ph] (cit. on p. 70).

[182] J. R. Ellis, K. A. Olive and Y. Santoso, *Calculations of neutralino stop coannihilation in the CMSSM*, Astropart. Phys. **18** (2003) 395, arXiv: hep-ph/0112113 [hep-ph] (cit. on p. 70).

[183] J. Hisano et al., *Non-perturbative effect on thermal relic abundance of dark matter*, Phys. Lett. **B646** (2007) 34, arXiv: hep-ph/0610249 [hep-ph] (cit. on p. 70).

[184] T. Plehn, *Yet Another Introduction to Dark Matter* (2017), arXiv: 1705.01987 [hep-ph] (cit. on pp. 70, 71).

[185] J. R. Ellis et al., *Calculations of neutralino-stau coannihilation channels and the cosmologically relevant region of MSSM parameter space*, Astropart. Phys. **13** (2000) 181, [Erratum: Astropart. Phys.15,413(2001)], arXiv: hep-ph/9905481 [hep-ph] (cit. on p. 70).

[186] J. R. Ellis et al., *Update on the direct detection of supersymmetric dark matter*, Phys. Rev. **D71** (2005) 095007, arXiv: hep-ph/0502001 [hep-ph] (cit. on p. 71).

[187] P. Binetruy, *Supersymmetry: Theory, experiment and cosmology*, 2006 (cit. on pp. 71, 85, 86).

[188] M. Drees and M. Nojiri, *Neutralino - nucleon scattering revisited*, Phys. Rev. **D48** (1993) 3483, arXiv: hep-ph/9307208 [hep-ph] (cit. on p. 71).

[189] J. R. Ellis, A. Ferstl and K. A. Olive, *Reevaluation of the elastic scattering of supersymmetric dark matter*, Phys. Lett. **B481** (2000) 304, arXiv: hep-ph/0001005 [hep-ph] (cit. on p. 71).

[190] C. Munoz, *Dark matter detection in the light of recent experimental results*, Int. J. Mod. Phys. **A19** (2004) 3093, arXiv: hep-ph/0309346 [hep-ph] (cit. on p. 71).

[191] J. R. Ellis, K. A. Olive and C. Savage, *Hadronic Uncertainties in the Elastic Scattering of Supersymmetric Dark Matter*, Phys. Rev. **D77** (2008) 065026, arXiv: 0801.3656 [hep-ph] (cit. on p. 71).

[192] A. L. Erickcek, *The Dark Matter Annihilation Boost from Low-Temperature Reheating*, Phys. Rev. **D92**.10 (2015) 103505, arXiv: 1504.03335 [astro-ph.CO] (cit. on p. 77).

[193] A. L. Erickcek, K. Sinha and S. Watson, *Bringing Isolated Dark Matter Out of Isolation: Late-time Reheating and Indirect Detection*, Phys. Rev. **D94**.6 (2016) 063502, arXiv: 1510.04291 [hep-ph] (cit. on p. 77).

[194] J. Billard, L. Strigari and E. Figueroa-Feliciano, *Implication of neutrino backgrounds on the reach of next generation dark matter direct detection experiments*, Phys. Rev. **D89**.2 (2014) 023524, arXiv: 1307.5458 [hep-ph] (cit. on pp. 77, 78).

[195] O. Philipsen, *The QCD equation of state from the lattice*, Prog. Part. Nucl. Phys. **70** (2013) 55, arXiv: 1207.5999 [hep-lat] (cit. on pp. 81–83).

[196] J. I. Kapusta and C. Gale, *Finite-temperature field theory: Principles and applications*, Cambridge University Press, 2011, ISBN: 9780521173223, 9780521820820, 9780511222801 (cit. on pp. 81–83).

[197] T. R. Slatyer, "Indirect Detection of Dark Matter", *Proceedings, Theoretical Advanced Study Institute in Elementary Particle Physics : Anticipating the Next Discoveries in Particle Physics (TASI 2016): Boulder, CO, USA, June 6-July 1, 2016*, 2018 297, arXiv: 1710.05137 [hep-ph] (cit. on p. 85).

[198] J. F. Navarro, C. S. Frenk and S. D. M. White, *The Structure of cold dark matter halos*, Astrophys. J. **462** (1996) 563, arXiv: astro-ph/9508025 [astro-ph] (cit. on p. 85).

[199] B. Moore et al., *Cold collapse and the core catastrophe*, Mon. Not. Roy. Astron. Soc. **310** (1999) 1147, arXiv: astro-ph/9903164 [astro-ph] (cit. on p. 85).

[200] A. V. Kravtsov et al., *The Cores of dark matter dominated galaxies: Theory versus observations*, Astrophys. J. **502** (1998) 48, arXiv: astro-ph/9708176 [astro-ph] (cit. on p. 85).

List of Figures

List of Tables